THERMODYNAMIC STUDY ON VAPOURIZATION OF NIOBIUM OXIDES FROM SLAG MELTS

BY

QIUJIN LI
B.ENG., M.ENG. (DALIAN UNIV. OF TECH., CHINA)

THERMODYNAMIC STUDY ON VAPOURIZATION OF NIOBIUM OXIDES FROM SLAG MELTS

THERMODYNAMIC STUDY ON VAPOURIZATION OF NIOBIUM OXIDES FROM SLAG MELTS

BY

QIUJIN LI, B.ENG., M.ENG.

A Thesis

Submitted to the school of Graduate Studies

In Partial Fulfilment of the Requirements

For the Degree

Doctor of Philosophy

McMaster University

DOCTOR OF PHILOSOPHY (2009) McMaster University

(Materials Science and Engineering) Hamilton, Ontario

TITLE: Thermodynamic Study on Vapourization of Niobium Oxides from Slag Melts

AUTHOR: Qiujin Li, B.Eng., M.Eng., (Dalian University of Technology, China)

SUPERVISOR: Dr. Kenneth S. Coley

NUMBER OF PAGES: xv, 187

ABSTRACT

The partitioning of niobium to slag and gaseous niobium oxide vapourizing from metal/slag may cause niobium losses and erratic recovery rates in steelmaking practices. Knowledge of the volatility and activities of niobium oxides in slag melts are of great value for both theoretical evaluation and practical applications in niobium microalloyed steels. Because of the multi-valence state of niobium ions in slags, the behaviour of niobium in metallurgical slags is complicated. So far, little systematic attempts have been made and activity data of niobium oxides in slags are extremely scarce. The aim of this study is to determine precise data on the vapour pressures of niobium oxides, and consequently, to obtain information on thermodynamic quantities of niobium oxides in slag melts.

The thermodynamic properties of niobium oxide in $CaO\text{-}SiO_2\text{-}NbO_x$ and $CaO\text{-}SiO_2\text{-}Al_2O_3\text{-}NbO_x$ slag melts were determined by employing the transpiration method from 1800-1873K under a controlled atmosphere. To confirm the validity of the transpiration method for the measurement of thermodynamic properties, the binary alloy system silver-gold was chosen for a comparison with the same property which has been measured by other recognized procedures. The agreement with literature results confirmed that the measurement yields reliable results for thermodynamic activity data by the transpiration method.

The vapourization of liquid Nb_2O_5 was studied as a function of partial pressure of oxygen in the system and this confirms that atmosphere control is the essential condition for the vapourization study. The gaseous niobium oxide species was verified to be NbO_2; hence, Nb_2O_5 vapourizes by the reaction $Nb_2O_5(l) = 2NbO_2(g) + 1/2O_2(g)$. Heat of vapourization was estimated by applying the second law method and comparison with the literature showed a fairly good agreement.

The thermodynamic properties of niobium oxide in the slag system of $CaO-SiO_2-NbO_x$ and $CaO-SiO_2-Al_2O_3-NbO_x$ were measured by varying the experimental conditions of slag basicities, slag compositions, temperature and oxygen partial pressures. From the basicity dependency of the activity coefficient for each oxide in this study, it is proposed that niobium oxide behaves as an amphoteric oxide and niobium pentoxide as an acidic oxide. On the other hand, it was observed in the redox equilibrium experiment that $NbO_{2.5}$ becomes predominant as the slag basicity increases. However, insufficient interaction parameters as well as parameter conversions prevent the application of the regular solution model. The co-relationship between the ionic diameter and ionic energy was discovered and shows good agreement with calcium oxide and silicon oxide. With the interaction parameter and converting parameter attained, the regular solution model shows good agreement for the activity coefficients between measurement and calculation.

ACKNOWLEDGEMENTS

This thesis has arisen from the years of research work since I joined McMaster University. In the course of this research, I have worked with a number of people who have contributed to this thesis. It is my great pleasure to convey my gratitude to them all.

I would like to record my deep gratitude to my supervisor, Dr. Ken Coley, for his supervision, advice and guidance over the years. He provided ongoing encouragement and support and his scientific intuition both inspired and enriched my growth both as a student and engineer.

I gratefully acknowledge Dr. McDermid and Dr. Malakhov for their advice, supervision and crucial contribution. Their involvement has nourished and developed my intellectual maturity.

Many thanks go out in particular to Dr. Gord Irons, the director for McMaster university steel research center. This thesis was made possible through the financial support of the steel research center and its participating member companies.

It is a pleasure to express my gratitude wholeheartedly to faculty members, researchers, staff and graduate students in the department of Materials Science and Engineering for providing a cooperative academic environment. I convey special acknowledgment to Fernando Guevara, HoYong Huang, Hualong Pan and Tom Zhou , my new and old friends with whom I shared many good times and lasting memories.

My parents deserve special mention for their inseparable support and love. My father, Rongkuan, fundamentally guided my learning character, showing me the joy of intellectual pursuit since childhood. My mother XiuMei , the one who sincerely raised me with her caring unconditional love. My sisters QiuHong and QiuXia, my brother XiangFeng and all my family members, thanks for being supportive.

Words fail me to express my appreciation to my love, best friend and life partner, Clive for his true love, encouragement and support. I could never have embarked and started all of this without his support and help. Thank you.

Finally, I would like to thank everybody who was important to the successful realization of this thesis.

TABLE OF CONTENTS

LIST OF FIGURES

Chapter 2

Chapter 3

Chapter 4

Chapter 5

Chapter 6

LIST OF TABLES

Chapter 2

Chapter 3

Chapter 4

Chapter 6

Appendix A

Appendix B

Chapter 1 Introduction

1.1 Research Background

Niobium is an alloying element used in strengthening high-strength-low-alloy (HSLA) steels which can be used in a variety of applications. The most important application area for high strength niobium microalloyed steels is in building automobiles and high pressure gas transmission pipelines, which require high levels of strength to contain the high-pressure gas as well as acceptable toughness.

Much attention has been paid to the use of niobium as a microalloying element to improve the mechanical properties of micro-alloyed steels (Patel *et al.*, 2001). The improved steel strength due to the microaddition of this element is attributed to the formation of carbide and carbonitrides of niobium and their effect on grain refinement and precipitation strengthening (Schulze *et al.*, 1988).

Although there are very beneficial results obtained when niobium is added to steels, the growth and acceptance of the production of niobium-microalloyed steels is still relatively limited. The limitation is mainly due to the very strong affinity of niobium to oxygen, which causes the partition of niobium to slag. Furthermore, gaseous niobium oxides vapourizing from metal/slag result in erratic recovery rates as experienced in

steelmaking practices.

The following formula can be used for the calculation of niobium recoveries (Sismanis and Argyropoulos, 1989):

$$R_{Nb} = \frac{m_{Nb}}{m_{FeNb}} \times 100\% \quad (1.1)$$

Where:

R_{Nb} niobium recovery

m_{Nb} mass of ferroalloy that was found in the liquid steel after chemical analysis

m_{FeNb} mass of the ferroalloy which was found to be transferred into the liquid steel by the weight sensor

The alloy recovery worsens in the vacuum degasser, creating a great concern in the steelmaking industry (Deeley *et al.*, 1981; Bonnet and Coley, 2001). Meanwhile, metal-oxygen reaction and the volatilization of niobium oxides can cause an alloy loss, affecting the usage of the materials at higher temperatures (Schulze *et al.*, 1988).

Specifically, niobium losses can be attributed to two reactions shown below:

(1) partition to slags by oxidation

$$[Nb] + x[O] = (NbO_x) \quad (1.2)$$

(2) formation of gaseous NbO_2

$$[Nb] + 2[O] = NbO_2(gas) \quad (1.3)$$

Where [] and () indicate solute in metal phase and slag respectively. The typical alloy recovery rate is reported as 90%. Supposing 0.04 wt% of niobium in HSLA steels, for one million Mg of annual output, it will result in a one million dollar loss. In addition, the erratic recovery rate is the primary concern.

Therefore, one of the major interests in ferroniobium and microalloyed steels is to optimize the process for higher recovery of niobium. It will be beneficial both in saving raw materials and energy. The reaction between slag and metal is known to mainly control the niobium recovery from slag to metal phase. Thus, knowledge of the activities of niobium oxides in slag melts is of great importance for better understanding the nature of niobium-containing slags.

The behaviour of niobium oxides in metallurgical slags is very complex due to the co-existence of the multi-valence niobium ions (Tsukihashi *et al.*, 1988). The high vapour pressure of NbO_2 in niobium oxide containing slags is another barrier for a systematic study. So far, few attempts have been made to measure the activities of niobium oxides and the volatility of niobium oxides under controlled atmosphere, consequently, the data is still inadequate.

When a liquid steel contains niobium, the loss of niobium through oxidation and subsequent vapourization is inevitable. This makes it important to determine the

thermodynamic properties of niobium oxide in slag to minimize the niobium loss. Thermochemical calculation shows that Nb_2O_5 is probably the most stable substance under the oxygen partial pressure used in practical ladle metallurgy; however, studies on the behaviour of Nb_2O_5 in steelmaking slags are quite limited.

Three phases of niobium oxides, NbO, NbO_2 and Nb_2O_5, are reported to be stable from room temperature to high temperature (Kamegashira *et al.*, 1981). Vapourization studies on these phases have been carried out by several investigators (Kamegashira *et al.*, 1981; Golubtsov *et al.*, 1960; Shchukarev *et al.*, 1959; 1962; 1966; Matsui and Naito, 1981; 1982;1983). These studies contribute to the identification of the gaseous species based on pure niobium oxides at high temperatures. However, the vapour pressures as well as the vapourization from steelmaking slags were rarely studied.

In the meantime, an effusion method coupled with mass spectrometry has been commonly employed for vapour pressure study; however, this method leads to some inconsistency in atmosphere control in the literature. Among the numerous methods for vapour pressure measurement, the transpiration method has been proven to be very useful for systems in which vapour pressures and dissociation pressures cannot be measured by more direct means (Richardson and Alcock, 1959) and are often used for studying vapour arising from condensed phases at high temperatures. Thus, a modified transpiration method was employed to measure the vapour pressure in this study.

In metallurgical operations, the distribution of niobium between liquid metal and

slag, as well as the partitioning between Nb^{5+} and Nb^{4+} valency states in the slag, is determined by the oxygen partial pressure, slag composition, and temperature. The oxides associated with these two predominant valencies of niobium are expected to exhibit inherently different properties, affecting both the physical and thermodynamic behaviour of slags containing these oxides.

The ternary system $CaO\text{-}SiO_2\text{-}NbO_x$ (this system is not truly ternary because niobium occurs in two different oxidation states in varying amounts under the experimental conditions) is a suitable model system for study because the acid-base relations can be varied over a wide range by changing the CaO/SiO_2 ratio in the melts. Furthermore, the addition of moderate amounts of Al_2O_3 to the ternary system will serve to evaluate the behaviour of Al_2O_3 as an amphoteric oxide in silicate melts.

The chosen $CaO\text{-}SiO_2\text{-}NbO_x$ system also provides an excellent starting point for an improved understanding of the properties of technologically important slags in the steelmaking and ferroalloy industries. These slags typically contain CaO and SiO_2 as the main constituents with varying amounts of alumina, magnesia, iron oxide, manganese oxide, and niobium oxide (especially in ferroniobium production). Data from the present work can be readily applied to systems that include some of these additional components through thermodynamic modeling, from which only a limited number of experimental check points (calibration points) are needed.

A fundamental thermodynamic link between the condensed and vapour phase is

given by activities and related quantities. Activities of condensed-phase components can be expressed in terms of partial vapour pressures with reference to the standard state pressure (Kubaschewski and Alcock, 1979). Hence, a measurement in the vapour phase can provide activity data for the condensed phase.

Studies on the vapourization of niobium in slags are of interest to the metallurgist because they provide the fundamental data and mechanisms contributing to niobium loss in ladle slags and RH degasser. Knowledge of the activity coefficient of niobium and its variation with composition and temperature in a melt can be used to determine the equilibrium solubility of niobium and its distribution between various phases in the melt.

Hence, knowledge of volatility and the activities of niobium oxides in slag melts are of great value for both theoretical evaluation and practical applications in niobium microalloyed steelmaking. Owing to the continuously increasing demand for this type of steel in recent years, there has been a persistent search for effective and economic ways to raise and stabilize the niobium recovery. This depends very much on the slag/metal reactions. Due to the multi-valence state of niobium ions in slags, the behaviour of niobium in metallurgical slags is complicated so that little systematic attempts have been made, resulting in extremely scarce activity data of niobium oxides in literature. Thus, the vapourization study on niobium oxides is important, not only from the technical point of view, but also from a pure scientific point of view in filling up the gap in knowledge.

1.2 Objectives of This Research

The transpiration method has been employed throughout the experimental work. The versatile method itself is not new; however, this method for the vapourization study in pure niobium oxide and niobium oxide containing slags has rarely been applied. This research has been divided by three stages and the objectives of each stage are presented below.

Stage I Validation and Calibration

- To establish and calibrate the transpiration method for vapour pressure and activity measurement by the designed self-consistency experiments
- To measure the vapour pressure of pure niobium oxide under various oxygen pressures in the temperature range of 1525-1600°C
- To verify the vapour species of niobium oxide under controlled atmosphere

Stage II Measurements of Vapour Pressure and Thermodynamic Properties of Niobium Oxide Containing Slags

- To measure the equilibrium vapour pressure of niobium oxides starting from $CaO\text{-}SiO_2\text{-}NbO_x$ slag melt by varying the following influential factors

- Variation of temperatures
- Partial pressure of oxygen controlled by CO_2/CO ratios
- Slag composition (slag basicity, initial content of Nb_2O_5, addition of Al_2O_3)

- To determine the thermodynamic properties of slag systems both in CaO-SiO_2-NbO_x and CaO-SiO_2-Al_2O_3-NbO_x

- To develop a potentiometric titration method and quantitatively measure Nb^{4+} and Nb^{5+} ionic species in the slag solution

Stage III Application of This Research

- To access the parameters for the application of the regular solution model and to predict the activity of niobium oxide in a multicomponent slag system

- To propose the secondary steelmaking process to minimize niobium losses and maximize the alloy recovery rate

1.3 Outline of This Thesis

Seven chapters are presented in this thesis, which cover the contents from

literature review, description of experimental work, experimental results, discussions and conclusions.

Chapter 2 is the literature review, in six sections, stating the previous research and current state of the art that is closely related to this thesis.

Chapter 3 describes the materials processing, experimental apparatus, general experimental procedures and subsequent chemical analysis.

Chapter 4 presents in detail in what is called self-consistency experiments, by which the systematic errors are detected and the precision and accuracy of the measurements are evaluated.

Chapter 5 provides the study on the vapourization of liquid Nb_2O_5 by the transpiration method under various oxygen pressures in the temperature range of 1525-1600°C.

Chapter 6 illustrates the systematic studies on the thermodynamic properties of niobium oxide containing slag in $CaO\text{-}SiO_2\text{-}NbO_x$ and $CaO\text{-}SiO_2\text{-}Al_2O_3\text{-}NbO_x$ systems; a total of 60 conditions and 120 experiments have been conducted by varying slag composition, oxygen partial pressure and temperature; the assessment of the interaction energy for the application of regular solution model as well as the application of the experimental results are all discussed in this chapter.

Chapter 7 is the summary and conclusions for the overall thesis while future work is also proposed.

Chapter 2 Literature Review

This chapter presents, in six sections, previous research and state of the art that is closely related to this thesis. Starting with the introduction of the reasons for measuring high temperature vapour pressure in section 1, section 2 summarizes the general measuring methods which are applied for high temperature vapours. Among these measuring methods, the transpiration method has been employed through this research and is explained in detail in section 3. In section 4, niobium oxides and their vapour species are summarized from previous work. Subsequently, section 5 addresses the thermodynamics of slags and section 6 explores niobium in slag.

2.1 The Roles for Measuring High Temperature Vapour Pressure

The development of high temperature chemistry, with an emphasis on the gas or vapour phase (Hastie, 1975; Haskell and Byrne, 1972; Schwerdtfeger and Turkdogan, 1970), can contribute much to the appreciation of the role of vapour pressure in materials applications at high temperatures.

The importance of high temperature vapourization studies lies mainly in two areas:

- measurement of thermodynamic properties of a component
- each stage of materials cycle

2.1.1 Attaining Thermodynamic Quantities

Among thermodynamic properties of components, the measurement of activities should be the focus of attention. This is because if it is possible to determine the vapour pressure and thereby the activity of one component of a mixture as a function of temperature, one can derive all partial thermodynamic quantities (Kubaschewski *et al.*, 1993), for instance,

$$\Delta\overline{G}_i = RT\ln a_i \tag{2.1}$$

$$\Delta\overline{H}_i = \frac{\partial(\Delta\overline{G}_i/T)}{\partial(1/T)} = R\frac{\partial\ln a_i}{\partial(1/T)} = -RT^2\frac{\partial\ln a_i}{\partial T} \tag{2.2}$$

$$\Delta\overline{S}_i = -\frac{\partial\Delta\overline{G}_i}{\partial T} = -R(\ln a_i + T\frac{\partial\ln a_i}{\partial T}) \tag{2.3}$$

Furthermore, if these quantities can be determined over the entire composition range ($0 \le x_i \le 1$) of a binary system, all integral thermodynamic quantities can, in principle, be obtained by means of a Gibbs-Duhem integration, yielding a complete thermodynamic description of the system. The thermodynamics of a higher-order system can be worked out in a similar way if additional information on the limiting binary systems is available (Turkdogan, 1980).

Generally, the activities of components in solution can be determined by the

following methods (Kubaschewski and Alcock, 1979):

- direct vapour pressure
- vapour effusion from Knudsen cells
- vapour transpiration and isopiestic techniques
- electrochemical cells
- calculation from phase diagrams
- partitioning between condensed phases
- equilibration with gas phases
- Langmuir evaporation and condensation

It can be seen that among the many experimental methods to determine thermodynamic activities of a component, vapour pressure methods comprise a large group. The general definition of the thermodynamic activity of a component i is

$$a_i = \frac{f_i}{f_i^0} \approx \frac{p_i}{p_i^0} \tag{2.4}$$

where

f_i fugacity of i

f_i^0 fugacity of i at standard state

This definition implicitly assumes that the vapour species i is monatomic or monomer. The only restriction on Equation 2.4 is that the pressures must not be so great that deviations from ideal gas behaviour are significant. As can be seen from Equation 2.4, a_i can be found from measurements of p_i over the alloy and p_i^0 over pure i. However, there are many alternative vapour methods for using Equation 2.4 indirectly to obtain a_i.

It should be pointed out that the assumption of the validity of the ideal gas will result in sufficient accuracy in the majority of cases of interest for metallurgical thermodynamics (Kubaschewski and Alcock, 1979). This is particularly true for low pressures and in the present case the pressures of interest are small fractions of an atmosphere.

As shown in Equation 2.4, the activity of a substance can be derived by measuring the ratio of its vapour pressures over the solution and in the pure state. The measurement of the partial pressure leads directly to the corresponding activity value, if the vapour pressure of the pure condensed form of the substance at standard state is known. Therefore, the vapour pressure method is so versatile that activities can be derived from measurements of any equilibria involving a solution and a gaseous phase.

2.1.2 The Role of Vapour Pressure in Materials Science

In addition to obtaining the thermodynamic properties of materials, high

temperature vapours also play a significant role at each stage of the materials cycle. For instance, the separation and transportation of ores in the period of orogenesis may have involved high temperature vapours (Hastie, 1975). The metallurgical extraction and refinement process can utilize high temperature vapours to advantage (Vidal and Poos, 1973).

Similarly, the preparation of product materials can be achieved by vapour solvation and transport processes (Haskell and Byrne, 1972). And finally, the disposal or recycling of these materials can utilize combustion or pyrometallurgical procedures.

Moreover, the growth of extremely pure crystals is a necessity for modern technology. Many of these techniques involve vapourization processes and some lie within the subfield denoted as chemical transport reactions. These reactions have been intensively discussed by Schaefer (Schaefer, 1964) who cites numerous examples.

On the other hand, in many high temperature systems, the rate at which material is lost through vapourization is a far more severe limitation than the fusion of materials. Hence, measurements of vapour pressures are essential in establishing upper temperature limits of usages of materials (Gilles, 1975).

2.2 General Methods for Measuring Vapour Pressures

Several reviews of vapour pressure measurements have been given in the past

(Komarek, 1971; Komarek, 1977; Kubaschewski, 1981; Komarek and Ipser, 1984); furthermore, there are a number of books devoting one or more chapters to experimental methods (Kubaschewski and Alcock, 1979; Nesmeyanov, 1963; Brodowsky and Schaller, 1989; Kubaschewski *et al.*, 1967). A comparison of various vapour pressure methods was given by Wahlbeck (Wahlbeck, 1986).

However, it must be pointed out that no new vapour pressure methods could be found in recent literature. It is rather the application and/or modification of well-established methods that may be of interest.

Fundamentally, the existing methods for measuring vapour pressure are divided into four groups:

- Static methods (pressure gauges, atomic absorption, and others)
- Dynamic methods (boiling point method, transpiration method)
- Effusion methods (Langmuir method, different variants of the Knudsen method)
- Equilibration methods (equilibration with gas mixtures, isopiestic method, dew point method).

2.2.1 Static Methods

Static methods (Nesmeyanov, 1963) are defined as those where a substance is

heated in an evacuated container until equilibrium is established with the corresponding gas phase. In practice, the actual measurements of the pressure can be done in different ways.

2.2.2 Dynamic Methods

Although several other methods, especially all effusion methods and some of the gas equilibration methods could actually be listed as dynamic, this term is restricted here to the boiling point and transpiration methods. The transpiration method has been employed throughout all the experiments in this study and will be discussed in detail in **Section 2.3**.

2.2.3 Effusion Methods

There exists an entire group of methods in which the vapour pressure is calculated from the rate of vapourization. Vapourization into a vacuum can occur either from an open surface [Langmuir method (Hilpert, 1978)] or through an orifice from a container in which the gas phase is saturated with the vapour [Knudsen method (Neckle, 1989)].

Although the Langmuir method is not an effusion in its strict sense (Margrave, 1959), it is still treated together with the Knudsen method due to their many similarities. Both methods are, in principle, based on the same relationship between vapourization rate and vapour pressure.

$$p_i = \frac{m_i}{tA}\sqrt{\frac{2\pi RT}{M_i}} \tag{2.5}$$

where m_i is the mass of the species i (with a molecular weight M_i) evaporating during the time t; A is either the surface of the substance from which vapourization occurs (Langmuir) or the area of the orifice of the Knudsen cell.

The Langmuir kinetic vapour pressure p_L is usually correlated with the equilibrium vapour pressure p_{eq} through α_L, the Langmuir sublimation coefficient (Richardson and Alcock, 1959).

$$p_L = \alpha_L \cdot p_{eq} \tag{2.6}$$

where $0 \le \alpha_L \le 1$. A Langmuir coefficient of unity means that sample molecules evaporate into a vacuum at the equilibrium rate. The Langmuir coefficients of most metals and other simple substance are close to unity (Hirth and Pound, 1963); whereas a Langmuir coefficient near zero indicates that the sample evaporates at kinetically determined rate with significant energy or entropy barriers (Merten and Bell, 1967). Some molecular and ionic systems vapourize at rates appreciably lower than are predicted from their equilibrium vapour pressures. Such systems may have Langmuir coefficients very much less than one (Paule and Margrave, 1967).

2.2.4 Equilibration Methods

This group of methods is defined as comparing all those methods where a condensed sample is brought into equilibrium with a gas phase (Anthonisamy *et al.*, 1996). The isopiestic method and the dew point method (which is, in principle, an inverse isopiestic method) belong to this group.

2.2.5 Summary of the Overall Methods

It is usually difficult to determine which method will be applied for vapour pressure measurements. In general, static methods are preferable for the measurement of the reaction pressure of a system below 1000°C and only one gas is involved (Kubaschewski, 1967). However, the dynamic method, for instance, the transpiration method, may be used to determine the rate of vapourization of two volatile components. There will be a detailed discussion shortly about the limitation and application of the transpiration method.

It seems that the Knudsen method has no serious sources of error, but is limited to a suitable cell material, which should be workable and must not react with the contents (Kubaschewski, 1967). In addition, the Langmuir method does not measure equilibrium vapour pressure. Nevertheless, these effusion methods can only be employed when the vapour species effusion is simple or well defined chemically (Merten and Bell, 1967).

2.3 The Transpiration Method

2.3.1 Introduction

The transpiration method, also called the transportation or entrainment method is one of the simplest and most versatile ways of studying heterogeneous equilibria involving gases. Thomson (Thomson, 1959) credits the French chemist and physicist Regnault (Regnault, 1845) with being the first to use this method.

It is used primarily for measuring vapour and dissociation pressures, but it may be applied to gas-solid or gas-liquid equilibria and chemical processes during vapourization (Merten and Bell, 1967). In valuable reviews, Kubaschewski and Evans (Kubaschewski and Evans, 1958), Margrave (Margrave, 1959), Richardson and Alcock (Richardson and Alcock, 1959) have discussed applications of the method. More recently, these experimental techniques have been employed by many researchers, for instance, Reyes and Gaskell (Reyes and Gaskell, 1983), Son and Tsukihashi (Son and Tsukihashi, 2003).

2.3.2 Principles

A steady, measured stream of inert or reactive gas is passed over or bubbled through the substance under investigation, which is maintained at a constant temperature. The gas removes the vapour or volatile component of the substance at a rate which is dependent upon their relative pressures and upon the rate of gas flow (Kubaschewski *et*

al., 1967).

In principle, the entraining gas should become saturated with the vapour (Lumsden, 1952). The flow is desired to be sufficiently slow so that the carrier gas is saturated with the vapour, which is condensed at some point "downstream" from the sample. The vapour is condensed or collected by absorption or chemical combination at a cooler portion of the apparatus. The amount of material condensed is determined by chemical means, by the weight gain of the condenser, or by the weight loss of the sample (Margrave, 1959).

Basically, the gases are assumed ideal, and the flowing gas is assumed to be saturated with the vapours of the materials being studied. The total pressure P_t is proportional to the total number of gaseous moles present, n_t. For each component in the gas, the partial pressure p_i is proportional to n_i, and by Dalton's law,

$$P_t = \sum p_i \text{ and } n_t = \sum n_i \tag{2.7}$$

Thus, for a flow gas, f, and one vapour species, v,

$$\frac{p_v}{P_t} = \frac{p_v}{p_v + p_f} = \frac{n_v}{n_v + n_f} \tag{2.8}$$

Where, n_v can be determined from the weight loss from the sample container or from the weight-gain of a condenser or trap in the flow system, if the molecular weight of

the vapour species is known or assumed; n_f results from volume of flowing gas; and P_t will be the atmospheric pressure if the system is in equilibrium with the atmosphere, as is the usual arrangement.

The transpiration method is in principle simple and capable of broad application to high temperature systems. However, in practice, there are some limitations for the applications, for example,

- the number of moles vapourizing cannot be known unless the molecular weight of the vapour is known
- the flowing gas must be saturated with the vapour
- a container with sample may show a weight loss at high temperature through diffusion, even when the flow rate is zero
- side reactions of the sample with the container or flow gas are often hard to prevent.

2.3.3 Common Description of Experimental Apparatus

The descriptions of transpiration apparatus vary greatly in literature, from an expanse of massive bottles filled with solutions for measuring solution vapour pressures to a small ceramic cell employed in some high-temperature studies (Rapp, 1968). These seemingly different systems, however, have a set of components that are common to all

transpiration apparatus. These common components are listed as follows:

- a source of carrier gas
- a conduction system for this gas into a saturation chamber
- a saturation chamber where the equilibrium partial pressure are maintained over a condensed system
- a conduction system for carrying the saturated carrier gas away from the saturation chamber
- a measuring system for evaluating the transpiration rate versus the carrier gas flow rate

Simultaneously, the functional behaviour of an interaction between each pair of these components requires the following considerations. The carrier gas must be constant in composition. The gas must be delivered to the saturation chamber at a constant rate. The temperature for the saturation chamber is constant.

2.3.4 Dependence of Vapour Pressure on Flow Rate of Carrier Gas

A typical transpiration cell is shown schematically in Figure 2.2 (Merten, 1959). The carrier gas is introduced at "a", flows around a heat shield "b", into an essentially isothermal region in the neighbourhood of the sample-containing boat "c". The vapour laden gas then passes through a capillary constriction "d" and into the condensing region

"e".

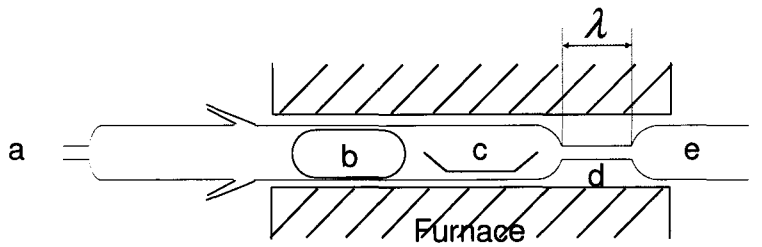

Figure 2.1 A typical transpiration apparatus (Merten, 1959): (a) carrier gas, (b) heat shield, (c) sample-containing boat, (d) capillary constriction, (e) condensing region.

The flow of vapour through the capillary of saturation chamber may be thought of as the sum of a slug-flow term and a diffusion term (Merten, 1959), so that the mass of the vapour passing any point along the capillary in unit time is given by

$$k = A\left(Vc - D\frac{dc}{dx}\right) \tag{2.9}$$

k mass flow rate of vapour

D interdiffusion coefficient of carrier gas and vapour

c vapour density

V linear flow velocity of gas mixture

A area of capillary

x distance along the capillary

At steady state, k must be constant over the length of the capillary if no condensation occurs in this region; by integrating Equation 2.9,

$$c = \frac{k}{VA} + B\exp\left(\frac{V}{D}x\right) \tag{2.10}$$

where B is a constant of integration.

Assumption:

- there is no temperature or total pressure gradient along the capillary
- D is independent of concentration
- the vapour concentration is zero at the exit end of the capillary.

In order to evaluate constant B for a capillary of length λ, supposing, $c = 0$ at $x = 0$, we have,

$$c_1 = \frac{k}{VA}\left(1 - \exp\left(-\frac{V\lambda}{D}\right)\right) \tag{2.11}$$

where c_1 is the vapour density at the inlet end of the capillary

let, $$V = \frac{v}{A} \tag{2.12}$$

v is the gas flow rate in volume units and assuming the vapour behaves as an ideal gas, and

$$p_1 = \frac{c_1}{M} RT = \frac{k}{v} \frac{RT}{M} \left(1 - \exp\left(- \frac{v\lambda}{DA} \right) \right) \tag{2.13}$$

where M is the molecular weight of the vapor species. Thus, if we determine k as a function of v with a given experimental arrangement, and T and p_1 are constant, we will obtain a curve of the form shown in Figure 2.2. For moderate v, diffusion effects are negligible and

$$p_1 = \frac{k}{v} \frac{RT}{M} \tag{2.14}$$

Equation 2.14 is essentially the expression which has generally been used to interpret transpiration measurements.

At $v = 0$, only diffusion flow is observed and

$$p_1 = \frac{k}{D} \frac{\lambda}{A} \frac{RT}{M} \tag{2.15}$$

Equation 2.13 has the form shown in Figure 2.2, where k is presented as a function of v for constant p. In the straight-line portion of the curve, the amount of vapour transported is proportional to the flow rate, and the simple expression of Equation 2.8 or 2.14 can be used directly to calculate p. The diffusion contribution, which is significant at low flow rates, vanishes as the flow rate is increased.

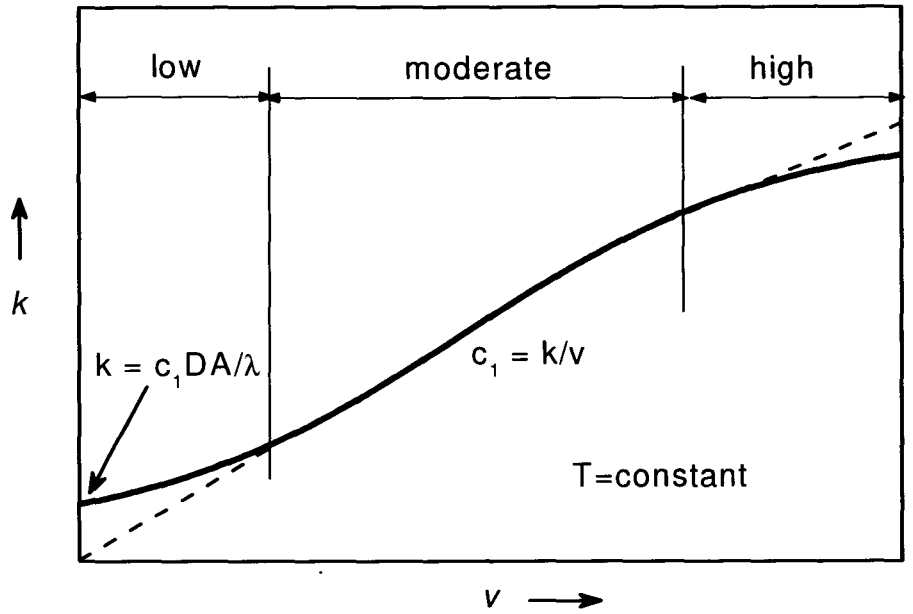

Figure 2.2 Variation of vapour transport with gas flow rate (Merten, 1959)

At higher flow rates, the measured values of k will fall below the curve in Figure 2.2 because saturation will not be achieved, and these points must be neglected in analyzing the results (Merten, 1959).

Most experiments have been conducted, targeting the moderate flow rate in Figure 2.2, where the mass flow rate of vapour is proportional to the flow rate of carrier gas. Experiments performed in this region need no correction for diffusion or kinetic effects. The flow rate range of the linear region will vary according to the experimental setup and system studied. Flow rates reported are usually in the range 1-70 mL (STP)/min. By selecting a capillary of the proper dimensions in order to minimize

diffusion effects and by selection a sufficiently large sample surface area in order to saturate the gas rapidly, one can usually design experiments so that the linear region extends a larger range of flow rate.

2.4 Niobium Oxides

2.4.1 Vapourization Reactions

The phase diagram of the Nb-O system at high temperature is shown in Figure 2.3 according to the work by Chang and Phillips (Chang and Phillips, 1969) and Naito and co-workers (Naito *et al.*, 1980). As can be seen, with oxygen, niobium forms three oxides: niobium pentoxide (Nb_2O_5), niobium dioxide (NbO_2) and niobium protoxide NbO and these three phases are relatively stable from room temperature to high temperature. However, these three types of niobium oxides behave very differently in vapourization reactions.

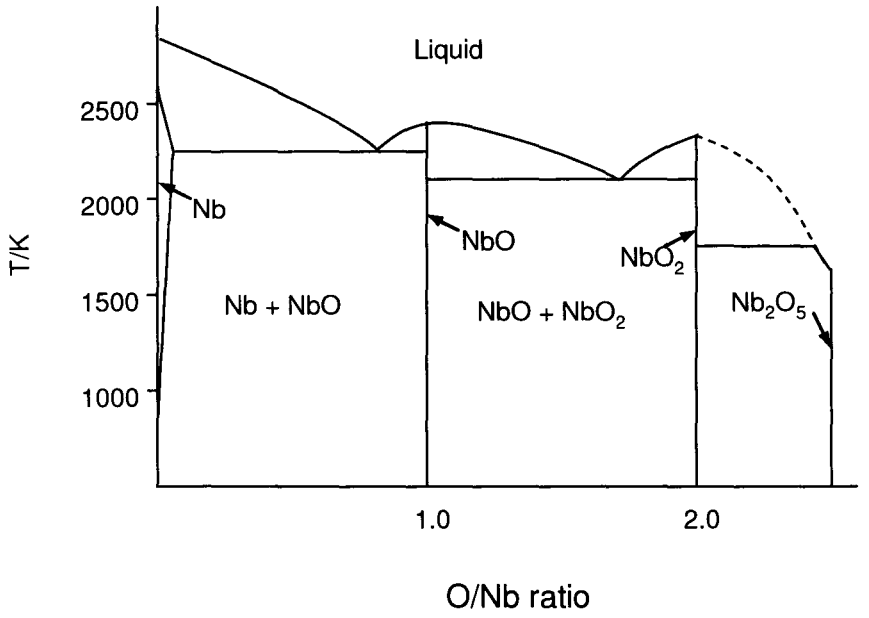

Figure 2.3 The phase diagram of the Nb-O system (Chang and Phillips, 1969).

2.4.1.1 Niobium Dioxide (NbO_2)

Shchukarev and co-workers (Shchukarev *et al.*, 1966) systematically characterized quantitatively the processes of vapourization of NbO and NbO_2. In their studies, the effusion method was employed and the volatilized products were simultaneously monitored by mass-spectrometric analysis.

In the temperature range of 1773-2473K, the vapour species being $NbO_2(g)$ and NbO(g) over NbO_2 solid phase were identified and it was suggested that $NbO_2(s)$ is a congruently vapourizing phase (Shchukarev *et al.*, 1966; Matsui and Naito, 1981). In addition, X-Ray diffraction showed that the solid phase contained only NbO_2, indicating

that the vapourization of niobium dioxide involves the processes,

$$NbO_2(solid, liqiud) \rightarrow NbO_2(gas) \quad (2.16)$$

$$NbO_2(solid, liqiud, gas) \rightarrow NbO(gas) + O(gas) \quad (2.17)$$

2.4.1.2 Niobium Monoxide (NbO)

The study by Shchukarev and co-workers (Shchukarev *et al.*, 1966) of the vapourization of NbO in the range of 1873-2473K suggested that the gaseous phase contains NbO_2 and NbO molecules. X-Ray diffraction of the residue remaining when vapourization of the niobium monoxide was complete indicated the presence of metallic niobium and NbO_2 with lattice parameters corresponding to those published by Alyamovskii and co-workers (Alyamovskii *et al.*, 1958). Thus NbO vapourizes incongruently and the vapourization involves the processes:

$$NbO(solid, liqiud) \rightarrow NbO(gas) \quad (2.18)$$

$$2NbO(solid, liqiud) \rightarrow NbO_2(gas) + Nb(solid) \quad (2.19)$$

2.4.1.3 Niobium Pentoxide (Nb_2O_5)

In the temperature range of 1432-1756K, Golubtsov and co-workers (Golubtsov *et al.*, 1960) studied the dissociation phenomenon of Nb_2O_5 in vacuum by the mass-

effusion method and suggested that the dissociation process is

$$Nb_2O_5(\text{solid}) \rightarrow 2NbO_2(\text{gas}) + 1/2O_2(\text{gas}) \qquad (2.20)$$

The results obtained by Kamegashira and co-workers (Kamegashira *et al.*, 1981) at high temperatures from 1803 to 1893 K, above the melting point of Nb_2O_5 (m.p.≈ 1769 K), indicated that Nb_2O_5 vapourizes incongruently and the residue approaches NbO_2. Semenov and Lopatin (Semenov and Lopatin, 2001) also proved that Nb_2O_5 dissociates into NbO_{2+x} when it is heated in a vacuum.

More recently, the vapourization process of NbO, NbO_2, and Nb_2O_5 in the niobium–oxygen system was investigated from the phase change of the solid residue after vapourization by Kamegashira and co-workers (Kamegashira, 1981), and it was confirmed that only the NbO_2 phase vapourizes congruently; NbO(s) is the incongruently vapourizing phase and Nb_2O_5(s) is subject to dissociation process. These observations are also supported by Matsui and Naito (Matsui and Naito, 1981; 1982; 1983), and Schulze *et al.* (Schulze *et al.*, 1988).

2.4.2 Dependence of Partial Pressure of Oxygen

As pointed out by Belton and Worrell (Belton and Worrell, 1970), for considerations of metal-oxygen systems which form condensed phases as well as metal or oxide gaseous species, the most useful type of diagram is where the logarithms of the

pressures of these species ($\log p_{Me_xO_y}$) are plotted against the logarithm of the oxygen pressure ($\log p_{O_2}$) for a chosen temperature.

Using the JANAF data (Chase, 1998), a typical predominance diagram plotted as $\log p_{NbO_x}$ vs. $\log p_{O_2}$ is shown in Figure 2.4 at 1873 K. Equilibrium oxygen pressures between the various condensed phases are shown by the vertical lines.

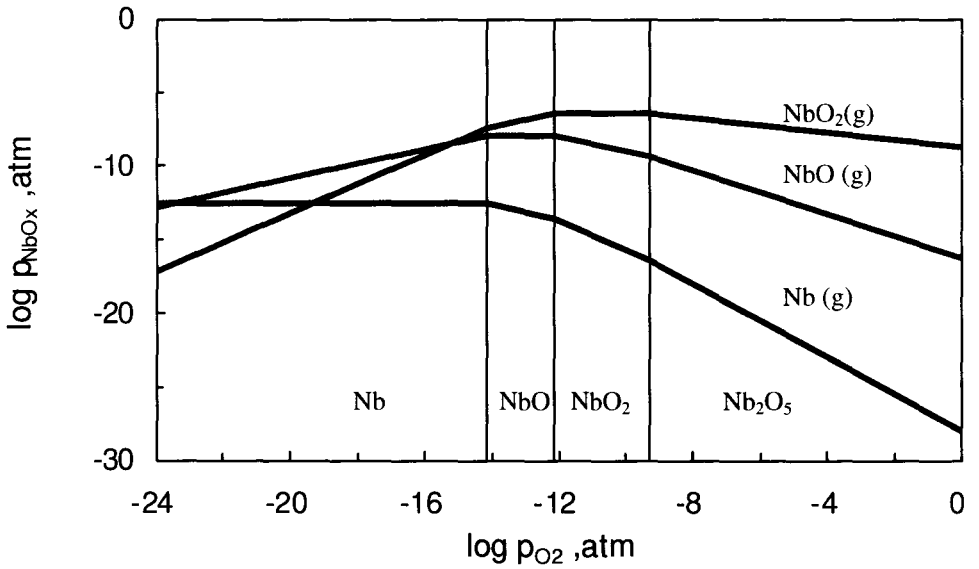

Figure 2.4 Stability diagram for the Nb-O system at 1873 K (Data from JANAF Tables, 1998)

As can be seen, oxygen pressure has several effects on the equilibrium pressures of the volatile species, depending on the chemical relation of the volatile species to the condensed phase. When the volatile species have the same composition as the condensed phase, the equilibrium pressures are independent of oxygen pressure, for instance,

$$NbO_2(s,l) = NbO_2(g) \tag{2.21}$$

However, when the volatile species have a different composition, the equilibrium pressures are a function of oxygen pressure, for example,

$$NbO_{2.5}(s,l) = NbO_2(g) + \frac{1}{4}O_2(g) \tag{2.22}$$

The pressure p_{NbO_2} for this equilibrium is given by

$$p_{NbO_2} = K_{22} \cdot \left(p_{O_2}\right)^{\frac{1}{4}} \tag{2.23}$$

where K_{22} is the equilibrium constant for Reaction 2.22.

2.4.3 Effect of Temperature on the Vapour Pressure

Kamegashira and co-workers (Kamegashira *et al.*, 1981) observed the partial pressures of NbO_2(g) and NbO(g) over NbO_2(s) and NbO_2(l), by the mass-spectrometric method, as a function of temperature shown in Figure 2.5. The equations for partial pressure gaseous species over NbO_2(s) were treated by the least squares method from two references (Kamegashira *et al.*, 1981; Shchukarev *et al.*, 1966), as listed in Table 2.1.

The partial pressures of NbO_2(g) and NbO(g) over NbO_2(s) obtained by Shchukarev and co-workers (Shchukarev *et al.*, 1966) are also shown in Figure 2.5 for

comparison. As can be seen, the partial pressures of $NbO_2(g)$ measured by Shchukarev *et al.* are considerably higher than those measured by Kamegashira *et al.* (Kamegashira *et al.*, 1981). And the partial pressures of NbO(g) by Shchukarev *et al.* are lower than the study by Kamegashira (Kamegashira *et al.*, 1981).

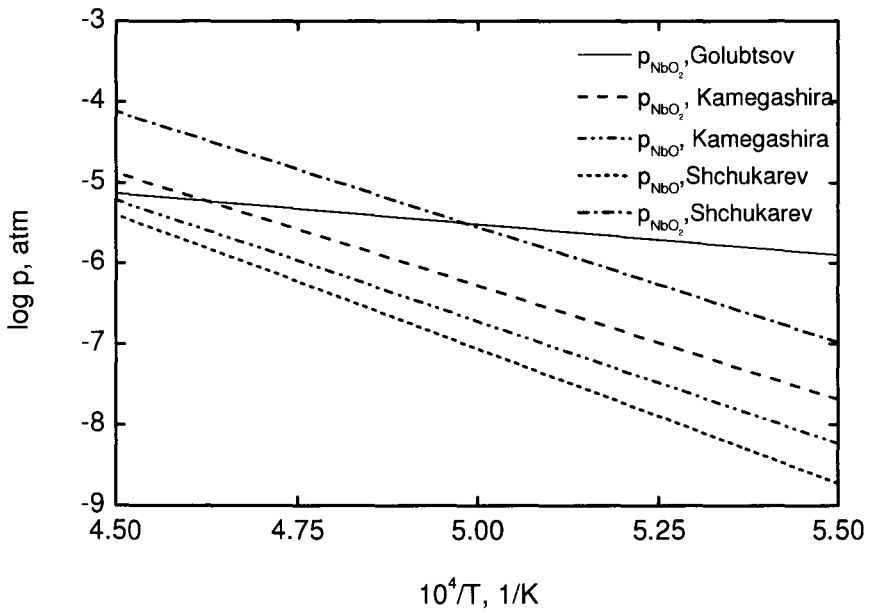

Figure 2.5 Equilibrium p_{NbO2} and p_{NbO} over $NbO_2(s)$ as a function of temperature (after Kamegashira and co-workers, 1981; Shchukarev and co-workers, 1962; Golubtsov and co-workers, 1960)

Kamegashira and co-workers believed that the vapour pressures of NbO_2 and NbO(g) measured in their investigation were reproducible on heating and cooling. X-ray analysis of the residue after vapourization indicated the existence of a single NbO_2 phase and O/Nb compositions of the residue were not changed from those of the starting sample ($O/Nb = 2.000 \pm 0.003$) within experimental error.

The sample powder used by Shchukarev *et al.*(Shchukarev *et al.*, 1966) for vapourization experiment was reported to be a single phase of NbO_2 with an O/Nb composition of 2.008. The disagreement between Kamegashira *et al.* and Shchukarev *et al.* may be mainly caused by the difference of the oxygen content of the NbO_2 samples.

Table 2.1. Equations for partial pressures of gaseous species over NbO_2(s)

Systems	$\log(P/Pa) = -(A\times10^4)/T+B$				Temperature,K	Reference
	NbO_2(g)		NbO(g)			
	A	B	A	B		
NbO_2(s)	2.913±0.049	13.29±0.23	2.945±0.085	13.04±0.41	2013-2188	Kamegashira
NbO_2(l)	2.393±0.065	10.90±0.29	2.716±0.130	12.05±0.59	2188-2323	(1981)
NbO_2(s)	2.86	13.75	3.33	14.59	1773-2173	Shchukarev
NbO_2(s)	2.38	11.52	2.82	12.24	2173-2373	(1962)

2.4.4 Remarks

Examination of Figure 2.4 shows that partial pressure of oxygen will have a significant effect on the measured vapour pressure. However, all observation on vapourization of niobium oxides were conducted by the effusion method coupled with mass spectrometry, in which the vapourization cell was installed in vacuum. It is easily discovered upon close observation of the experimental apparatus, that inside the cell, there is no oxygen partial pressure control resulting in the possible oxidation of NbO_2. Therefore, these workers used a mass spectrometer to analyze the vapour effusing from a

Knudsen cell that contained NbO_x under "oxidizing" conditions.

As in the literature (Matsui and Naito, 1981), the partial pressure of oxygen was 1.7×10^{-8}atm in the tungsten Knudsen cell. In this case, niobium dioxide will be oxidized to form niobium pentoxide through Reaction 2.24.

$$2NbO_2(s,l)+\frac{1}{2}O_2(g)=Nb_2O_5(s,l) \qquad (2.24)$$

The newly formed Nb_2O_5 layer will cover the NbO_2 condensed phase. Therefore, the NbO_2 vapour will be in equilibrium with Nb_2O_5 and will have lower pressure than with NbO_2 if NbO_2 were the stable condensed phase. From the above analysis, a conclusion can be drawn that the control of oxygen partial pressure becomes a crucial condition in vapourization studies of niobium oxides.

2.5 Thermodynamics of Slags

2.5.1 Structure Model of Silicates

The principal features of the atomic arrangement in silica were initially studied by Zachariasen (Zachariasen, 1932) and Warren (Warren, 1934) from X-ray diffraction measurements. For binary silicate systems MO-SiO_2 (M = Ca, Mg, Mn, Fe, Pb and so forth), it is generally accepted that silicate slags consist of 3-dimensional interconnected

networks of SiO_4^{4-} tetrahedra in which silicon atoms are covalently bonded to four oxygen atoms (Mysen, 1990). These SiO_4^{4-} tetrahedrons are joined together in chains or rings by bridging oxygen; whereas, in the molten state, an open structure with a cristobalite-like arrangement predominates (Nukui *et al.*, 1978), as shown in Figure 2.6.

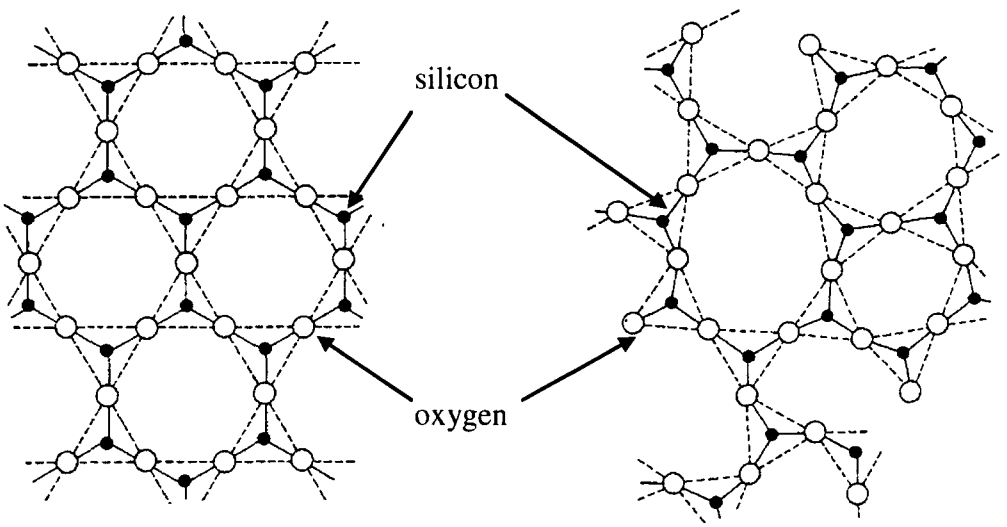

Figure 2.6 Schematic representation of the silica structure (Richardson, 1974) (a) in crystalline (b) in molten state

Many structure-based thermodynamic models of binary silicate melts over certain ranges of compositions have been proposed. Among these significant contributions, one should cite the work of Masson *et al* (Masson *et al.*, 1970; Masson, 1977), Gaskell (Gaskell, 1977), Fincham and Richardson (Fincham and Richardson, 1954), Toop and Samis (Toop and Samis, 1962), Kapoor and co-workers (Kapoor *et al.*, 1974), Niwa and

Yokokawa (Niwa and Yokokawa, 1969), Borgianni and Granati (Borgianni and Granati, 1979), and Lin and Pelton (Lin and Pelton, 1979).

For a solution very rich in the basic oxide MO, the melt consists essentially of M^{2+}, O^{2-} and SiO_4^{4-} ions (Flood and Knapp, 1963). According the model which was first introduced by Flood and Knapp (Flood and Knapp, 1963), the entropy in this composition region may be calculated by assuming a random distribution of O^{2-} and SiO_4^{4-} anions. As the concentration of SiO_2 is increased, the SiO_4^{4-} tetrahedra start to join together to form polymeric anions. Masson *et al* (Masson *et al.*, 1970) successfully modeled the MO-SiO_2 melts for SiO_2 concentrations up to about 40 mol pct SiO_2. For pure molten SiO_2, the structure consists of a three dimensional network of bridged silica tetrahedra (Masson *et al.*, 1970), thus Masson's model no longer holds.

For small additions of MO to SiO_2, Fincham and Richardson (Fincham and Richardson, 1954) proposed that the gradual addition of metallic oxides tends to break these bridging oxygen (O^0) bonds forming non-bridging oxygen (NBO), O^-, as can be seen in Figure 2.7. A simple equation can describe this reaction

$$O^o + O^{2-} = 2O^- \qquad (2.25)$$

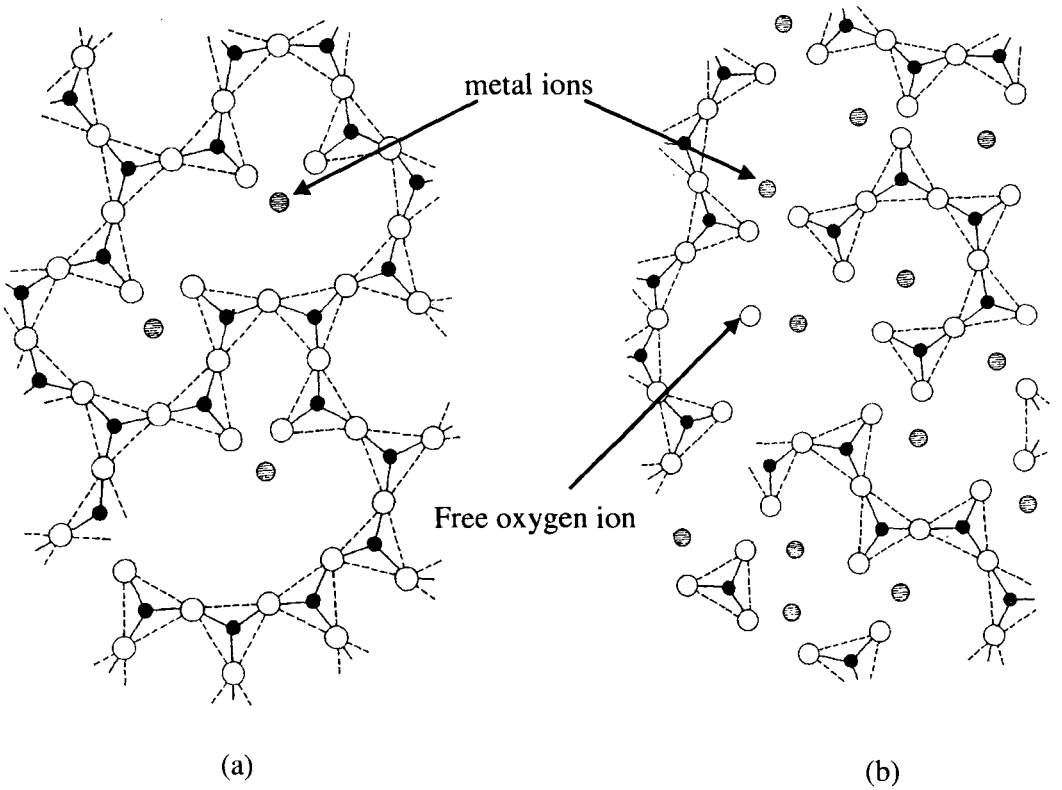

Figure 2.7 Stages in the breakdown of the lattice of molten silica brought about by the addition of a divalent metal oxides, such as CaO. The concentration of metal oxides increases from (a) to (b) (Richardson, 1974).

To apply to the entire ranges of the composition, Lin and Pelton (Lin and Pelton, 1979) introduced a model for MO-SiO_2 melts in which only simple structural units (silica tetrahedra, O^{2-} ions and oxygen bridges) are distributed and polyanions are not considered a priori. However, once the distribution of the simple structural units has been made, the chain length distribution of the polymeric anions can be calculated a posteriori (Lin and Pelton, 1979). Lin and Pelton's model is highly significant that it permits a posterior calculation of the ionic constitution by an approach which avoids the limitations

of classical polymer theory, and in so doing, provides the means for determining the composition at which the formation of ring ions becomes important (Gaskell, 1981).

2.5.2 Acidic and Basic Melts

In the liquid state some oxides have a weaker tendency to form free O^{2-} ions whereas others are clearly ionic in behaviour. The former oxides are usually called "acid" whereas the latter ones with free O^{2-} ions are called "basic" (Hallstedt *et al.*, 1994). The division between acidic and basic melts is usually taken as the composition at which just sufficient oxygen ions are donated by the cations to satisfy all the oxygen-ion bonds of the acidic polymers (Bodsworth and Bell, 1972).

In the liquid state, acidic oxides are acceptors of oxygen ions, O^{2-}; the oxides, such as SiO_2, P_2O_5, have a weaker tendency to form free oxygen ions but form anion complexes in molten slags (network formers).

Whereas basic oxide which are clearly ionic with free O^{2-} are donors of oxygen ions. The oxides, for instance, CaO, MgO, MnO, FeO and so forth, which break down the anion complexes in the melt are known as network modifiers and are cataloged to be basic oxides (Bodsworth and Bell, 1972).

Neutral oxides, such as Al_2O_3 and Cr_2O_3 are defined as amphoteric oxides, which can be either basic or acidic depending on the oxide present. In the case of Al_2O_3, three

reactions may take place as shown in Equation 2.26 to 2.28:

$$Al_2O_3 = 2Al^{3+} + 3O^{2-} \quad (2.26)$$

$$Al_2O_3 + 5O^{2-} = 2AlO_4^{5-} \quad (2.27)$$

$$Al^{3+} + 4O^{2-} = AlO_4^{5-} \quad (2.28)$$

As can be seen in Equations 2.30 and 2.31, Al^{3+} is stable in acidic oxides whereas AlO_4^{5-} is stable in basic oxide melts (Sano *et al.*, 2001).

In alkaline silicate melts containing alumina, when the molar ratio of Al_2O_3/MO (MO is a basic oxide) is less than unity, Al-O coordination would be tetrahedral (Doweidar, 1998); when this ratio exceeds 1.0, Al^{3+} ions would have octahedral coordination with oxygen and enter interstices in the structure (Doweidar, 1998). These structural changes in aluminosilicate melts could affect their physical properties (Turkdogan and Bills, 1960). Further investigation (Park *et.al.*, 2004) indicates that Al_2O_3 behaves as an amphoteric oxide as a function of composition in CaO-SiO_2-Al_2O_3 slag system. That is, the alumina behaves as network former up to about 10 mass pct Al_2O_3, while it acts as a network modifier, in compositions greater than 10 mass pct Al_2O_3.

2.5.3 Slag Basicity

Over the years, many empirical expressions of slag basicity have been proposed and a number of these have been useful from an operating point of view. Slag basicity can be divided by two approaches.

The first approach, the ratio of the basic to acidic oxides has been helpful to the plant metallurgist. In simple slags where lime and silica are the major constituent oxides, the basicity is usually defined by the concentration ratio, $\%CaO/\%SiO_2$, which is called the "v" ratio (Turkdogan, 1984).

However the simple $\%CaO/\%SiO_2$ ratio ignores the effects of other oxides. For instance, the ratio $(CaO+MgO)/(Al_2O_3+SiO_2)$ implies that lime and magnesia behave as equivalent basic oxides and that alumina and silica have the same degree of acidity, neither of which is the case (McLean *et al.*, 2001). Therefore, in practice, this approach can lead to some conflicting conclusions.

The other approach is the introduction of activity of free oxygen ion, $a_{O^{2-}}$, in the slag melts by Toops and Samis (Toops and Samis, 1962). The introduction of $a_{O^{2-}}$ progressed the understanding of the reactivity of the slag especially from the view of the ionic theory in metallurgical slags, for example, sulfide capacity and phosphate capacity (Toop and Samis, 1962). However, single ion activities such as $a_{O^{2-}}$ can not be defined thermodynamically and can not be measured (Sano and Tsukihashi, 2001). Thus several methods for the estimation of $a_{O^{2-}}$ have been proposed.

One such estimation which evaluates the electron donor power of a slag, was achieved by Duffy and Ingram (Duffy and Ingram, 1976). They realized that when "probe" ions such as Pb^{2+} were added to glasses the shifts in frequency of the absorption

band involved with the 6s→6p transition observed in the UV region of the spectrum can be related to the basicity of a glass or slag. By making numerous measurements, they found out that the "optical basicity" of an oxide AO, Λ_{AO}, is related to the Pauling electronegativity, χ, of the cation by the following equation:

$$\Lambda_{AO} = \frac{0.74}{\chi - 0.26} \tag{2.29}$$

Therefore, it is possible to calculate the optical basicity, Λ, for metallurgical slags of any composition involving these oxides.

$$\Lambda = X_{AO}\Lambda_{AO} + X_{BO}\Lambda_{BO} + \cdots \tag{2.30}$$

where, Λ is the optical basicity of the slag and Λ_{AO} is the optical basicity value of one component , X is the equivalent cation fraction that can be obtained by

$$X = \frac{\text{mole fraction of component} \times \text{Number of oxygen atoms in oxide molecule}}{\sum(\text{mole fraction of component} \times \text{Number of oxygen atoms in oxide molecule})} \tag{2.31}$$

Thereafter the concept of the optical basicity was introduced and applied to metallurgy by Duffy and co-workers (Duffy *et al.*, 1978). In this approach, the optical basicities of a slag is considered to estimate $a_{O^{2-}}$ or more correctly the chemical potential of the O^{2-} ion. However, the measurements of optical basicities in metallurgical slags are not easy even in the glassy state (Duffy and Ingram, 1976).

2.5.4 The Regular Solution Model and Its Application to Metallurgical Slags

The application of mathematical models for representing some of the thermodynamic properties of slags has gone through many stages of empirical and theoretical development, and the search for a better model is ongoing. From the practical point of view, the regular solution model appears most appealing for empirical formulation of the composition dependence of the activity of oxides in complex and metallurgical slags (Jiang *et al.*, 1993).

2.5.4.1 Understanding the Regular Solution Model

A solution is said to be regular, by definition, when the entropy of mixing is equal to the ideal configurational entropy, and the enthalpy of mixing varies with composition (Hildebrand, 1929) represented by Equation 2.32 for a ternary system composed of n_1, n_2 and n_3 moles of components 1, 2 and 3 per unit volume of solution:

$$\Delta H = \frac{\alpha_{12} n_1 n_2 + \alpha_{13} n_1 n_3 + \alpha_{23} n_2 n_3}{n_1 + n_2 + n_3} \tag{2.32}$$

where the coefficients $\alpha_{12}, \alpha_{13}, \alpha_{23}$ are constants for the binary systems 1-2, 1-3 and 2-3 at constant temperature and pressure. Partial differentiation with respect to n_1 for constant n_2 and n_3 gives,

$$\left(\frac{\partial H}{\partial n_1}\right)_{n2,n3} = \frac{-\alpha_{23}n_2n_3 + (n_2+n_3)(\alpha_{12}n_2+\alpha_{13}n_3)}{(n_1+n_2+n_3)^2} \tag{2.33}$$

Since the entropy of mixing is assumed to be ideal, Equation 2.33 gives the partial molar excess Gibbs energy of solution of the components 1, 2 and 3. Substitution of n_i by mole fraction $x_i = \frac{n_i}{n_1+n_2+n_3}$ gives,

$$RT\ln\gamma_1 = \alpha_{12}x_2^2 + \alpha_{13}x_3^2 + (\alpha_{12}+\alpha_{13}-\alpha_{23})x_2x_3 \tag{2.34}$$

$$RT\ln\gamma_2 = \alpha_{12}x_1^2 + \alpha_{23}x_3^2 + (\alpha_{12}+\alpha_{23}-\alpha_{13})x_1x_3 \tag{2.35}$$

$$RT\ln\gamma_3 = \alpha_{13}x_1^2 + \alpha_{23}x_2^2 + (\alpha_{13}+\alpha_{23}-\alpha_{12})x_1x_2 \tag{2.36}$$

where the activity coefficients γ_i are relative to the pure liquid components. Correspondingly, for a multicomponent system, the general form of the equation for the regular solution model (Lumsden, 1961) is given by

$$RT\ln\gamma_i(\mathrm{RS}) = \sum_j \alpha_{ij}x_j^2 + \sum_j\sum_k (\alpha_{ij}+\alpha_{ik}-\alpha_{jk})x_jx_k \tag{2.37}$$

here, $i \neq j$ or k, and $k > j$, $\alpha_{ij} = \alpha_{ji}$, $\alpha_{ii} = \alpha_{jj} = \alpha_{kk} = 0$. If the melts are not strictly regular solution, Equation 2.41 can be modified (Ban-Ya, 1993) as given in Equation 2.38

$$RT \ln \gamma_i(\text{real solution}) = RT \ln \gamma_i(\text{RS}) + I' \qquad (2.38)$$

where I' is the conversion factor , associated with the conversion from a theoretical Regular Solution (RS) standard state to the conventional standard states (e.g. pure solid or liquid) (Ban-Ya, 1993).

2.5.4.2 Application of Regular Solution Model

In 1961, Lumsden (Lumsden, 1961) was first to apply the regular solution model (RSM) to polymeric melts showing a good representation of the activity data for the PbO-B_2O_3 and FeO-Fe_2O_3-SiO_2 melts. Nowadays, the greatest contribution to the use of regular solution model in slag has been by Ban-Ya and his co-workers. Particularly, many α_{ij} parameters were calculated by Ban-Ya.

Application of the regular solution model to polymeric melts implies that cations, such as Cu^+, Ca^{2+}, Fe^{3+} and Si^{4+} are almost randomly distributed within a three-dimensional matrix of oxygen anions (O^{2-}) (Lumsden, 1961). In the melts with regular solution behaviour, the molecular/ionic species, such as SiO_2 or SiO_4^{4-} were taken as "dissociated" ionic species consisting of Si^{4+} cations and O^{2-} anions. The composition is given in terms of atom fractions of cations; accordingly, the melt is considered to be composed of oxides in the form of $CuO_{0.5}$, CaO, $FeO_{1.5}$, SiO_2.

Prior to applying the regular solution model for silicate melts, two parameters

need to be known, namely:

(1) the value of the interaction energy (α_{ij})

(2) the conversion factor (I').

The determination of the regular solution binary interaction energies has been primarily illustrated by Lumsden for calculating the activities of components in simple melts. Since then, a number of investigators (i.e., Richards and Thorne 1961; Fujita and Maruhashi, 1970; Nagabayashi *et.al.*, 1989) have examined the applicability of the RSM to various slags systems. However, there are inconsistencies between the apparent binary interaction energies (α_{ij}) obtained by different groups of workers.

These inconsistencies are largely due to the differences in the selected thermochemisty data as well as the choice of activity composition data, thus making the interaction energies not readily transferable from one system to another.

During the initial work on the evaluation of the RSM and determination of the model parameters, it became apparent that not only the selection of the thermodynamic data, but also the method employed for determination of the binary interaction energies could influence the results. In particular, the use of multiple linear regression analysis as a quick and convenient method of determining the model parameters had to be ruled out (Jahanshahi and Wright, 1992). Ban-Ya and co-workers used a graphical method to

verify regular solution behaviour as well as optimizing for the "best" values of the binary interaction energies. This graphical method showed advantages in its ability to indicate subtle differences between sets of data for a complex slag system and present the possible source of errors in the data sets (Ban-Ya, 1993).

The use of conversion factor for converting the calculated activity coefficients from a theoretical regular solution standard state to the conventional standard states has been practiced by some of investigators. The conversion factors were determined by Jahanshahi and Wright (Jahanshahi and Wright, 1992) using the selected thermochemical data and the activity-composition data from the database, in conjunction with some of the published phase diagrams. It was also found that slag melts containing strongly electronegative cations such as Si^{4+} is likely to be responsible for the considerable differences in the temperature dependent term of the conversion factor for SiO_2 (Jahanshahi and Wright, 1992).

2.6 Niobium in Slags

2.6.1 Redox Equilibria of Niobium in Silicate Melts

Many investigations of redox systems with respect to steelmaking have focused on Fe^{3+}/Fe^{2+} ratios in slags which are in equilibrium with metallic iron or with a gas phase (Jahanshahi and Wright, 1993). However, such data are scarce on other redox

system in slags. Particularly, redox equilibria of niobium in silicate melts has been rarely studied. One work known to the author is the systematic study by Schwerdtfeger and his colleagues (Schwerdtfeger *et al.*, 2000). In their study, slag melts containing small content of NbO_x in the $CaO\text{-}SiO_2\text{-}NbO_x$ systems has been investigated at 1600°C with controlled oxygen pressure and their results are summarized in Figure 2.8.

Similar to other transition metals, niobium can be present in silicate melts in different valence states in certain ranges of oxygen pressure. The oxidation-reduction equilibria of niobium oxides in solution in molten silicate would be expected from the stoichiometry of the reaction

$$Nb^{4+} + \frac{1}{4}O_2 = Nb^{5+} + \frac{1}{2}O^{2-} \tag{2.39}$$

Thus, the Nb^{5+}/Nb^{4+} ratio can be presented as in Equation 2.40

$$\frac{Nb^{5+}}{Nb^{4+}} = \frac{\gamma_{Nb^{4+}}}{\gamma_{Nb^{5+}}\left(a_{O^{2-}}\right)^{1/2}}\left(p_{O_2}\right)^{\frac{1}{4}} \tag{2.40}$$

If $K' = \frac{\gamma_{Nb^{4+}}}{\gamma_{Nb^{5+}}\left(a_{O^{2-}}\right)^{1/2}}$, Equation 2.40 can be rewritten as,

$$\frac{Nb^{5+}}{Nb^{4+}} = K'\left(p_{O_2}\right)^{\frac{1}{4}} \tag{2.41}$$

where the factor K' contains the activity coefficients of the niobium ions and the activity of oxygen anion. However, if the niobium content in the melt is sufficiently low, it can be expected that activity coefficients of the niobium ions and the activity of the oxygen anion approach to constant values, at given contents of the other components, so that K' becomes a constant (Schewerdrfeger, 1990), but K' depends on the contents of the majority components of the melts. Hence, plot of $\log\left(\frac{Nb^{5+}}{Nb^{4+}}\right)$ against $\log p_{O_2}$ should result in a straight line with a slope of $\frac{1}{4}$. The dependence of Nb^{5+}/Nb^{4+} ratios on $\left(p_{O_2}\right)^{\frac{1}{4}}$ is fulfilled within the scatter of the data as shown in Figure 2.8.

Schwerdtfeger also stated that the Nb^{5+}/Nb^{4+} ratio has dependence of slag basicity defined as CaO/SiO_2 ratio. Specifically, there is an increase of Nb^{5+}/Nb^{4+} ratio with slag basicity that is, the higher valence state of niobium is stabilized. This effect can be explained, by assuming that one or both metal species form complexes with oxygen anions. The oxidation reaction of Nb^{4+} to Nb^{5+} can be written as

$$Nb^{4+} + \frac{1}{4}O_2 + \frac{7}{2}O^{2-} = NbO_4^{3-} \tag{2.42}$$

$$\frac{NbO_4^{3-}}{Nb^{4+}} = \frac{\gamma_{Nb^{4+}}}{\gamma_{NbO_4^{3-}}}\left(a_{O^{2-}}\right)^{\frac{7}{2}}\left(p_{O_2}\right)^{\frac{1}{4}} \tag{2.43}$$

Or
$$NbO_3^{2-} + \frac{1}{4}O_2 + \frac{1}{2}O^{2-} = NbO_4^{3-} \tag{2.44}$$

$$\frac{NbO_4^{3-}}{NbO_3^{2-}} = \frac{\gamma_{NbO_3^{2-}}}{\gamma_{NbO_4^{3-}}}\left(a_{O^{2-}}\right)^{\frac{1}{2}}\left(p_{O_2}\right)^{\frac{1}{4}} \tag{2.45}$$

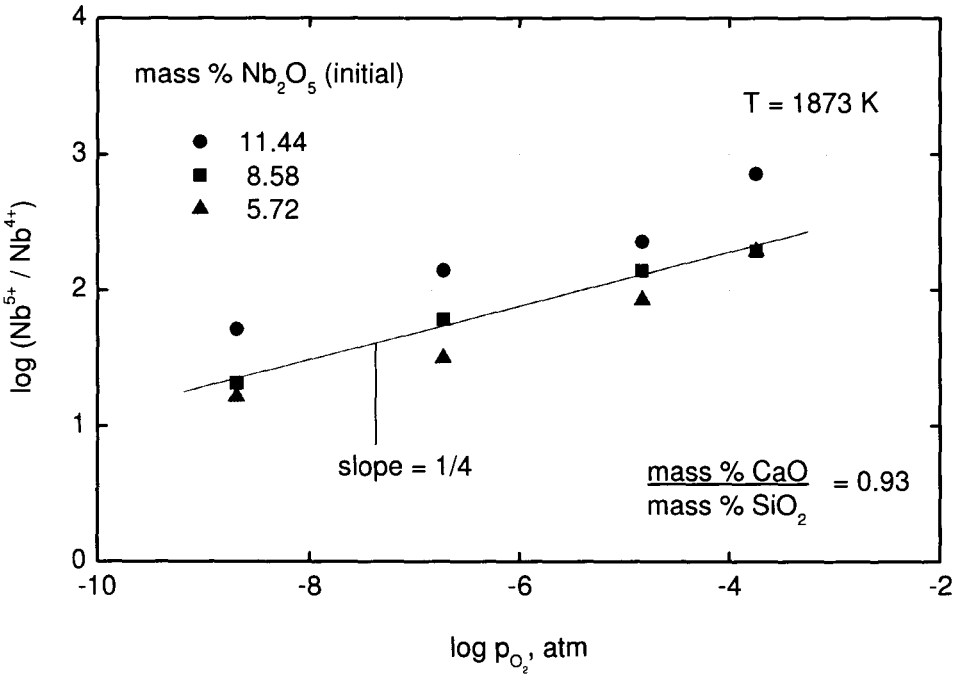

Figure 2.8 Redox equilibrium of niobium in $CaO\text{-}SiO_2$ base melts with fixed CaO/SiO_2 ratio and three difference initial Nb_2O_5 contents (Schwerdtfeger *et al.*, 2000)

According to Equations 2.43 and 2.45, the ratio Nb^{5+}/Nb^{4+} depends in the same manner on oxygen pressure as in Equation 2.41. Although the oxygen anion activity $a_{O^{2-}}$ cannot be determined, increasing the CaO/SiO_2 ratio causes an increase of $a_{O^{2-}}$ due

to the depolymerization of the silicate anions and the ratio Nb^{5+}/Nb^{4+} varies proportionally with $\left(a_{O^{2-}}\right)^{\frac{7}{2}}$ and $\left(a_{O^{2-}}\right)^{\frac{1}{2}}$ respectively.

2.6.2 Partitioning of Niobium between Slag Melts and Carbon Saturated Iron

Sato and co-workers (Sato *et al.*, 1987), Inoue and Suito (Inoue and Suito, 1983) studied the reaction of niobium in slag. Whereas, Tsukihashi (Tsukihashi *et al.*, 1988) investigated in detail the effect of Na_2O additions to the $CaO\text{-}CaF_2\text{-}SiO_2$ system on the partitioning of niobium between this slag melts and molten carbon saturated iron at 1300°C.

Tsukihashi and co-workers (Tsukihashi *et al.*, 1988) found that niobium was shown to exist mainly as Nb^{5+} in the $CaO\text{-}Na_2O\text{-}CaF_2\text{-}SiO_2$ system, equilibrated with carbon-saturated iron containing a certain content of niobium in a graphite crucible under a CO atmosphere. The partition values of niobium ((wt%Nb)/[wt%Nb])increase with increasing Na_2O content in $CaO\text{-}CaF_2\text{-}SiO_2$ melts, from 6 to 100 when about 2% Na_2O was added to the slag, as shown in Figure 2.9.

For niobium partitioning, the following reactions are assumed (Tsukihashi *et al.*, 1988)

$$Nb(l) + \tfrac{5}{2}CO(g) = NbO_{2.5}(l) + \tfrac{5}{2}C(s) \qquad (2.46)$$

$$Nb(l) + 2CO(g) = NbO_2(l) + 2C(s) \quad (2.47)$$

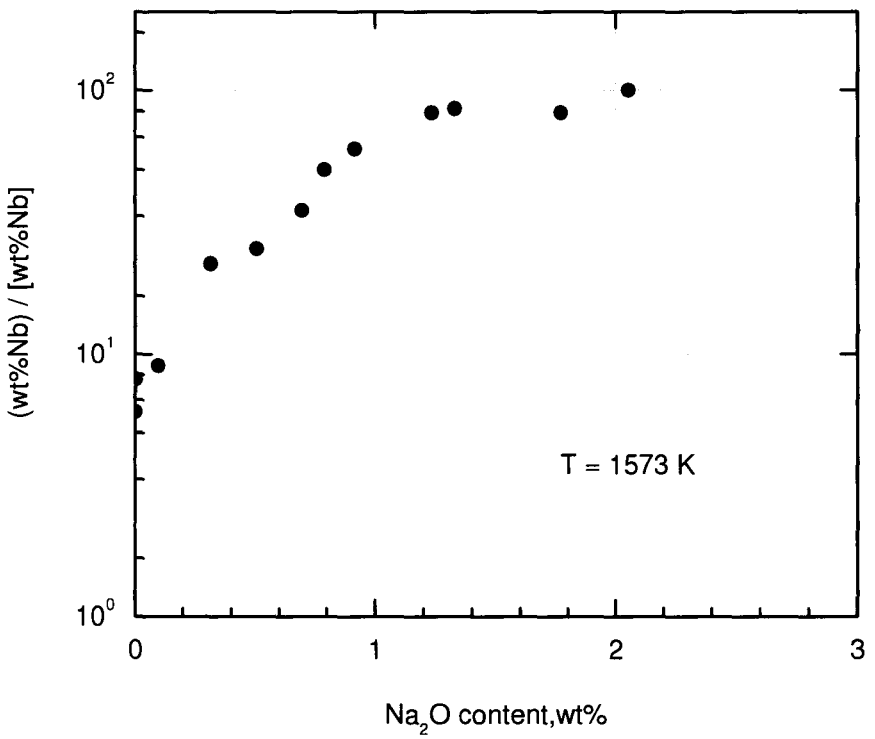

Figure 2.9 Effect of Na_2O to CaO-CaF_2-SiO_2 melts doubly saturated with CaO and $3CaO.SiO_2$ on partition ratios of niobium at 1300°C (Tsukihashi *et al.*, 1988)

The activity coefficient of niobium in carbon saturated iron was taken as 7.73×10^{-3} at 1300°C for this calculation. Mole fractions of $NbO_{2.5}$ and NbO_2 were obtained from the measured ratios of Nb^{5+}/Nb^{4+} and the total content of niobium in slag. As shown in Figure 2.10, the calculated activity coefficients of $NbO_{2.5}$ and NbO_2 decrease with increasing Na_2O content, indicating that NbO_2 and $NbO_{2.5}$ behave as acidic oxides in CaO-Na_2O-CaF_2-SiO_2 melts as concluded by Tsukihashi *et al.*.

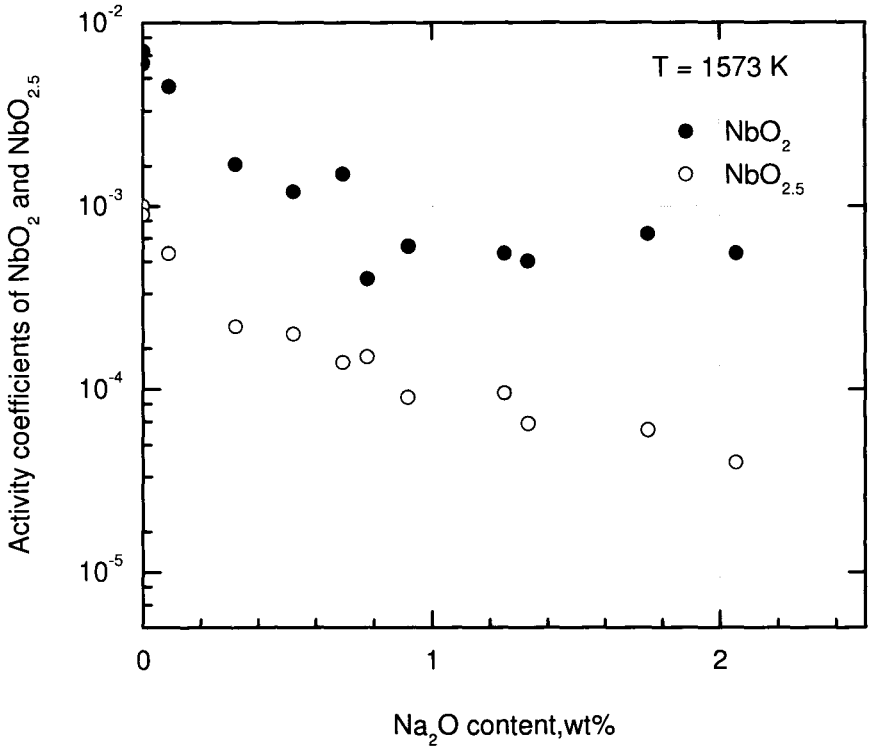

Figure 2.10. The activity coefficients of NbO_2 and $NbO_{2.5}$ for the CaO-Na_2O-CaF_2-SiO_2-NbO_x system doubly saturated with CaO and $3CaO.SiO_2$ at 1300°C (Tsukihashi *et al.*, 1988).

Niobium partitioning behaviour was also investigated by Chen and co-workers (Chen *et al.*, 1989) due to hot metal produced in China containing niobium. The equilibrium of niobium between slag and molten iron at 1600°C was studied for the direct alloying of steel with Nb_2O_5 bearing slag.

As shown in Figures 2.11-2.13, niobium partition between liquid iron and Nb_2O_5-bearing slag is influenced by slag basicity, oxygen activity and total FeO content. The partition ratio decreases with the increase of silicon content in the molten iron. With

silicon content remaining constant, the partitioning ratio $(Nb_2O_5)/[Nb]$ decreases with the increase of slag basicity (CaO/SiO_2), as shown in Figure 2.11.

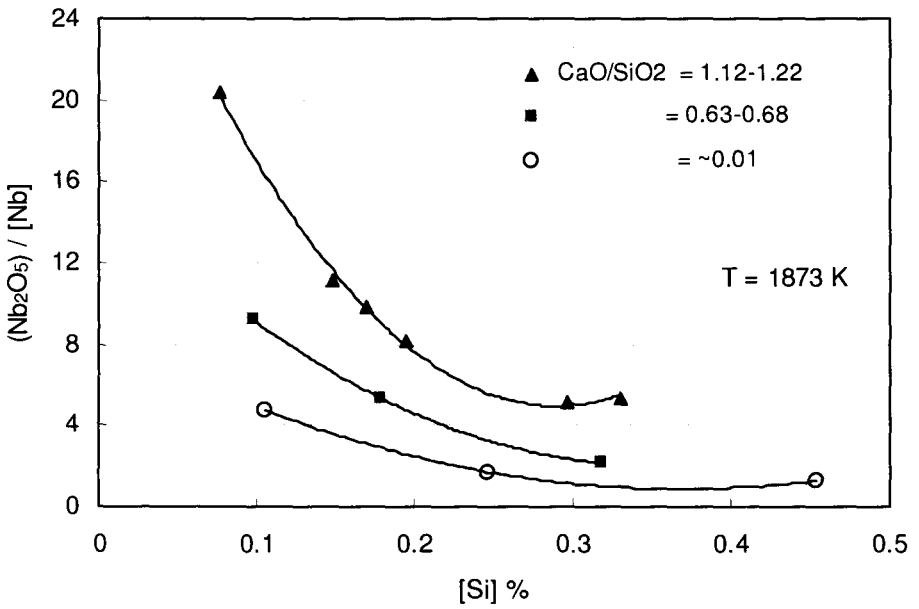

Figure 2.11 Relation between $(Nb_2O_5)/[Nb]$ and [%Si] at different ratio of CaO/SiO_2 at 1873K (Chen *et al.*, 1989)

Figures 2.12 and 2.13 show that the partitioning ratio of niobium increases when oxygen activity ($a_{[O]}$) or total FeO content increases. This indicates that lower $a_{[O]}$ and total FeO content are favorable to niobium oxide in slag reduced into molten iron.

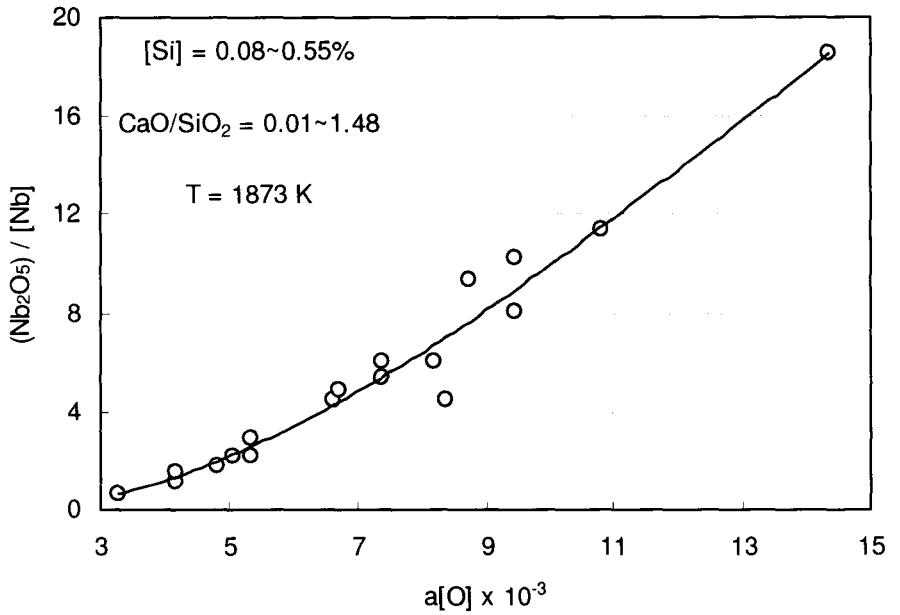

Figure 2.12 Relation between Nb_2O_5/[Nb] and a[O] at 1873K (Chen *et.al.*, 1989)

From these experimental results, it is clear that slag basicity, oxygen potential and total FeO content have a significant influence on the niobium partition ratio between slag and molten iron. However, from the insight of the experimental control, it was found that those experiments were conducted by argon protective gas and a solid electrolyte oxygen cell was used for measuring the oxygen potential in molten iron. While the oxygen potential was studied in the range from 3×10^{-3} to 14×10^{-3} at 1600 °C, the oxygen partial pressure in this system can easily be calculated according to the data given in the literature (Rao, 1985),

$$O_2 = 2[O] \qquad \Delta G^0 = -274235 + 15.57T(J/mol) \qquad (2.50)$$

Hence, the partial pressure of oxygen will be about 1.8×10^{-11} atm at 1600°C. In this circumstance, Nb_2O_5 will be equilibrium with NbO_2, which needs to be taken into account for the partitioning behaviour. Therefore, a more detailed atmosphere control and valence state of niobium in the slag needs to be analyzed.

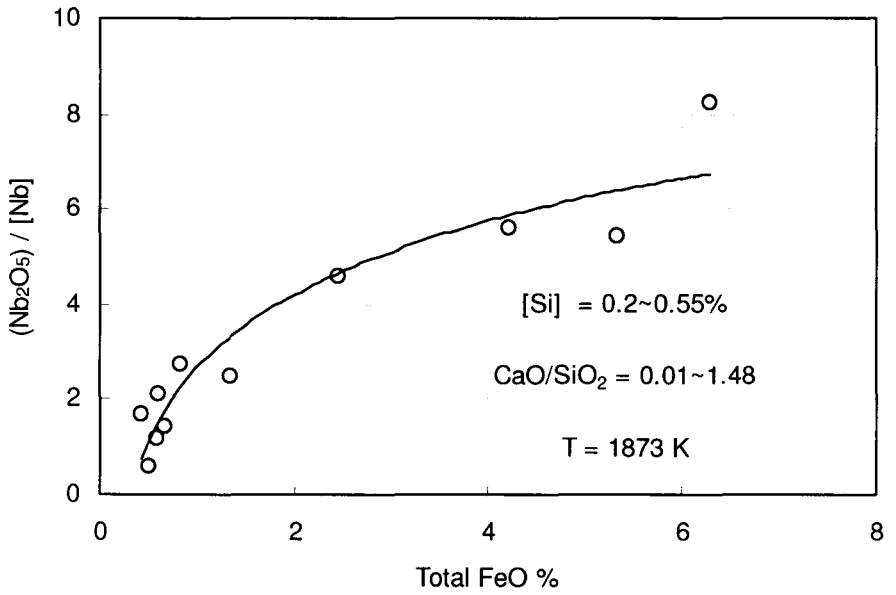

Figure 2.13 Relation between $(Nb_2O_5)/[Nb]$ and total FeO at 1873K (Chen *et.al.*, 1989).

2.7 Summary

The vapour pressure method is the most popular method for obtaining thermodynamic properties of a substance. Among the various method of vapour pressure measurements, the transpiration method has proved the most versatile method and is excellent in measuring low vapour pressure and heterogeneous reactions. Hence, the

transpiration method will be employed in all experiments.

Although the vapour pressures over pure NbO_2 and NbO have been measured by means of the effusion method combined with the mass spectrometric method, these results showed a disagreement even though the same methods have been employed. In the meantime, the dissociation vapour pressure of Nb_2O_5 was measured only in the range of a solid state and the effect of oxygen partial pressure on the vapourization of niobium oxides has not been studied. Vapourization studies of niobium oxide from steelmaking slags have not yet been undertaken.

All previous work, although useful, did little to resolve the effect of melt composition on the activity coefficient of NbO_x in silicate melts. The reason for this lack of progress can largely be attributed to the use of complex melt compositions in which the effects of chemical composition have been difficult to quantify because of their dependence on changing compositional variables. The present study is specifically concerned with determining the activity-composition relations of NbO_x in the simple $CaO\text{-}SiO_2\text{-}NbO_x$ and $CaO\text{-}SiO_2\text{-}Al_2O_3\text{-}NbO_x$ systems.

In the present study, activities of NbO_2 and $NbO_{2.5}$ were determined with the transpiration method covering the isothermal liquidus section in the $CaO\text{-}SiO_2\text{-}NbO_x$ quasi-ternary system at 1600°C, and the effects of slag basicity, Al_2O_3 addition were investigated at 1600°C. Furthermore, the oxidation state of niobium in the slags was evaluated according to the results of chemical analysis.

Professor Julian Szekely in his 1987 Extractive Metallurgy Lecture, he emphasized the fact that "Both process optimization and process control require a quantitative representation of the process", he also stressed the concept that "Calculations and measurements are not alternatives, but most often must be pursed in a complementary fashion." With an attempt to optimize the metallurgical processes, studies on the vapourization of niobium in slags are of interest to the metallurgist because they provide fundamental data and the mechanisms of niobium losses in ladle slags and the RH degasser. Knowledge of the activity coefficient of niobium and its variation with composition in a melt can be used to determine the equilibrium solubility of niobium and its distribution between various phases in the melt.

Chapter 3 Experimental Details

Experimental apparatus, general experimental procedures and subsequent chemical analysis are presented in this chapter. Section 1 describes the materials preparation and carrier gases purification; the design and construction of the apparatus which is used in the application of the transpiration method explained in section 2. The general experimental procedures for measuring vapour pressure of niobium oxide are illustrated in section 3 along with the analytical methods. In addition to the drift correction of ICP, the calibration work, both in temperature and mass flow controller, the measurements precision are assured and presented in detail in this chapter.

3.1 Materials Processing

3.1.1 Premelting of Slag Samples

The starting materials for preparing the master slag samples were calcium oxide (CaO), silica (SiO_2), niobium pentoxide (Nb_2O_5) and alumina (Al_2O_3) all being of analytical reagent grade quality. These materials where properties are listed in Table 3.1 were dried at 510°C overnight, and cooled in a desiccator. These oxides were weighed and carefully transferred to a mill, in which the oxides were fully mixed and ground.

About 15 grams of oxide mixture was melted in a platinum crucible at a

temperature above the liquidus and then allowed to quench in air. This premelting process was repeated to ensure slag homogeneity. These slags were subsequently ground and were subsampled for use in vapourization experiments and multiple samples were taken for chemical analysis by inductively coupled plasma (ICP).

Table 3.1 Properties of Starting Materials

Oxide	Purity, %	Density, kg/m^3	Melting Point, °C	Formular weight	Supplier
CaO	99.95	3250-3380	2572	56.08	Alfa Aesar
SiO_2	99.995	2200-2600	1710	60.09	Alfa Aesar
Nb_2O_5	99.95	4600	1520	265.81	Alfa Aesar
Al_2O_3	99.9	3965	2045	101.96	Alfa Aesar

In the vapourization study on niobium pentoxide, those experiments involve a strict procedure of sample preparation because the vapour pressure measurement is based on the weight loss of the sample, transported by the carrier gas. Care has been taken not to introduce any impurities whilst handing the sample. All samples removed from the furnace were placed in a desiccator before weighing. Initially, the Nb_2O_5 powder (99.95% purity, Alfa Aesar) was pressed into a pellet of 6 mm in diameter and heated in air at 1173 K for about 24 hours to ensure the composition to be stoichiometric.

3.1.2 Carrier gases and Oxygen Partial Pressure Control

As stated in Chapter 2, the control of oxygen partial pressure becomes crucial in

the vapourization study of niobium oxide, either in slag melts or in the pure state. In this experimental work, the role of the CO_2 and CO gas mixture is twofold: one is that the partial pressure of oxygen is assured by admitting a mixture of CO_2/CO to the reaction zone; the other is that this gas mixture serves as a carrier gas to remove the vapour from the saturation chamber.

The mixing ratio of CO_2 and CO gases was determined by measuring the flow rates of each gas with a calibrated mass flow controller. The oxygen partial pressures were calculated from the mixing ratio and the temperature using the JANAF thermodynamic tables.

Considering the reaction between CO_2 and CO at equilibrium, the oxygen partial pressures were calculated from the mixing ratio and the temperature as follows,

$$CO + \frac{1}{2}O_2 = CO_2 \tag{3.1}$$

where $$\Delta G^0 = -281765 + 85.815T \tag{3.2}$$

therefore, $$p_{O_2} = \left(\frac{p_{CO_2}}{p_{CO}}\right)^2 \cdot \exp\left(\frac{2\Delta G^0}{RT}\right) \tag{3.3}$$

In an experimental run, it was required that the CO_2/CO ratio in the carrier gas be low enough that a measurable weight loss be obtained in a certain time and be high

enough that the change in composition of the melt, due to removal of NbO_2, be insignificant. It was determined that these conditions were met with gas mixtures of $0.02 < CO_2/CO < 8.0$ at 1873K. Correspondingly, the partial pressure of oxygen would be controlled in the range of 10^{-10} to 10^{-5} atm, which is prevailing in refining operations.

3.1.3 Purification of Gases

Initially, the high-purity CO_2-CO gas (supplied by Air Liquide) was passed through silica gel and drierite (anhydrous calcium sulfate) to eliminate moisture. However, drierite is known to adsorb CO_2 gas and it required in excess of an hour to obtain saturation. Calcium chloride proved to be a superior material for the removal of moisture from the gas mixture and subsequently stable flow rates were assured.

In addition to eliminating moisture, traces of CO_2 were removed from CO by passing the gas through Ascarite (sodium hydroxide). The protection and coolant gas, argon (UHP grade) was purified by passing it through silica gel and drierite (anhydrous calcium sulfate) to eliminate any moisture. In addition, Ar was deoxidized by passing it through copper turnings heated at 873K. The purification procedure is illustrated in Figure 3.1. The individual gas flow rates were controlled using calibrated mass flow controllers and the gaseous composition was monitored by a gas chromatograph at the gas inlet.

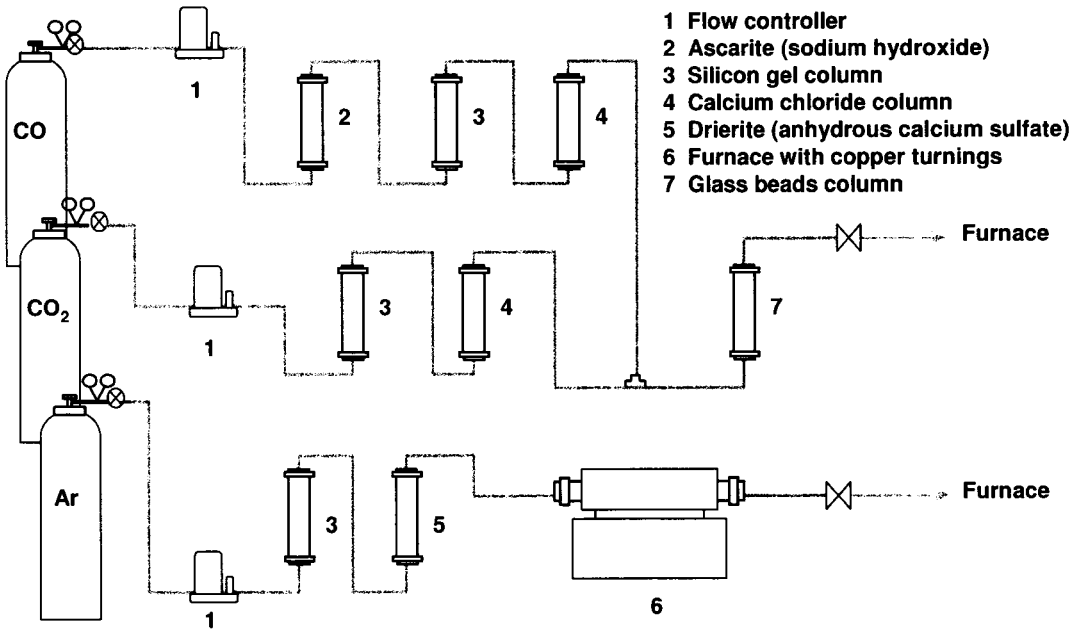

Figure 3.1 Gas purification trains for CO, CO_2 and Ar.

3.2 Apparatus

3.2.1 Design of the Apparatus

The transpiration apparatus is mainly composed of four systems as listed below:

- Gas purification system and admission system
- Saturation chamber made of alumina crucible and alumina discs
- Flow rate controlling system
- Furnace and temperature controlling system

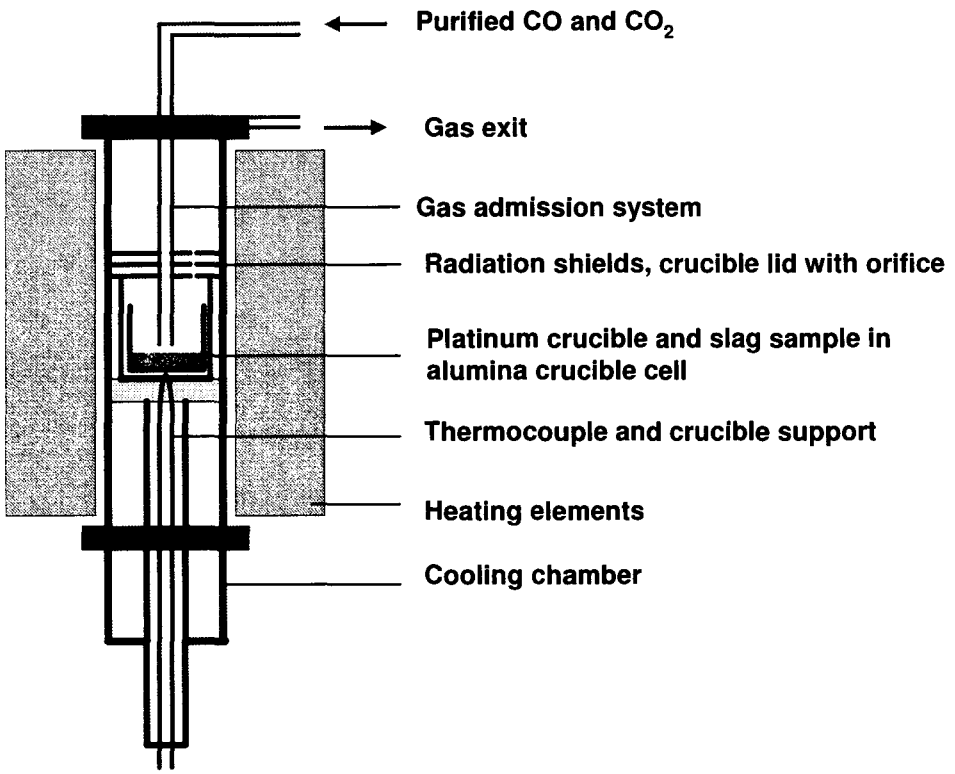

Figure 3.2 Experimental apparatus –transpiration reaction cell

This arrangement with the exclusion of the gas purification system is schematically shown in Figure 3.2. As can be seen, the slag sample was held in a platinum crucible and was placed in the saturation cell, 40 mm i.d.× 40 mm. This saturation cell is closed except for an alumina lance through which the flow gas was introduced and a small orifice through which the gases can escape. This apparatus facilitates saturation of the flow gas, since it may be blown against the sample's surface to attain maximum gas sample contact. With a relatively small orifice, the flow through

the orifice is small enough not to upset equilibrium inside the cell and great enough to make the effect of any back diffusion negligible

3.2.2 Furnace

All the experiments were conducted in a vertical tube furnace which had a 1000 mm long by 45 mm i.d alumina reaction tube fitted with water-cooled stainless steel endcaps. All joints were sealed by O-ring systems. The temperature as well as cooling and heating rate was controlled by an Eurotherm 2416 programmable controller. Temperature readings were measured by a Pt-6 pct Rh/Pt-30 pct Rh thermocouple, which is located at right bottom of the crucible as shown in Figure 3.2.

The vertical temperature gradient over the expected height of the slag phase was less than 1°C and any radial temperature gradient was minimized by means of an alumina lid and two alumina radiation shields located above the lid. The hot zone of the furnace was about 40 mm and the accuracy of the temperature measurements was certified to be within ±1°C. The temperature profile of the furnace, as illustrated in Figure 3.3, was measured with the presence of the reaction crucibles. The actual temperature was read from a calibrated B-type thermocouple which was inserted in the crucible support within 5mm of the bottom face of the crucible.

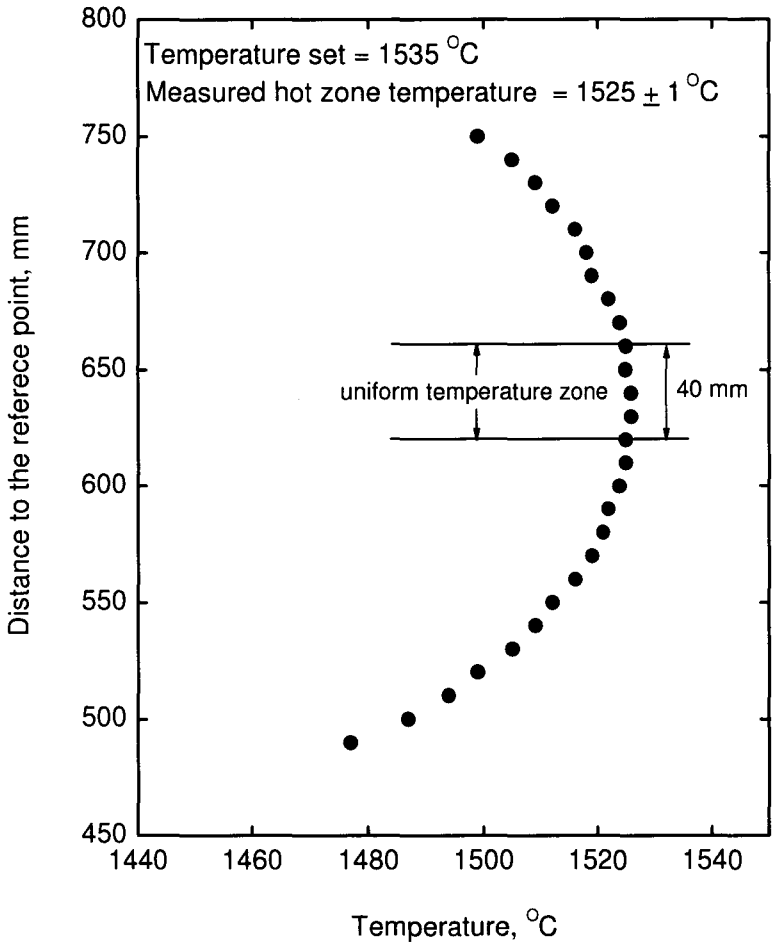

Figure 3.3 Temperature profile of the furnace and the uniform temperature zone is about 40 mm high located about 640 mm above the reference point.

The temperature at the specimen-setting position was measured before and after the run by using a Pt-6 pct Rh/Pt-30 pct Rh thermocouple. The measuring thermocouple was compared periodically with other standardized thermocouples. The temperature measurement was always made after the atmosphere of CO_2/CO mixture had been

replaced with argon of the similar flow rate to prevent the deterioration of the thermocouple.

3.2.3 Calibration of Flow Controller

The mass flow controller was factory calibrated for nitrogen gas. For proper use, it needs to be recalibrated for the target gas to ensure accurate flow control. This calibration was conducted under room temperature for CO_2 and CO gases. The linear calibration curves were also compared with 3 measurements conducted within 180 days. As shown in Figure 3.4, the variation of flow rates among these measurements was not significant and it ensured the precision of flow rate control during longer experimental time periods. However, the calibration was still updated over the course of the research.

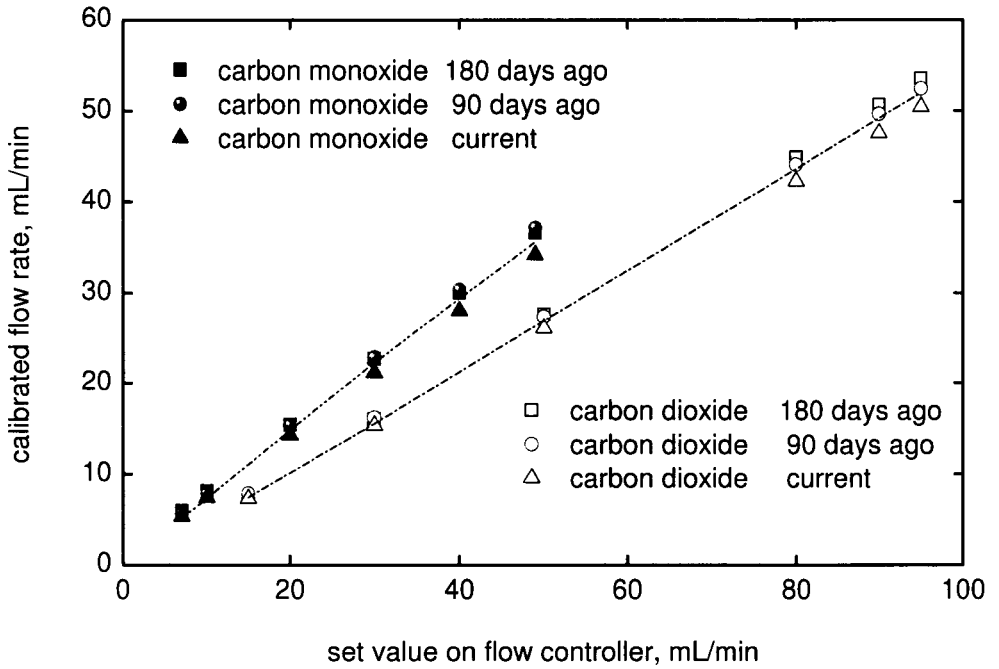

Figure 3.4 Calibration curves for flow rate control on carbon monoxide and carbon dioxide, conducted at room temperature with comparison of three measurements in 180 days.

Table 3.2 Total flow rate checkout for calibrated CO and CO_2 flow controllers

p_{O2}, atm	CO flow controller		CO_2 flow controller		CO_2/CO	total flow,mL/min	
(at 1873K)	set	cal	set	cal		average	error
1.00E-05	6.1	4.6	64.7	35.1	7.63	39.7	± 0.1
1.00E-06	15.9	11.7	52.4	28.2	2.41	39.9	± 0.1
1.00E-07	31.0	22.7	32.7	17.2	0.76	39.9	± 0.1
1.00E-08	44.0	32.2	15.7	7.7	0.24	39.7	± 0.1

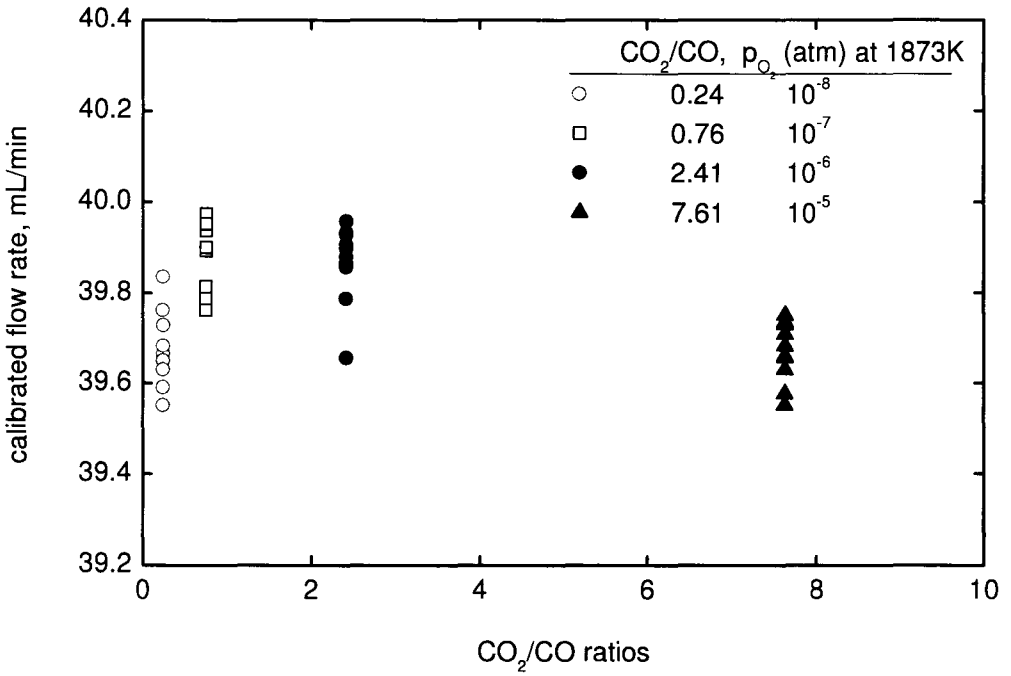

Figure 3.5 Overall flow rate verification for four oxygen partial pressures with total flow rate of 40 mL/min

Individual flow rate and the total flow rate of gas mixture were verified as shown in Figure 3.5. The four ratios of CO_2/CO, as listed in Table 3.2, were frequently used in these vapourization experiments. The total flow rate was with an error of ± 0.1 mL/min, which is propagated to the error of the oxygen partial pressure of ± 2%.

3.3 General Experimental Procedure

3.3.1 Vapourization Experiments

For each experiment, the platinum crucible encased with a protective alumina crucible held approximately 1g of the premelted slag and was placed in the water-cooled chamber. After attaining the desired temperature, the reaction cell crucible was raised slowly into the furnace hot zone.

The CO_2/CO gas mixture, which was delivered by a thin alumina tube onto the surface of the slag sample, were prepared from the purified gases, blended in a column of glass beads and then introduced into the furnace with a controlled flow rate for a given length of experimental time. The experiment was terminated by lowering the crucible from the hot zone into the cooling chamber and quenched with a strong argon stream.

The quenched slag samples were analyzed by ICP technique for major components. Specifically, the total amount of niobium in the slag was determined. The Nb^{4+} content was determined by a potentiometric redox titration method. This scheme involved dissolution of the slag in acid solution as stated in the next section.

3.3.2 Chemical Analysis

3.3.2.1 Making Solutions

In wet methods of analysis, obtaining a suitable solution is the first step. Slag containing niobium oxide can be decomposed in a number of ways. Generally, this slag is brought into solution by means of the fusion processes (Scott, 1939). Fusion with alkaline fluxes is usually very effective. However, this introduces material that may be undesirable and may cause measurement inconsistencies. A more efficient method to dissolve the slag sample has been developed.

While the acid attack is the preferred method, hydrofluoric acid is the usual choice. When niobium pentoxide is dissolved in aqueous hydrofluoric acid, oxyfluoniobic acid (pentafluoniobic acid), H_2NbOF_5 will be formed (Kolthoff and Elving, 1964).

To carry out the procedure, the quenched slag samples were dissolved by adding 4 mL hydrofluoric acid (49 pct HF diluted with purified water 1:3) to a polyethylene tube container. The container was tightly capped and was heated in a hot water bath (maintained at 70°C) for 2 hours.

A further dissolution was conducted by adding 6 mL of concentrated hydrochloric acid to the container and let it digest for 2 hours. The resultant clear solution was transferred to a 100mL polythene flask. To avoid any loss of solution, the platinum crucible, the polythene tube container and cap were rinsed five times with 1M hydrochloric acid. The rinse solution was added to the flask as well. Finally, 1M hydrochloric acid was added to the flask to the graduation mark.

3.3.2.2 ICP testing

In the dissolution procedure, the final concentration of fluoric ion is less than 1%, which meets the allowed level for the ICP testing. To obtain a good reading from the ICP, the pH value in the final solution should be consistent in all the solutions. Therefore, it was found that the results from solution diluted by 1M hydrochloric acid was more consistent than the solution diluted by distilled water.

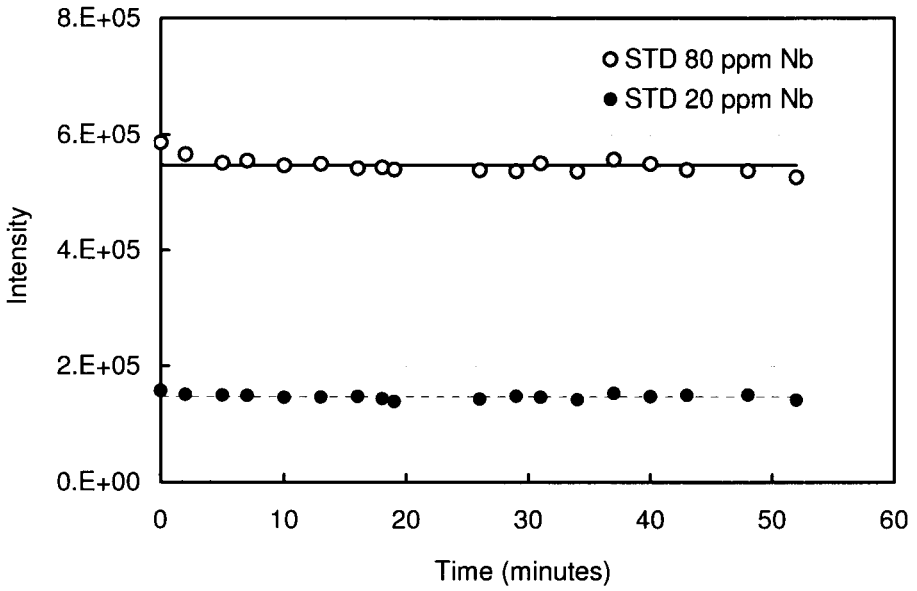

Figure 3.6 Intensity variation of STD 20ppm and STD 80 ppm with time

The performance of the ICP (*i.e.* adjust the flow rate of argon, observation height, cleaning the torch) was optimized. However, the drift pattern of ICP was monitored by the 80ppm and 20ppm niobium standard solutions respectively. By optimizing the

performance of the ICP and applying the newly developed correction method, the intensity drift in 52 minutes was less than 5% as shown in Figure 3.6.

3.3.3 Potentiometric Titration

3.3.3.1 Principles

The volatility of niobium oxides dissolved in slag is strongly dependent on the oxidation state. From the ionic theory viewpoint, niobium exists in slag melts as Nb^{2+}, Nb^{4+}or Nb^{5+} or oxygen complex (Tsukihashi, 1988). For a better understanding of the physicochemical properties, it is necessary to determine the niobic ionic species in the slag solution.

In ranges of intermediate oxygen pressure all three ions, Nb^{2+}, Nb^{4+} and Nb^{5+}, can be present. When this occurs, the precise determination of the various valency states by chemical analysis is not possible because the internal equilibrium among the three valency states is shifted during dissolution (Tsukihashi, 1988). Thus, only two valency states are present in the aqueous solution, *e.g.* Nb^{2+} and Nb^{4+}, or Nb^{4+} and Nb^{5+}.

Niobium concentration in slag was determined by ICP, indicated by Nb_{total}. Assuming all the niobium ions Nb^{4+} are oxidized to Nb^{5+} by oxidant (Ce^{4+} in this experiment). The amount of oxidized ions is indicated as Nb_{obs}. The amount of niobium ions prior to oxidation is indicated by Nb^{4+} and Nb^{5+}. The quantity of niobium in the Nb^{5+}

valency state was calculated as the difference between total and oxidized niobium. Namely, in the case of Nb^{4+} and Nb^{5+}

$$Nb^{4+} + Nb^{5+} = Nb_{total} \tag{3.4}$$

where

$$Nb^{4+} = Nb_{obs} \tag{3.5}$$

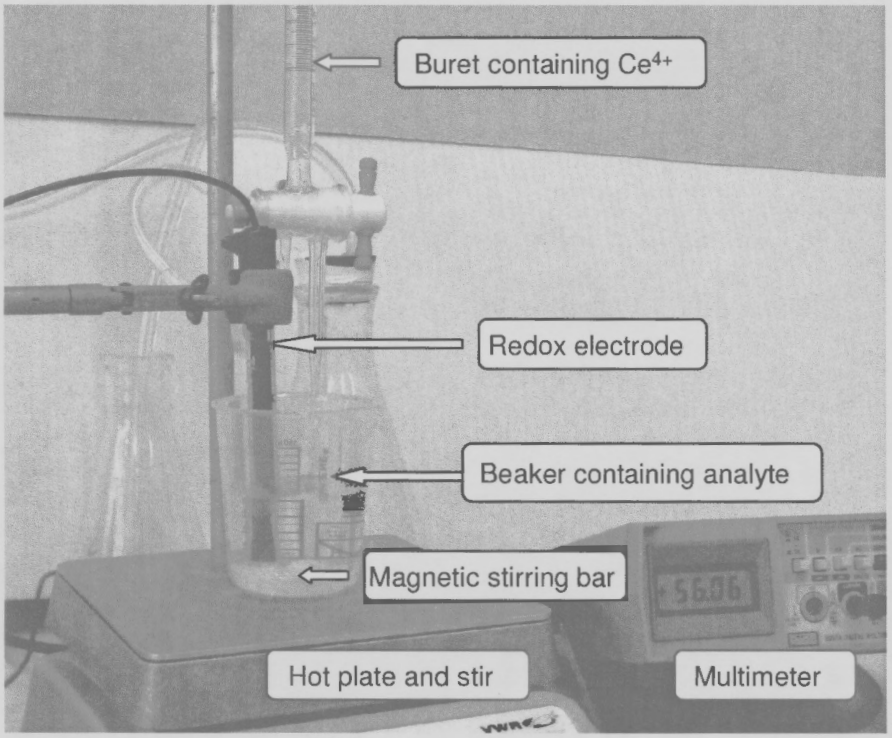

Figure 3.7 Arrangement for potentiometric titration of Nb^{4+} with Ce^{4+}

The content of Nb^{4+} is determined by redox titration with standardized cerium

(IV), the course of which can be monitored potentiometrically. The titration reaction is

$$Ce^{4+} + Nb^{4+} \rightarrow Ce^{3+} + Nb^{5+} \quad (3.6)$$

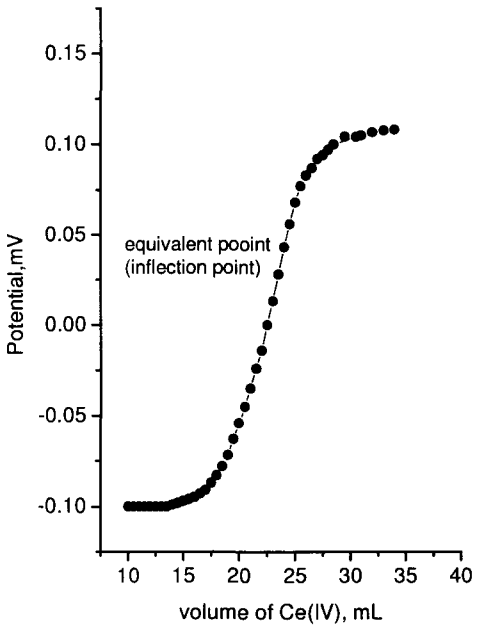

Figure 3.8. A typical titration curve of 40mL solution containing Nb^{4+} with standardized 0.001NCe^{4+}

As shown in Figure 3.7, Ce^{4+} was added from the buret to create a mixture of Ce^{4+}, Ce^{3+}, Nb^{5+} and Nb^{4+} in the beaker, which was mounted on the top of the hot plate and stirred. The temperature was controlled at 40°C. The electrode (Thermo Scientific, Orion 967800) which was used to perform potentiometric titrations combines a platinum redox and a silver/silver chloride reference electrode in one body. The multimeter measures the voltage driving electrons from the reference electrode, through the meter and out at the Pt electrode.

A typical titration curve for Reaction 3.6 is presented in Figure 3.8, which shows the potential as a function of the volume of the addition of Ce (IV). The equivalence point is marked by a steep rise in the voltage (inflection point)

3.3.3.3 Standardized Ceric Titrant

The commercial ceric titrant is previously standardized against sodium oxalate in acid solution before any usage:

$$2Ce^{4+} + Na_2C_2O_4 = 2Ce^{3+} + 2CO_2 + 2Na^+ \qquad (3.7)$$

Procedure: Prepare 1 L of 1 M H_2SO_4 by slowly adding 59 mL of concentrated acid to about 700 mL of water then diluting to 1 L. Dry about 1.5 g of primary-standard sodium oxalate, $Na_2C_2O_4$, at about 110 °C for at least 1 hr. Cool in the desiccator. Weigh about 0.2 g samples (to the nearest 0.1 mg) and place a sample of $Na_2C_2O_4$ into the 400 mL beaker. Dissolve each sample in about 250 mL of 1 M H_2SO_4. Heat each solution to 80 - 90 °C, and titrate with Ce^{4+} while stirring with a magnetic stirring bar. The potential is recorded as a function of the volume of added ceric solution. The equivalence point is marked by a steep rise in the voltage. The temperature should not drop below 60 °C. Determine a blank by titrating an equal volume of the 1M H_2SO_4. Correct the titration data for the blank, and calculate the concentration of the ceric solution.

Chapter 4 Self-Consistency Experiment

4.1 Introduction

In the preliminary study, the dissociation vapour pressure of pure Nb_2O_5 was measured as a function of temperature under controlled partial pressure of oxygen by the transpiration method. Comparing the experimental results with literature as shown in Figure 5.3 (see page 107, in Chapter 5), it exhibited both agreement and disagreement. An agreement was demonstrated in terms of the slope, which includes the information regarding the enthalpy of vapourization. However, the disagreement with respect to the absolute values of vapour pressures was significant among these measurements.

The partial pressure of oxygen was precisely controlled by the CO_2/CO ratios in the current study whereas it was inexplicit in the experimental condition in the literature (Golubtsov *et al.*, 1960; Kamegashira *et al.*, 1981; Matsui and Naito, 1982). Although the absolute value of these measurements were not comparable with respect to different conditions in oxygen partial pressure, it is still essential to develop a method by which self-consistency can be proven.

The activities of the components of a liquid alloy system can be determined in favourable cases from the partial pressure of the vapour in equilibrium with liquid alloy. A number of examples of recent applications of vapour pressure method can be found in

the literature. Onderka *et al.* measured lead vapour pressures over liquid Cu-Fe-Pb alloy at 1500°C by employing the transpiration method (Onderka *et al.*, 1993); Gingerich and coworkers studied the thermodynamics of ternary liquid Au-Cu-Ge alloys by using a Knudsen effusion apparatus (Miller and Gingerich, 1994); Hilpert and coworkers determined thermodynamic activities for various aluminum alloys of technical interest based on iron, nickel, or titanium (Albers *et al.*, 1992; Eckert *et al.*, 1996; Kapala *et al.* 1996) and for other high melting metal systems, e.g., Hf-Ni alloys, by using a vapour pressure method (Bencze and Hilpert, 1996).

Assuming that vapour over the alloy behaves as an ideal gas and the vapor species i is monatomic or monomeric, the thermodynamic activity of a component i is given by the expression

$$a_i = \gamma_i \cdot x_i = \frac{f_i}{f_i^0} \approx \frac{p_i}{p_i^0} \tag{4.1}$$

where f_i , p_i are the fugacity and the partial pressure of i, respectively, and f_i^0 , p_i^0 are the fugacity and the vapour pressure of i at some standard state. The quantities p_i and p_i^o can be determined by the transpiration method.

Thus, the measurement of the partial pressure over the solution leads directly to the corresponding activity value, if the vapour pressure of the pure condensed form of the substance at standard state is known at the temperature under consideration.

The transpiration method has been established in measuring vapour pressure of pure Nb_2O_5, and it should be applicable for other vapour pressure measurements. On the other hand, experience in high-temperature vapour-pressure measurements has shown large systematic errors, even among experienced investigators (Geiger *et al.*, 1987).

A sound development of a technique for the measurement of thermodynamic property of matter requires a comparison with the same property which has been measured by other recognized procedures. The agreement in the results tends to confirm the validity of the method.

The binary alloy system silver-gold is excellent for this purpose. This system was chosen as a test system because thermodynamic data are available from various investigations by different techniques (Wachter, 1932; McCabe *et al.* 1953). Furthermore no anomalies are expected in this system such as a minimum in the logarithmic plot of the activity coefficient versus concentration, which was observed in some binary systems in the range of lower concentrations (Peltner and Herzig, 1980).

This chapter is called "self-consistency experiments" because the aim of this study was to compare the activity of silver in silver-gold alloys measured by the transpiration method with that by other methods, so that it allows us to detect systematic errors and to evaluate the precision and accuracy of our measurements. More specifically, the objectives of these self-consistency experiments are:

- To validate the transpiration method for vapour pressure measurement
- To estimate the systematic error in determining the activity
- Comparing by well-established data, e.g. Ag, Au and Au-Ag
    - Measuring vapour pressure above liquid Ag, Au and Ag-Au alloy,
    - Calculating activity of silver in Ag(l)=Ag (in Ag-Au)(l)

In this chapter, vapour pressures above pure liquid gold, silver and silver-gold alloys were measured by employing the transpiration method; the thermodynamic activity of silver in liquid silver-gold alloys was determined by measuring the vapour pressure of silver over alloys and pure silver. The activity of gold was computed from that of silver. Results indicate agreement with the literature both in terms of activity and vapour pressures above the alloys at fixed temperature. Therefore, the measurement which yields thermodynamic activity data demonstrated reliable results for a_i by the transpiration method.

4.2 Experimental

The materials used in these experiments were pure gold (99.9985% purity, Alfa Aesar) and pure silver(99.99% purity, Alfa Aesar). In addition, three gold-silver alloys with a mole fraction of silver from 0.2 to 0.8 were prepared by melting weighed amounts

of gold and silver in a graphite crucible and quenched under the protection of purified argon. The melts were subsequently heat treated at the temperature 50°C below the melting point for 15 hours. The composition of each alloy was established by ICP analysis.

All the weighing was carried out on a Sartorius electrobalance on which weight changes of 0.01mg could be measured accurately to 0.01%. All the sample weights were approximately 2g.

The ultra high purity (UHP) argon gas admitted as carrier gas was further purified by passing it through silica gel and drierite (anhydrous calcium sulfate) to eliminate any moisture. The gas stream was also passed over copper turnings heated to 873 K to remove oxygen. The flow rate was controlled by calibrated flow controller accurately to 0.1%. The insertion and removal of samples from the furnace was carried out under a fast-flowing stream of argon to avoid back-fusion of air down the open-ended reaction tube and over the sample.

The measurement method as well as temperature control are as described in the previous chapter. Additionally, a weighed sample was contained in an alumina crucible which has been reduced to constant weights by heating to 1500°C in a fast-flowing stream of argon for approximately 6 hours. An alumina crucible containing the sample was placed in the bottom of an alumina reaction tube and was then raised into the hot zone of the furnace. This operation was performed in approximately 20 minutes so that

the refractory should not be subjected to too great a thermal shock.

After a measured volume of gas had been passed, the sample was quenched by slowly withdrawing it from the furnace. The sample was then transferred to a stainless steel water cooling chamber. The time required for this procedure was approximately 30 minutes. Coming to thermal equilibrium with its surroundings, the sample was weighed again or in the case of silver-gold alloys submitted for chemical analysis.

4.3 Results and Discussion

4.3.1 Equilibrium Flow Rates

The experiment was initially conducted to measure the weight loss per liter of transporting gas as a function of flow rates at a fixed temperature for pure gold and pure silver respectively. Having proved the validity of the technique in this way, experiments were conducted on liquid silver-gold alloys.

As can be seen from Figure 4.1, these measurements exhibit a typical shape of equilibrium vapour pressure against flow rate. As the flow rate of carrier gas was varied, three regions of interest can be described. They are,

(1) At low flow rates, an abnormally high loss of sample was recorded due to the vapour species leaving the reaction zone by some means other than saturation of

the transporting gas. The cause of the high values recorded was considered to be twofold (Alcock and Hooper, 1959):

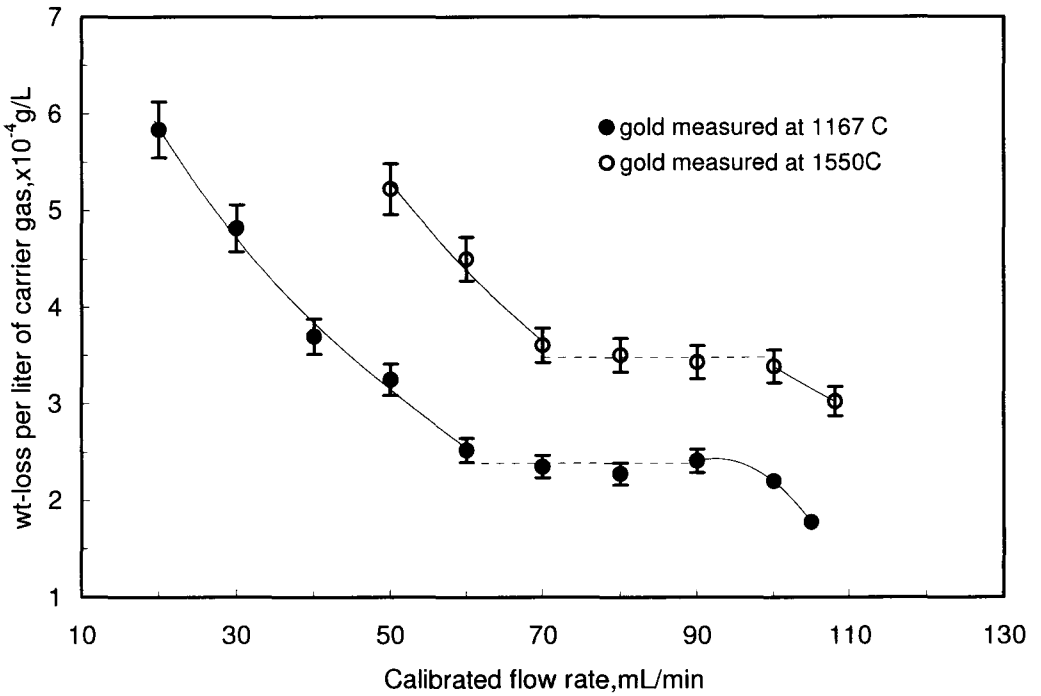

Figure 4.1. Weight loss per liter of carrier gas (Ar) as a function of flow rate, for gold at 1550°C and for silver at 11670°C

(a) The difference in molecular weight between the carrier gas and volatile product causes them to segregate from one another;

(b) The concentration gradient set up on the surface of melts gives rise to diffusive flow of the vapour molecules from the reaction zone. Therefore, not all the molecules would be transported by the carrier gas.

Kvande and Wahlbeck (Kvande and Wahlbeck, 1976) also point out that a considerable amount of sample vapour is transported by a diffusion mechanism as well as by bulk hydrodynamic flow at a very small flow rate of carrier gas.

The loss in weight of the sample was used to determine $n_{v.}$, thus, diffusion of vapour out of the sample region will lead to an error. However, another region was observed in this experiment, namely,

(2) At a moderate flow rate of carrier gas, 60-90 and 70-100 ml/min respectively for gold and silver, most vapour transported is independent of flow rates. The region where the rate of vapourization is rapid enough to saturate the carrier gas so that the equilibrium vapour pressure is independent of the rate of flow of the carrier gas.

As can be seen, the transpiration method should only be used in cases where the measured vapour pressure is independent of the rate of flow (Alcock and Hooper, 1959). Experiments performed in this region need no correction for diffusion or kinetic effects (Lepore and Van Wazer, 1948; Alcock and Hooper, 1960). Alcock and Hooper (Alcock and Hooper, 1959) in a study of the vapour pressure of gold by the transpiration technique found that saturation could be achieved over a range of flow rates, 42-90 mL/min, as shown in Figure 4.2.

(3) At high flow rates, the carrier gas is not saturated with sample vapour and the

weight loss per the weight loss per liter tends to decrease because the carrying gas is moving too quickly to become saturated with the volatile product.

Merten and Bell (Merten and Bell, 1967) have discussed the kinetic aspects of the transpiration method, and found that at high flow rates, saturation of the carrier gas may be prevented by incomplete mixing in the gas stream or by insufficiently rapid vapourization of the sample.

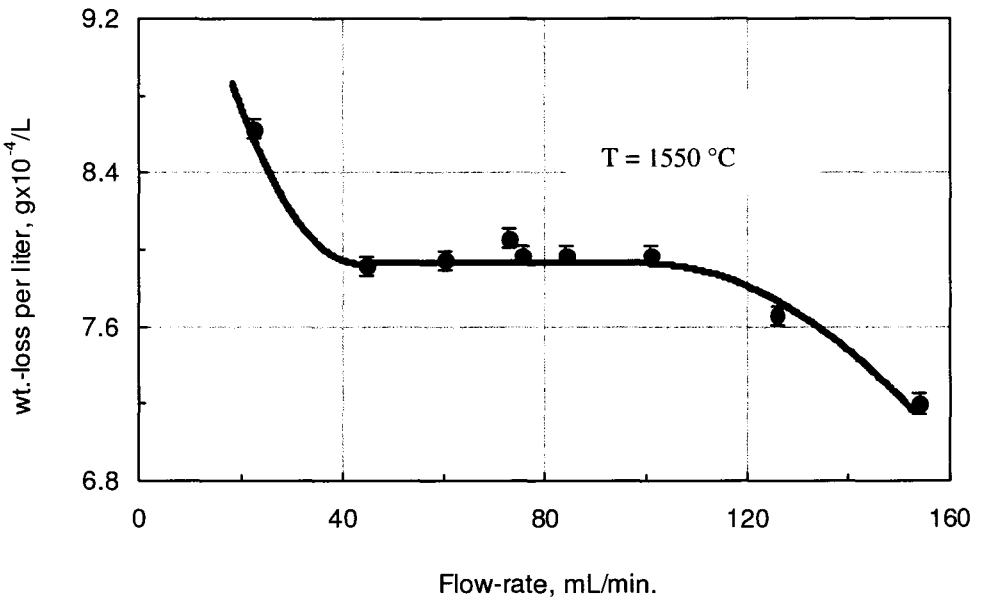

Figure 4.2 Weight of gold lost per liter of carrier gas as a function of flow rate at 1550°C (Alcock and Hooper, 1959)

In conclusion, when the carrier gas flow rate is low, the vapour pressure shows a high value as the result of the diffusion of volatile species, but when the carrier gas flow

rate is high, on the contrary, the vapour pressure shows a low value due to the unsaturation of volatile species in flowing gas. On the basis of results, both in literature and this experiment, it is proposed that the value of the vapour pressure obtained by the measurement in a proper intermediate flow rate region should be considered as the saturated vapour pressure.

Consequently, over a range of flow rates, the experimentally determined vapour pressures uncorrected for diffusional and kinetic effects have been found to be essentially independent of flow rate. An experimental plateau region for various vapour pressures is established under certain carrier gas and temperature conditions by finding flow rates high enough that diffusional loss is negligible and yet low enough that the carrier gas is saturated with vapour.

The reproducibility of measurements in the plateau was satisfactory. The equilibrium value of sample weight loss per liter of transporting gas was found by drawing the best horizontal line through the plateau points. The random errors of the technique were estimated in each series of measurements by taking the arithmetic mean of the plateau results and calculating the standard deviation from it.

Table 4.1 Experimental results

Materials	flow rate in plateau region mL/min	wt.loss per liter $x10^{-4}$g/L	vapor pressure atm	temperature °C	standard deviation %
Gold	60 - 90	2.38±0.09	2.7×10^{-5}	1550	4%
Silver	70 - 100	3.48±0.08	7.2×10^{-5}	1167	3%

The vapour pressures of liquid gold and silver have been measured by the transpiration technique at 1550°C and 1167°C respectively and the result is summarized in Table 4.1. Comparison of the silver vapour pressure-flow rate curve in Figure 4.1 with that of gold shows a considerable difference and is probably due to the difference in magnitude of the vapour pressure being measured.

4.3.2 Vapour Pressure and Thermodynamic Properties

As shown in Figure 4.1, the plateau regions where the weight loss per liter of carrier gas is independent of flow rate of carrier gas result in the equilibrium flow rate for gold and silver at 60-90 mL/min and 70-100 mL/min respectively. The following experiments were conducted by choosing the flow rate of 80 ml/mL for gold and 100 mL/min for silver respectively.

The temperature effect on the vapour pressure of the gold and silver curve is demonstrated in Figure 4.3. Both silver and gold were found to deviate from experimental data as straight-line as in the plots of log p vs. 1/T by least-square method. Vapour pressure attained from the plateau region in Figure 4.1 was also plotted as a comparison. It can be seen that both measurements show agreement as in Figure 4.3 for both silver and gold at 1167°C and 1550°C respectively. The agreement between two runs of the experiments indicates the good reproducibility of the experimental results.

As seen in Figure 4.4 and 4.5, the vapour pressure of gold and silver are also

compared with the literature respectively. The vapour pressure of gold was measured by Grieveson *et al.* (Grieveson *et al.*, 1959) independently by the transpiration and Knudsen methods when monatomicity of the vapour is assumed. In addition, the gold Standard Vapour pressure of the reference material 745 was measurements over the pressure range 10^{-8} to 10^{-3} atm. The temperature range corresponding to these pressures is 1300-2100 K. These results were based on a series of interlaboratory measurements on the vapour pressure of gold (Paule and Mandel, 1970). The uncertainty in the associated temperature was approximately ±9K in the laboratory report, while the temperature was controlled within ±1K in this study.

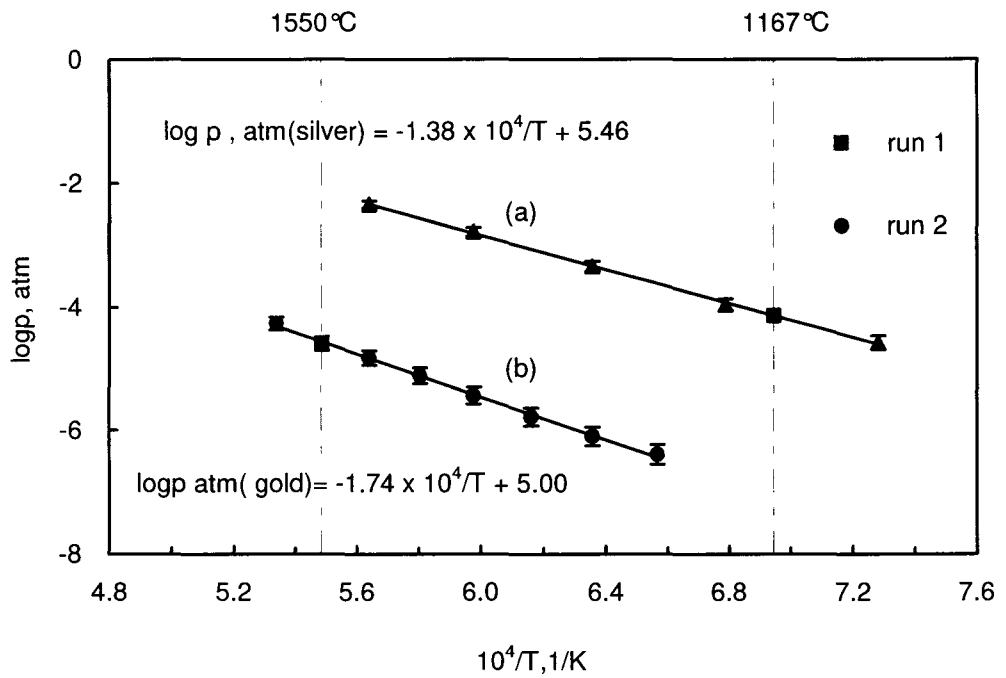

Figure 4.3 Vapour pressure as a function of temperature (a) vapour pressure of silver above liquid silver (b) vapour pressure of gold above liquid gold.

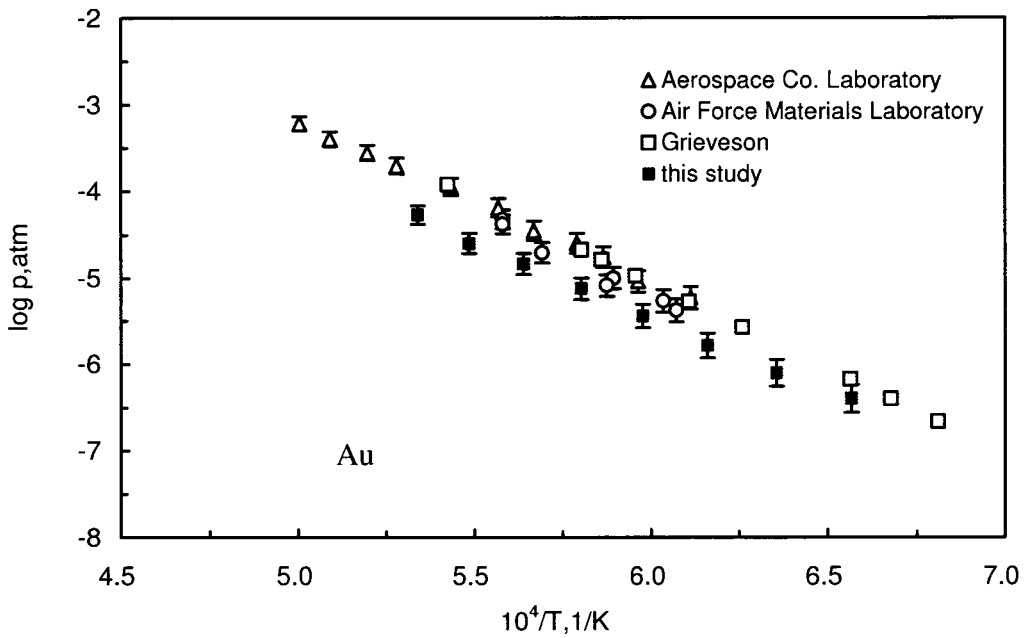

Figure 4.4 Comparison of vapour pressure for gold as a function of temperature with laboratories (Paule and Mandel, 1970) and Grieveson *et al.*,(Grieveson *et al.*, 1959).

The vapour pressure of silver has been measured by the Knudsen orifice effusion method 750 °C to 1050°C using radioactive Ag^{110} as a tracer (Schadel and Birchenall, 1950). In addition, the present data for silver is also compared with previous measurements and estimates summarized by Nesmeyanov (Nesmeyanov, 1963). The results for Ag, (Figure 4.6) agree well with the literature. However, the present results for Au (Figure 4.5) are in good agreement with literature only in the slope.

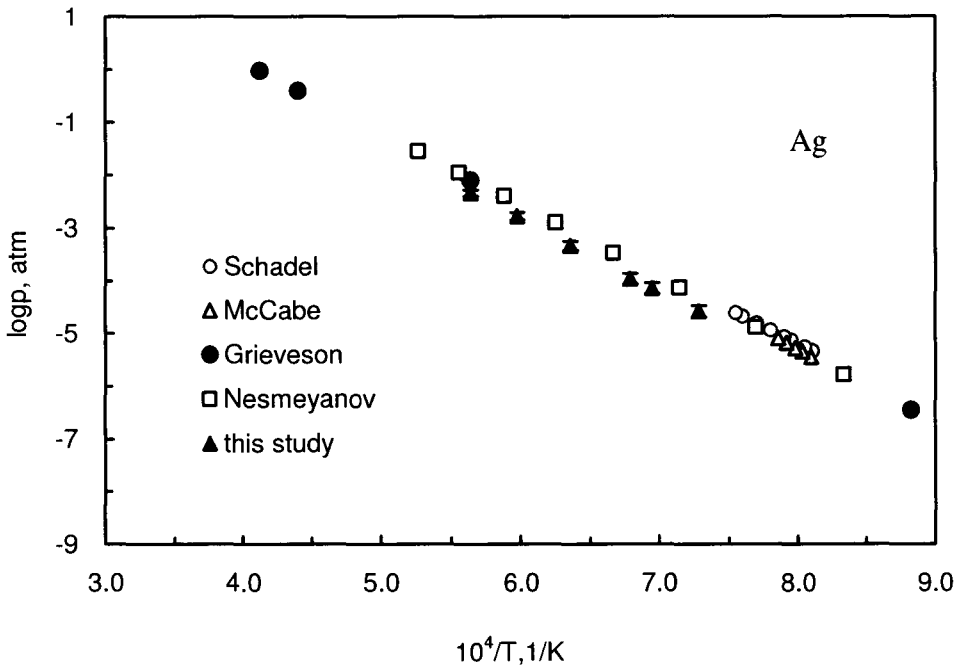

Figure 4.5 Comparison of vapour pressure above liquid silver as a function of temperature with literature measured in the same temperature range.

Vapour pressure data against temperature were also fitted to the analytical form

$$\log p = \frac{A \times 10^4}{T} + B \tag{4.2}$$

where p in atm and T in K, using the least-square methods. The values for the constants A and B for each materials as well as heat of vapourization, as calculated from the analytical expression using the Clausus-Clapeyron relation, are presented in Table 4.2.

Table 4.2 Comparison of the vapour pressure of gold and silver by least-square treatment

metal	logp,atm = A x 10^4/T + B				
	A	B	Temperature	Heat of vaporization	reference
			K	kJ/mol	
Au	-1.98	6.80	1400-2000	378	Grieveson et al., 1959
	-1.80	5.81	1336-3200	321	Oriani, 1956
	-1.79	5.83	1300-2100	343	Paule,R.C.et al., 1970
	-1.74	4.98	1523-1873	326-340	this study
Ag	-1.37	5.62	1238-2425	262	Grieveson et al, 1959
	-1.33	5.46	1233-2443	255	Schadel and Birchenall, 1950
	-1.50	6.70	1235-1273	287	McCabe and Birchenall, 1953
	-1.38	5.72	1200-2400	264	Nesmeyanov, 1963
	-1.38	5.46	1370-1785	259-269	this study

4.3.3 The Activities of Silver and Gold in Liquid Silver-Gold Alloys

As can be seen from Figure 4.1, the vapour pressure of silver is about 200 times higher than that of gold if compared using the same temperature. Therefore, silver is the more volatile component which makes it possible to determine silver activities in liquid Ag-Au alloys directly by vapour pressure methods. Since more silver than gold was vapourized during the runs, the change in weight over a series of measurements was attributed entirely to silver loss in computing the vapour pressure. In addition, since the vapour pressure of gold is less than that of silver, the effect of gold on the measurements

may be safely neglected under these particular conditions.

Three compositions of silver-gold alloys were prepared following the procedure as stated in the previous section. The vapour pressure above the liquid Ag-Au at 1350 K was shown in Figure 4.6. The solid line, representing the partial vapour pressure of silver above the liquid solution, was computed from the activity of liquid silver-gold alloys from Oriani's data. In Figure 4.6, the agreement between the two sets of data is excellent.

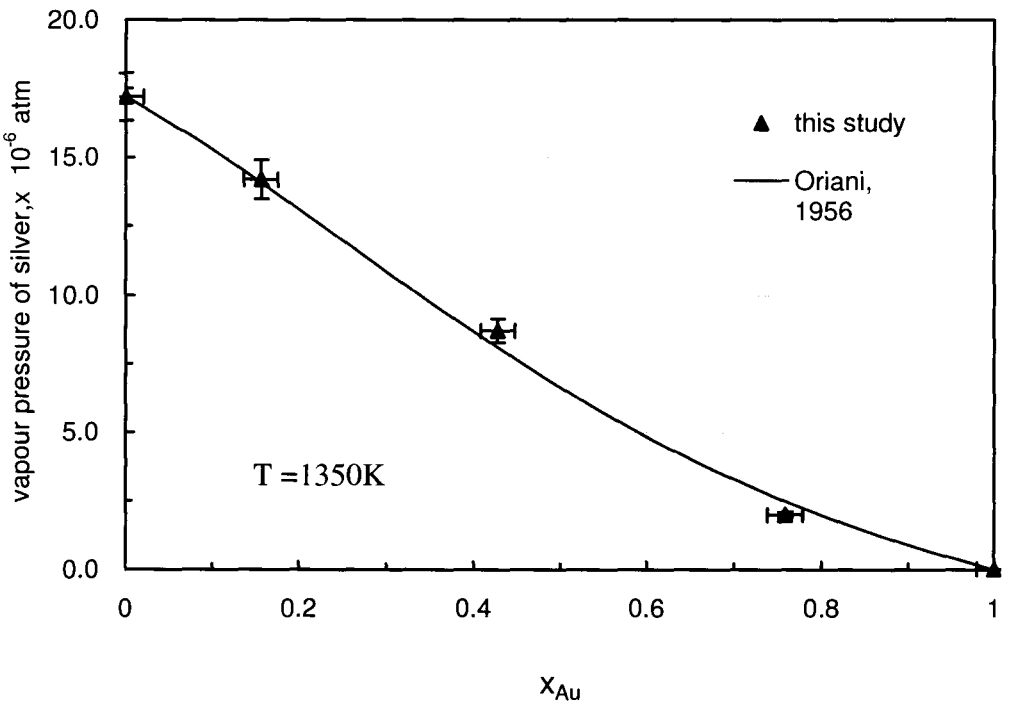

Figure 4.6 Vapour pressure of silver above liquid silver-gold alloys at 1350K

The activities of silver in liquid silver-gold alloys were determined directly by

measuring the vapour pressure of silver over the alloys and pure silver, which is the reference state at this temperature. A plot of the activity values at 1350K vs mole fraction is shown in Figure 4.7. The activity of gold was derived from that of silver by applying the Gibbs-Duhem relation, using graphic integration. Good agreement between calculated and literature points shows that the data for silver consistent with those for gold. Activities and activity coefficients for silver and gold are listed in Table 4.3

Table 4.3 Measurement of the thermodynamic activity for different Au-Ag alloys at 1350K

		measured at T = 1350 K				Gibbs-Duhem equation	
X_{Ag}	X_{Au}	p_{Ag}, atm (above liquid Ag-Au alloy)	p_{Ag},atm,(reference state)	a_{Ag}	r_{Ag}	a_{Au}	r_{Au}
0.241	0.759	2.00×10^{-6}	1.72×10^{-5}	0.116	0.481	0.705	0.929
0.844	0.156	14.20×10^{-6}		0.826	0.979	0.084	0.535
0.572	0.428	8.71×10^{-6}		0.506	0.885	0.344	0.803

As can be seen, the gold-silver system exhibits negative deviation from Raoult's law at 1350K. The agreement between the two sets of data is excellent, both of Oriani's curves falling within the experimental error (±11%) of the present study. This agreement indicates that the results are independent of the relative amounts of materials which effuse through the orifices, as long as the transpiration technique is maintained. The present transpiration method extablishes an excellent check of the consistency and the reliability of the experimental results.

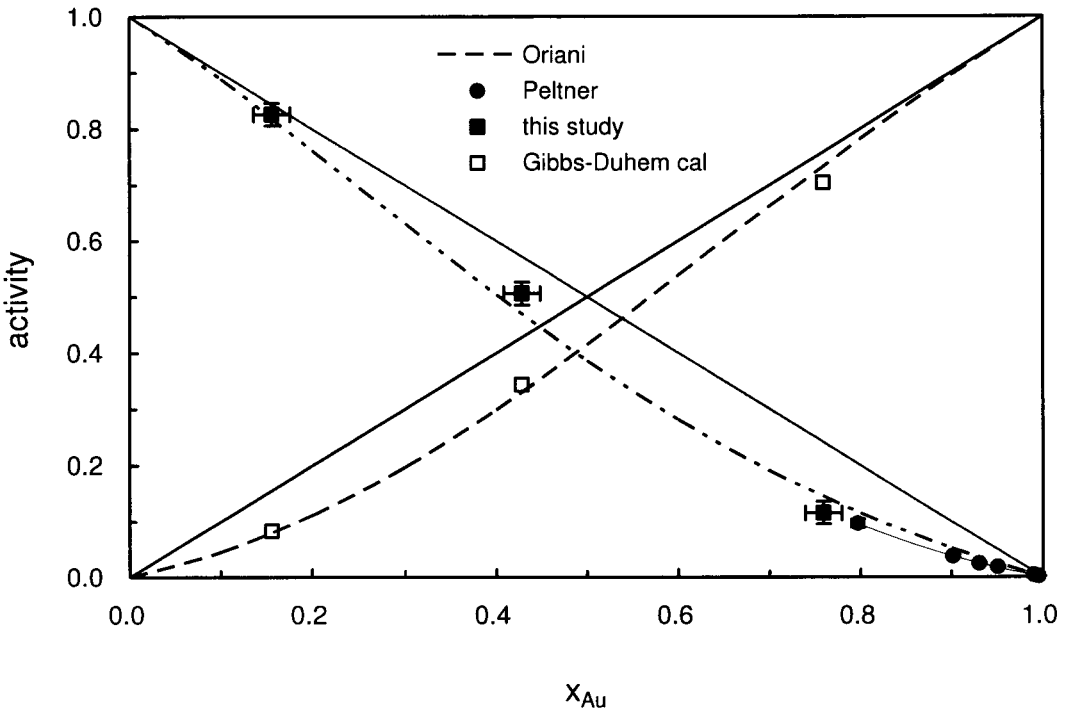

Figure 4.7 Activities for silver and gold alloys as a function of mole fraction of silver at 1350 K

4.4 Conclusions

The variation of weight loss per liter of carrier gas against flow rate exhibits the typical chair shaped transpiration curves. Three regions have been observed and the plateau region showing the equilibrium vapour pressure has indicated the validity of the transpiration method for vapour pressure measurement.

The comparison of vapour pressure of pure silver and pure gold both indicated

some deviation with literature data attained by different vapour pressure techniques. The disagreement of the vapour pressure of gold is significant. However, the heat of vapourization, both in silver and gold, shows good agreement with literature, exhibiting great consistency for these measurements.

The transpiration technique for the determination of the thermodynamic activity a_i of component i in a binary liquid alloy is presented and applied to liquid gold-silver alloys as a test. The reliability and the sensitivity of the technique are demonstrated with gold-silver alloys in the concentration range of 20-80 mol% of Ag at 1350K. It has been found that this technique yields reliable results for a_i and the transpiration method, compared with other techniques applied in literature, yield the same thermodynamic properties, demonstrating the accuracy and validity of this method.

Chapter 5 Vapour Pressure of Niobium Oxide

5.1 Introduction

To determine the activity of niobium oxide in slag melts by the transpiration method, the vapour pressure of pure liquid niobium oxide as the reference state needs to be known. However, the existing vapour pressure data of niobium oxides show disagreement among the measurements in the literature, consequently, this will result in inconsistency in the estimation of the activity of niobium oxide in the slag melts if the literature data is referenced; on the other hand, there is a vacancy in the vapour pressure of niobium oxide measured under controlled partial pressure of oxygen in the system.

Golubtsov and coworkers (Golubtsov *et al.*, 1960) studied the volatility of niobium oxides by the method of labeled atoms in a specially-built effusive Knudsen chamber and the vapour pressures of NbO_2 were obtained by the thermal dissociation of solid Nb_2O_5 in vacuo. It was shown that Nb_2O_5 in a current of air at 1350 K does not volatilize, and under these conditions Nb_2O_5 is a thermally stable compound. Nb_2O_5 in vacuo at a temperature above 1150 K is subjected to thermal dissociation into gaseous niobium oxide and oxygen.

Matsui and Naito (Matsui and Naito, 1983) measured the vapour pressure of Nb_2O_5(s,l) by the mass spectrometry method in the temperature range 1726-2271K to

determine the enthalpy and entropy of fusion of Nb_2O_5. The partial vapour pressures of $NbO_2(g)$ over $Nb_2O_5(s,l)$ were measured showing a factor of 5 lower than those by Golubtsov *et al.* although the slope in the plot of vapour pressures vs. reciprocal temperature was observed to be in fair agreement with each other.

Comparing these two studies on the dissociation vapour pressure of niobium pentoxide, the commonality is that Nb_2O_5 evaporates as NbO_2 gas and O_2 gas and the equilibrium species in the gas do not have the same stoichiometry as the condensed phase, therefore, niobium pentoxide evaporates incongruently.

However, the observation of Nb^+ with a heat of evaporation equal to that of niobium metal in Golubtsov's results, indicated that niobium metal was contained in the condensed phase. Therefore, it is doubtful that those measurements corresponded to equilibrium between the gases and solid Nb_2O_5. There was also no partial pressure of oxygen control in Matsui and Naito's study. Above all, it can be concluded that the nature of the gaseous species in equilibrium with Nb_2O_5 was sufficiently in doubt to warrant further investigation.

In this chapter, the vapourization of liquid Nb_2O_5 was studied by the transpiration method under various oxygen pressures in the temperature range of 1525-1600°C. The chemical system was analyzed according to the Gibbs Phase Rule; followed by the application of the transpiration method, the equilibrium flow rate of carrier gas, which is a mixture of CO and CO_2 with specific ratios, was determined. The variation of vapour

pressure of niobium oxide with partial pressure of oxygen confirms that atmosphere control is the essential condition for this vapourization study. The gaseous species was found to be NbO_2, hence the vapourization reaction of Nb_2O_5 was confirmed. The heat of vapourization was estimated by applying the second law method and compared with previous studies.

5.2 Chemical System

For a pressure measurement to be meaningful, the chemical system must be well defined (Gilles, 1975). A number of intensive parameters (temperature, pressure, molar fraction of a constituent) characterizing the system is expressed by the variances, namely, the Gibbs phase rule,

$$F = C - P + 2 \tag{5.1}$$

Considering a two component system ($C = 2$), four phases ($P = 4$) can exist in equilibrium only at unique points in pressure-temperature space, and such systems cannot be studied as functions of temperature. If two condensed and one gas phase ($P = 3$) are in equilibrium, one degree of freedom ($F = 1$) remains; when the temperature is chosen and fixed, the pressure is fixed and attempts to measure it are worthwhile. If only a single condensed phase and a gaseous phase ($P = 2$) are in equilibrium, the pressure depends not only the temperature but also on the composition of one of the phases.

The vapourization reactions of niobium pentoxide can be expressed in three fundamental equilibrium relationships:

$$[NbO_2] \leftrightarrow (NbO_2) \tag{5.2}$$

$$[Nb_2O_5] \leftrightarrow 2(NbO_2) + 1/2(O_2) \tag{5.3}$$

$$[Nb_2O_5] \leftrightarrow 2[NbO_2] + 1/2(O_2) \tag{5.4}$$

The square and round brackets refer to condensed and gaseous phases respectively. Reaction (5.3) is reactive and not strictly congruent vapourization. The oxide molecules undergo a modification of the oxidation state with oxygen desorption (or inversely, absorption) (Pichelin and Rouanet, 1992). Reaction (5.4) which can be described as non-congruent vapourization is oxide decomposition with oxygen mass transfers in the gas phase.

According to Reaction (5.3) and (5.4), oxygen partial pressure remains the most significant intensive parameter of the complex oxide vapourization under atmospheric pressure at a fixed temperature. In fact the speed of decomposition of the oxide in condensed phase is a lot larger than the vapourization reaction (two orders of magnitude) (Pichelin and Rouanet, 1992). Therefore, the initial vapourization system of the condensed phases attains equilibrium instantly.

The chemical system is composed of condensed phases and a gas phase which is

made of vapour species and carrier gases (carbon monoxide and carbon dioxide).The equilibrium behavior of the condensed phases must conform to the phase rule. In the temperature range of interest, Nb_2O_5 is liquid and NbO_2 can be solid, thus, the system with a gas phase will be univariant. This condition guarantees the pressure measurement in a niobium pentoxide system to be meaningful.

5.3 Results and Discussion

5.3.1 Equilibrium Flow Rate

The difficult part of the transpiration technique is to achieve saturation of the carrier gas. Validating saturation requires measuring each runs vapour pressure with a different flow rate. If, over a range of flow-rates, the same mass of volatile species is transported for a given volume of gas, then the carrier gas is considered to be perfectly saturated.

Hence, the transported NbO_2 was determined as a function of the flow rate of carrier gas as an initial step. The oxygen pressure was controlled by CO_2/CO ratio and maintained at 1×10^{-6} atm at 1873K for all flow rates. The plateau region indicating the equilibrium vapour pressure appeared at flow rates between 25 to 56 mL/min as shown in Figure 5.1. The extensive plateau, shown in Figure 5.1, represents the establishment of equilibrium in the transpiration method. The quantity "weight loss per liter" is directly

proportional to the pressure of volatile oxide.

At 1873K, measurements were made over a twofold range in flow rate and the pressures obtained were constant within a range of 10%, indicating that the carrier gas was saturated with the NbO_2 and that diffusion effects were negligible. The vapour pressure of NbO_2 measured was 7.0×10^{-6} atm. The equilibrium value was estimated by taking the arithmetic mean of the plateau points and the standard deviation was calculated from it. The standard deviation was $\pm 0.015\times10^{-4}$ g/L (g/normal liter of carrier gas).

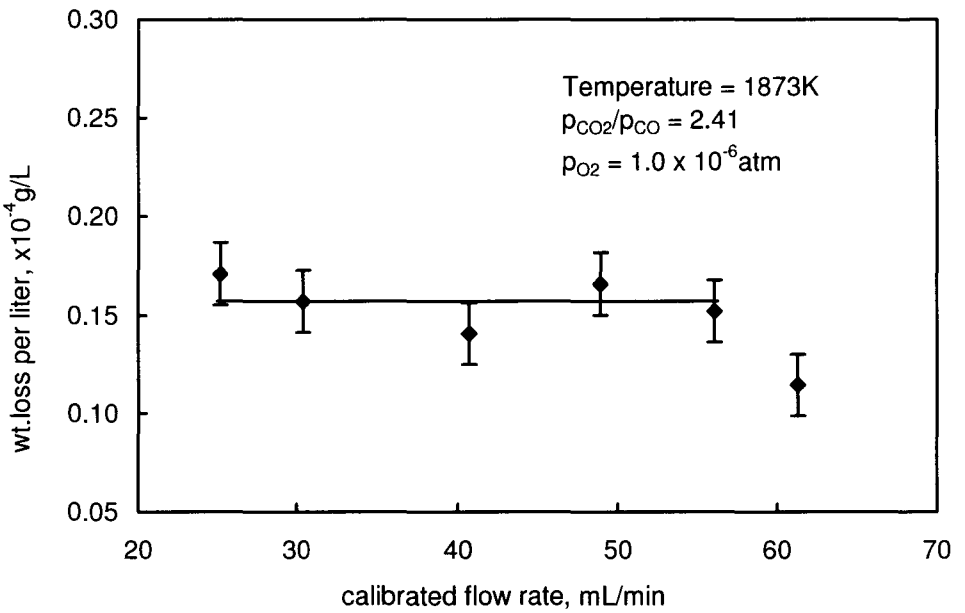

Figure 5.1 Weight loss of NbO_2 per liter of carrier gas as a function of flow rate at constant $p_{O_2} = 10^{-6}$ atm and $T = 1873K$, the plateau region appears at flow rate of 25-56 mL/min.

5.3.2 p_{NbO2} versus p_{O_2} at a Constant Temperature

The effect of oxygen partial pressure on the pressure of the volatile oxide was studied at 1873K. A carrier gas of known oxygen partial pressure was made by mixing carbon monoxide and carbon dioxide from two flow controllers to give a total pressure of 1atm. The flow controllers were independently calibrated beforehand with the requisite gas.

Attainment of equilibrium conditions was ascertained by the plateau region which is characteristic of isothermal equilibrium vapourization in a transpiration experiment in Figure 5.1. Hence, in the present study, the vapour pressure measurements were carried out at a flow rate of 40 mL/min for experiments. The dissociation vapour pressure of Nb_2O_5 was measured as a function of partial pressure of oxygen at 1873 K as shown in Figure 5.2.

From the dissociation Reaction (5.3), the equilibrium constant is given by

$$K = \frac{(p_{NbO_2})^2 (p_{O_2})^{1/2}}{a_{Nb_2O_5}} \tag{5.5}$$

We also know that, $$\Delta G^0 = -RT \ln \frac{(p_{NbO_2})^2 (p_{O_2})^{1/2}}{a_{Nb_2O_5}} \tag{5.6}$$

Thus, $$\ln(p_{NbO_2}) = -\frac{1}{4}\ln p_{O_2} - \frac{\Delta G^0}{2RT} \quad (5.7)$$

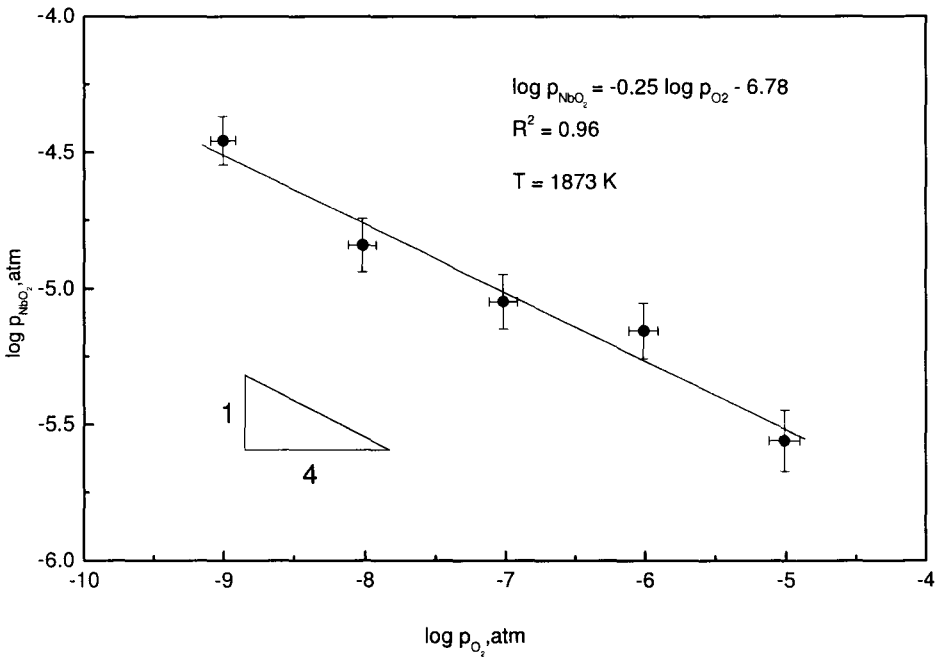

Figure 5.2. Dissociation vapour pressure of Nb_2O_5 as a function of partial pressure of oxygen at 1873 K, flow rate of carrier gas was 40 mL/min.

Therefore, according to Equation 5.7, the logarithm of vapour pressure of NbO_2 should have a linear relationship with logarithm oxygen partial pressure with a slope of $-\frac{1}{4}$ at a fixed temperature. By least-square treatment of the experimental data, a linear relationship between the logarithm scale of vapour pressure and partial pressure of oxygen indicated consistency with Equation 5.7. It can be seen in Figure 5.2 that the pressure of the gaseous oxide was directly proportional to the partial pressure of oxygen.

5.3.3 Determining the Niobium-Containing Vapour Species

The variation of the partial pressure of niobium-containing species in the equilibrium vapour would be expected to depend on the oxygen pressure through the equilibrium (5.8),

$$Nb_2O_5 = \left(\frac{2}{x}\right)Nb_xO_y(g) + \frac{1}{2}\left[5 - \left(\frac{2y}{x}\right)\right]O_2(g) \qquad (5.8)$$

where Nb_xO_y is the unknown gaseous species. Therefore, a log-log plot of the partial pressures of niobium-containing vapour species vs. oxygen pressure should yield a straight line with a slope of $-\frac{x}{4}\left[5-\left(\frac{2y}{x}\right)\right]$.

The most likely species were presumed to be, NbO, NbO_2, or Nb_2O_5 in the current experimental conditions. Correspondingly, the slopes expected for these species were, -3/4, -1/4 and 0 respectively. It seems that these slopes were sufficiently different; therefore, an experimental determination could be made to distinguish the possibilities.

The variation of partial pressure of niobium vapour species with oxygen partial pressure was determined at 1600°C. The partial pressure of the niobium-containing vapour species was calculated from the usual transpiration formula as shown in Equation 5.9,

$$p = \frac{\text{weight of } Nb_2O_5 \text{ loss}}{\text{mol wt of } Nb_2O_5} \cdot \frac{\text{total pressure}}{\text{moles of carrier gas}} \tag{5.9}$$

In this formula, p is the partial pressure of the niobium-containing vapour species under the assumptions:

(i) the controlled partial pressure of oxygen by CO_2/CO ratios is large enough that any oxygen produced or consumed by the vapourization is negligible;

(ii) if each gaseous molecule contains two niobium atom, i.e , Nb_2O_5, the partial pressure calculated from the above formula (5.9) would give the correct values for their pressures; however, if assuming vapour species contained one niobium atom, i.e., NbO or NbO_2, its partial pressure would be given by twice the value of the formula.

Variation of pressure of volatile Nb species (NbO_2 was assumed) with oxygen pressure over liquid Nb_2O_5 at 1600°C is shown in Figure 5.2. By least-square treatment of the experimental data, the slope of the line that best fit the data was -1/4, corresponding to the vapour species of NbO_2. In view of the scatter of the data, lines of slope -3/4 and 0 (corresponding to NbO and Nb_2O_5 as vapour species respectively) could not fit at all with the experimental data. Therefore, the only possible vapour species that can account for the slope of the log-log plot is NbO_2. Thus, Nb_2O_5 vapourizes according to the equilibrium (5.10),

$$Nb_2O_5(l) = 2NbO_2(g) + 1/2O_2(g) \tag{5.10}$$

5.3.4 Temperature Effect on p_{NbO_2} at a Constant p_{O_2}.

In the temperature range of 1798-1873K, the partial vapour pressure of $NbO_2(g)$ over $Nb_2O_5(l)$ calculated from the total weight loss measurements is shown as a function of reciprocal of temperature at 10^{-6} atm of O_2 in Figure 5.3.

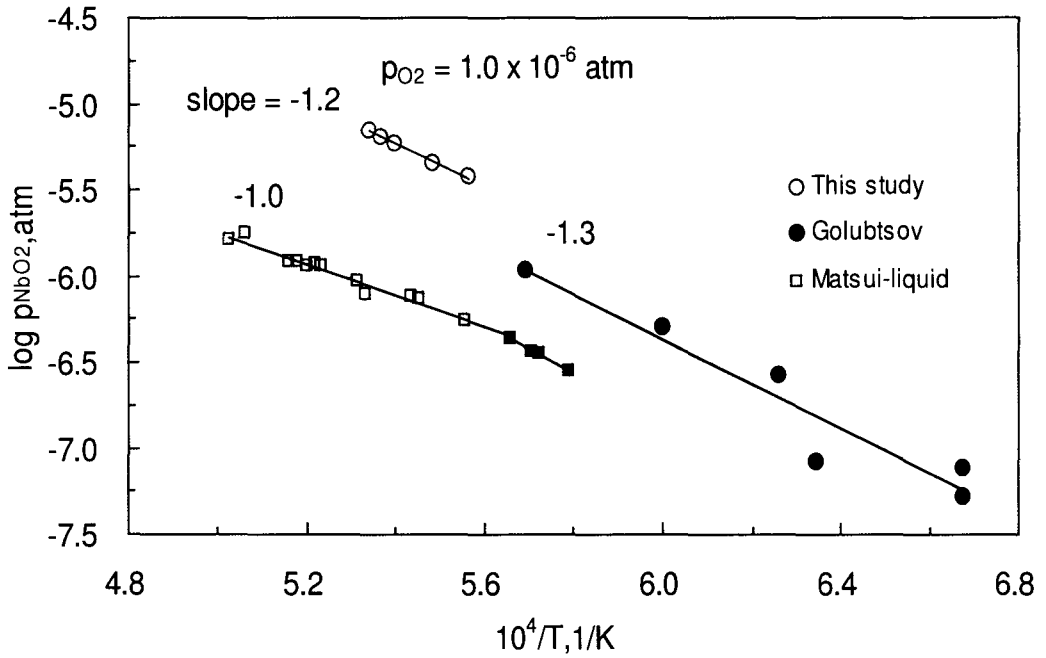

Figure 5.3. Dissociation vapour pressure of Nb_2O_5 as a function reciprocal of temperature at constant partial pressure of oxygen for the present study. As a comparison with the results by Golubtsov *et al.*(1960) and Matsui and Naito (Matsui and Naito, 1983).

The present results are shown together with the previous results by Golubtsov *et al.*. (Golubtsov *et.al.*, 1960) and Matsui and Naito (Matsui and Naito, 1983), whose results are about a factor of 10 lower than the present results, although the slope in the

plot of logarithm of vapour pressure vs. reciprocal temperature is observed to be in fairly good agreement with each other. The results of a least-square treatment of the vapour pressure obtained by the transpiration method is given as follows:

$$\log p_{NbO2,}atm = \frac{(-1.2 \pm 0.2)\times 10^4}{T} + (1.5 \pm 0.2) \qquad 1798 \le T \le 1873 \quad K \qquad (5.11)$$

Although the Knudsen cell method was employed in both Golubtsov and Matsui experiments, a factor of 5 of disagreement was indicated between the two authors. When you analyze the Knudsen cell, the NbO_2 vapour was in equilibrium with oxygen which is not controlled by the vacuum outside of the Knudsen cell, but controlled by the equilibrium indicated in Equation 5.10. As stated earlier, the dissociation vapour pressure of Nb_2O_5 was strongly associated with the partial pressure of oxygen. If there is no control of oxygen partial pressure, the measurement of vapour pressure of NbO_2 becomes ambiguous. Therefore, the present study with well controlled oxygen partial pressure is more convincing in the study of dissociation pressure.

The enthalpy of vapourization can be calculated from the slope of the graph in which vapour pressure was plotted against the reciprocal of temperature. The change in enthalpy of Nb_2O_5 liquid on vapourization was calculated in the usual manner from the slope of the vapour pressure curve. In the temperature range of study, the data give a constant 229.7 ± 38.2 kJ/mol. The present data differ from those of 191.4 ± 34.9 kJ/mol by Matsui and Naito, where it can be seen that the slope of the curve is different from this

study. There is no basis for comparing the two sets of data.

5.4 Conclusions

A vertical furnace with saturation cell was adapted as the transpiration apparatus for reliable vapour pressure measurements. The equilibrium nature of volatilization was established by a plateau in the plot of isothermal vapour pressure against the flow rate of the carrier gas.

The vapourization of liquid Nb_2O_5 was studied by the transpiration method under various oxygen pressures. The vapour pressure of NbO_2 above the liquid Nb_2O_5 was observed as a function of the partial pressure of oxygen. The results of a least-square treatment of the vapour pressure obtained by the transpiration method are given as follows:

$$\log p_{NbO_2} = -0.252 \log p_{O_2} - 6.777 \qquad \text{at } 1873\text{K}$$

The gaseous niobium oxide species was confirmed to be NbO_2; hence, Nb_2O_5 vapourizes by the reaction

$$Nb_2O_5(l) = 2NbO_2(g) + 1/2O_2(g)$$

At 10^{-6} atm of oxygen pressure the partial pressure of NbO_2 in the range of 1525-

1600°C can be expressed by the equation

$$\log p_{NbO2,}atm = \frac{(-1.2 \pm 0.2)\times 10^4}{T} + (1.5 \pm 0.2) \qquad 1798 \le T \le 1873 \quad K$$

The enthalpy of vapourization in that temperature range is 229.7 ± 38.2 kJ/mol although the slope in the plot of logarithm of vapour pressure vs. reciprocal temperature is observed to be in fairly good agreement with that of literature.

Chapter 6 Thermodynamic Properties of Niobium Oxide Bearing Slags

The thermodynamic properties of niobium oxide in the slag system of $CaO-SiO_2-NbO_x$ were measured by varying the experimental conditions of slag basicities, slag compositions, temperature and oxygen partial pressures. The effect of slag basicities on the vapour pressure of NbO_2, activity of NbO_x, activity coefficient of NbO_x and Nb^{5+}/Nb^{4+} ratios were studied in detail. The dependence of the NbO_2 vapour pressure, activity and activity coefficient on temperature is also addressed in this chapter. A niobium oxide bearing aluminate slag system of similar composition to that used in actual steel refining was studied by varying the factors of slag optical basicity and temperature. In order to predict the activity coefficient and activity of a niobium oxide bearing slag system, a regular solution model has been applied. However, insufficient interaction parameters as well as parameter conversions prevent the application of the regular solution model. The co-relationship between the ionic diameter and ionic energy was discovered and shows good agreement with calcium oxide and silicon oxide. With the interaction parameter and converting parameter attained, the regular solution model shows a good agreement on the activity coefficients between measurement and calculation.

6.1 Establishment of the Transpiration Method for $CaO\text{-}SiO_2\text{-}NbO_x$ System

An important variable in the transpiration technique is the flow rate of carrier gas. At very low flow rates, diffusive flow becomes significant; this leads to an overestimation of the equilibrium vapour pressure. On the other hand, at very high flow rates an apparently low value for the vapour pressure may result. Equilibrium conditions are indicated by a measured vapour pressure that is independent of flow rate in a range between these two extremes.

Experiments on $CaO\text{-}SiO_2\text{-}NbO_x$ melts were conducted to determine the equilibrium conditions in terms of the flows rate of carrier gas, which were chosen in the range of 20 to 70 ml per minute. Corresponding to the overall experimental design in slag compositions, three slag melts were prepared and the compositions listed in Table 6.1.

Table 6.1 Compositions of Slag Melts and Experimental Conditions

sample	Temperature	Compostion				Carrier Gas	
		Nb_2O_5	CaO	SiO_2	CaO/SiO_2	CO_2/CO	p_{O2}
	K	wt%	wt%	wt%	wt%/wt%		atm
slag 1	1873	10.0	50.0	40.0	1.3	0.06	$1.0x10^{-6}$
slag 2	1873	10.0	45.0	45.0	1.0	0.06	$1.0x10^{-6}$
slag 3	1873	5.0	47.5	47.5	1.0	0.06	$1.0x10^{-6}$

The preparation of slag melts and the experimental procedure was consistent with procedures stated in Chapter 3. The oxygen potential in these experimental runs was controlled by the CO_2/CO ratio, which gives $6x10^{-10}$ atm at 1873K. Data collected on the $CaO\text{-}SiO_2\text{-}NbO_x$ melts with three compositions at 1600°C are presented in Figure 6.1.

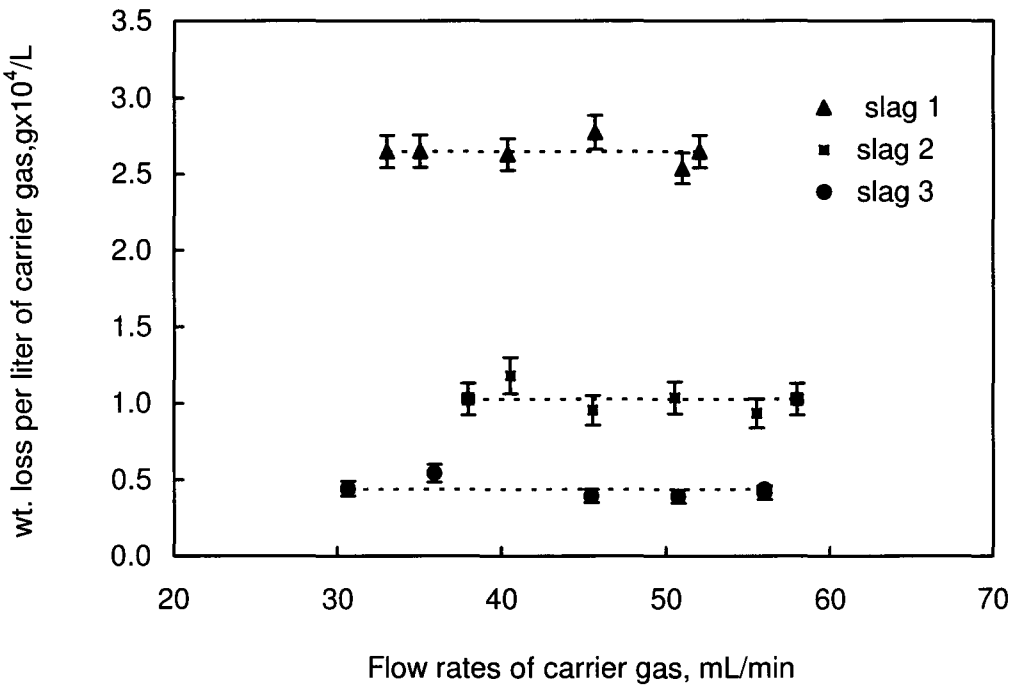

Figure 6.1 Weight loss of niobium dioxide as a function of flow rate of carrier gas at 1873K in $CaO\text{-}SiO_2\text{-}NbO_x$ melts.

As shown in Figure 6.1, plateau regions where the weight loss of niobium dioxide per liter of carrier gas was independent of carrier gas flow rate were observed for the three conditions. Based on the location of the plateau region in Figure 6.1, the flow rate of carrier gas was chosen to be 45 mL/min for all experiments in the $CaO\text{-}SiO_2\text{-}NbO_x$

slag system.

As shown in Figure 6.1, the higher basicity, as defined by CaO/SiO_2 mass percent ratios, will give higher vapour pressures of niobium dioxide.

In order to reinforce these observations, factors and ranges have been determined by Design of Experiment (DOE), as presented in Table 6.2; CO_2/CO ratios were designed to be low enough to ensure measurable weight loss and high enough for an insignificant change in activity due to removal of NbO_2.

Table 6.2 Designed Experimental Factors and Ranges

Factors	Conditions			
flow rate, mL/min	45			
T, K	1773-1873			
exp.time, min	1320			
initial Nb_2O_5, wt%	5%		10%	
CaO/SiO_2	0.8	1.0	1.2	1.5
CO_2/CO	0.24	0.76	2.41	7.63
p_{O2}, atm	$1.0x10^{-8}$	$1.0x10^{-7}$	$1.0x10^{-6}$	$1.0x10^{-5}$

Two series of experiments are reported in this chapter. The first was conducted in the system $CaO\text{-}SiO_2\text{-}NbO_x$ with two initial amounts of Nb_2O_5 and four slag basicities at $p_{O_2} = 10^{-5}, 10^{-6}, 10^{-7}$ and 10^{-8} atm. The second series was conducted at $p_{O_2} = 10^{-6}$ and 10^{-8} respectively with the addition of varying amounts of Al_2O_3 to the system $CaO\text{-}SiO_2\text{-}NbO_x$.

6.2 Calculations of Activities and Activity Coefficients of Nb_2O_5 and NbO_2

6.2.1 Determining Vapour Pressure of NbO_2

The equilibrium partial pressure of NbO_2, p_{NbO_2}, shown on the plateau regions in Fig. 6.1, was obtained from the measured weight loss of Nb, w, converting to loss of NbO_2, considering NbO_2 is the singular vapour species, which has been validated in the previous chapter. The volume of carrier gas passes, corrected to standard temperature and pressure, V_c, as,

$$p_{NbO_2} = \frac{n_v}{n_v + n_f} \cdot P_t \tag{6.1}$$

The total pressure P_t is 1 atm, therefore,

$$p_{NbO_2} = \frac{\frac{w}{92.9} \times 124.9}{\frac{w}{92.9} \times 124.9 + \frac{V_c}{22.4}} \tag{6.2}$$

where 92.9 and 124.9 are the molecular weights of Nb and NbO_2 respectively.

6.2.2 Calculation of Activities and Activity Coefficients

The activity of niobium oxide in slag melts was derived from the vapour pressure, partial pressure of oxygen and equilibrium constant for reaction (6.3) as described below:

$$NbO_{2.5}(l,\text{in slag}) = NbO_2(g) + \frac{1}{4}O_2(g) \tag{6.3}$$

Where *s*, *l* and *g* denote the standard states of pure substances, solid, liquid and gas, respectively.

The equilibrium constant for reaction (6.3) is given in Equation (6.4),

$$K = \frac{p_{NbO_2} p_{O_2}^{1/4}}{a_{NbO_{2.5}}} \tag{6.4}$$

In which, p represents partial pressure and a_i is the activities of the various species and K is the equilibrium constant. The reference state for $NbO_{2.5}$ is pure liquid in the temperature range of interest at 1-atm total pressure.

If Nb_2O_5 was a pure liquid, which gives activity of Nb_2O_5 of unity, the equilibrium constant K can be determined by measuring the vapour pressures of NbO_2 under controlled oxygen potentials at constant temperature, as presented in Chapter 5.

With the known equilibrium constant at 1873 K for reaction (6.3), the activity of

Nb_2O_5 in silicate slags is easily calculated by measuring the vapourization of NbO_2 from slag melts shown in Equation (6.5).

$$a_{NbO_{2.5}} = \frac{p_{NbO_2} p_{O_2}^{1/4}}{K} \tag{6.5}$$

Under the controlled atmosphere, there are two valence states for niobium in the slag melts, thus, it is also known,

$$NbO_{2.5}(l, \text{in slag}) = NbO_2(s \text{ or } l, \text{in slag}) + \frac{1}{4}O_2(g) \tag{6.6}$$

$$\Delta G_2^{\circ} = 214159.74 - 27.28T \text{ (Chase, 1998)}$$

where, ΔG_2° is the standard free energy of reaction (6.6).

Thus,
$$a_{NbO_2} = \sqrt{\frac{\exp(-\Delta G_2^0 / RT) \cdot a_{Nb_2O_5}}{p_{O_2}^{1/2}}} \tag{6.7}$$

With knowledge of the mole fraction of Nb^{5+} and Nb^{4+} from potentiometric titration measurements, the activity coefficients of NbO_2 and Nb_2O_5 can be determined by

$$\gamma_{Nb_2O_5} = a_{NbO_{2.5}} / x_{Nb^{5+}} \tag{6.8}$$

And $$\gamma_{NbO_2} = a_{NbO_2}/x_{Nb^{4+}} \quad (6.9)$$

Where, x is the mole fraction of the ionic species. Therefore, measuring the vapourization of niobium oxide from both pure substance and slag melt will result in the thermodynamic properties of the slags.

6.3 Experimental Results

6.3.1 Effect of Slag Basicity

A total of eight compositions of slag melts with four CaO/SiO_2 ratios and two different initial Nb_2O_5 contents have been prepared and analyzed following the procedure described in Chapter 3. Measurements for each composition of slag were conducted for a range of oxygen partial pressure from 10^{-5} to 10^{-8} atm at a constant temperature of 1873K. The data used to construct the graphs are presented in Appendix B.

6.3.1.1 Vapour Pressure of NbO_2

The dependence of vapour pressure of NbO_2 on slag optical basicity in the CaO-SiO_2-NbOx slag system is shown in Figure 6.2, in which temperature and initial content of Nb_2O_5 remained constant. The data used in calculating the optical basicity are given in Table 6.3. It can be seen that the measured vapour pressure of NbO_2 insignificantly rises with increased slag basicities at a fixed oxygen partial pressure. This dependence of

vapour pressure of NbO_2 on slag basicity showed consistency in the oxygen range of 10^{-5} to 10^{-9} atm in the $CaO\text{-}SiO_2\text{-}NbO_x$ slag system. As the partial pressure of oxygen over liquid slag at a given temperature is lowered, Nb_2O_5 will reduce to a liquid solution richer in NbO_2 and leaner in Nb_2O_5 therefore the vapour pressure of NbO_2 increases accordingly. As a result, the vapour pressure of NbO_2 increases with decreasing oxygen partial pressure.

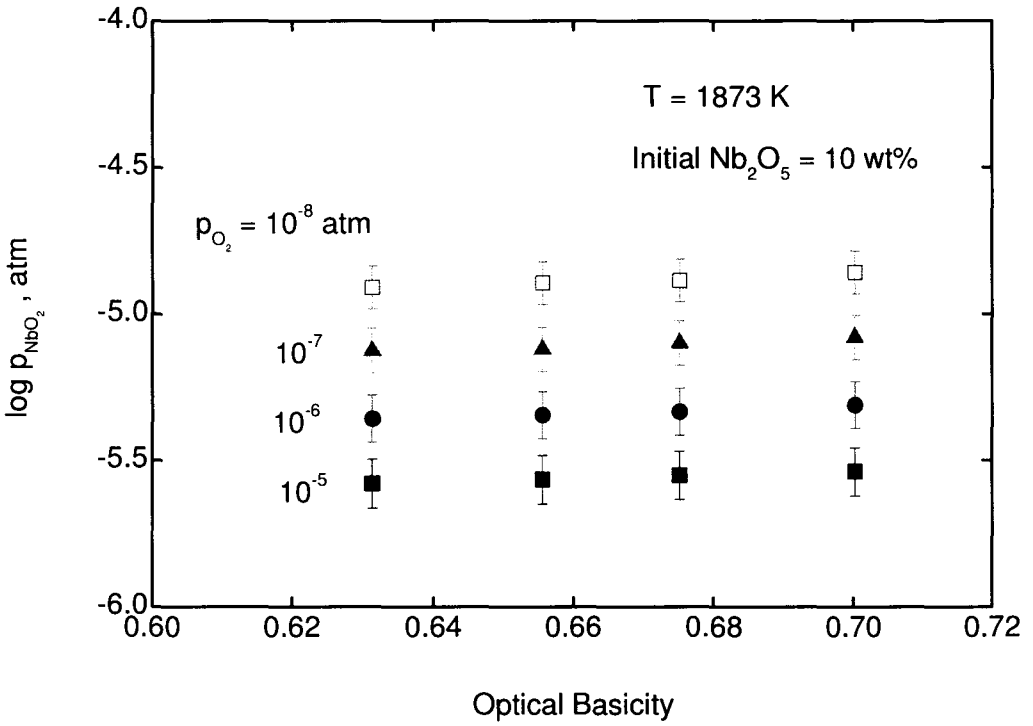

Figure 6.2. Dissociation vapour pressure of niobium oxide as a function of optical basicity in $CaO\text{-}SiO_2\text{-}NbO_x$ system at 1873K containing 10 mass pct Nb_2O_5.

Table 6.3 Data used to compute optical basicity

Materials	number of oxygen	optical basicity	reference temperature
CaO	1	1	2572
SiO_2	2	0.48	
$AlO_{1.5}$	1.5	0.597	
NbO_2	2	0.55	
$NbO_{2.5}$	2.5	0.55	1710

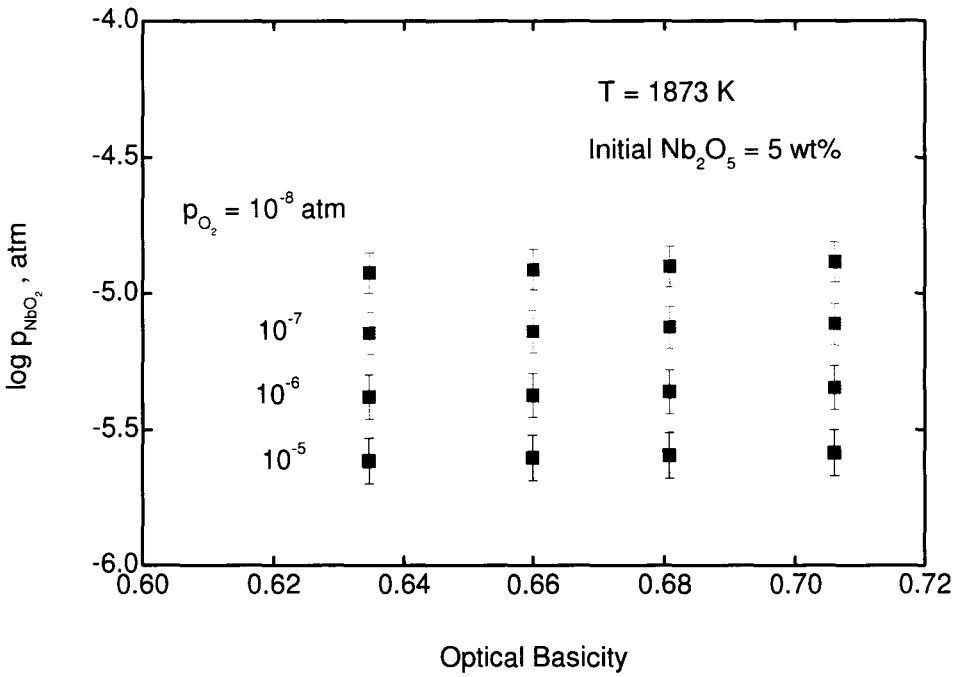

Figure 6.3. Dissociation vapour pressure of niobium oxide as a function of optical basicity in $CaO\text{-}SiO_2\text{-}NbO_x$ system at 1873K containing 5 mass pct Nb_2O_5.

The consistency of the vapour pressure of NbO_2 as a function of slag optical basicity is also presented in Figure 6.3, where CaO/SiO_2 ratios remain the same whereas initial Nb_2O_5 content was reduced to 5wt% in the $CaO\text{-}SiO_2\text{-}NbO_x$ slag system. Comparing Figure 6.2 and 6.3 with different initial Nb_2O_5 content, it can be seen that the higher the initial content, the higher the vapour pressure of NbO_2 if all other conditions remain the same.

Although vapour pressure of NbO_2 shows a negligible increase with increasing basicity, attention should be given in interpreting this result, as a repartitioning of the Nb^{4+}/Nb^{5+} ratio can compensate the effect of basicity, shown in the next section where Nb^{4+}/Nb^{5+} changes significantly with basicity. A more informative plot would be that of activity coefficient versus basicity which is shown in Figure 6.10 (page 128).

6.3.1.2 Activities

The effect of slag basicity on the activity of niobium oxide in the present slag system has been investigated at two levels of niobium content in the $CaO\text{-}SiO_2\text{-}NbO_x$ system, as shown in Figure 6.4 for 10wt% Nb_2O_5 and Figure 6.5 for 5wt%, respectively. The activity of niobium oxide with respect to the pure liquid state was evaluated based on the oxygen partial pressures previously determined.

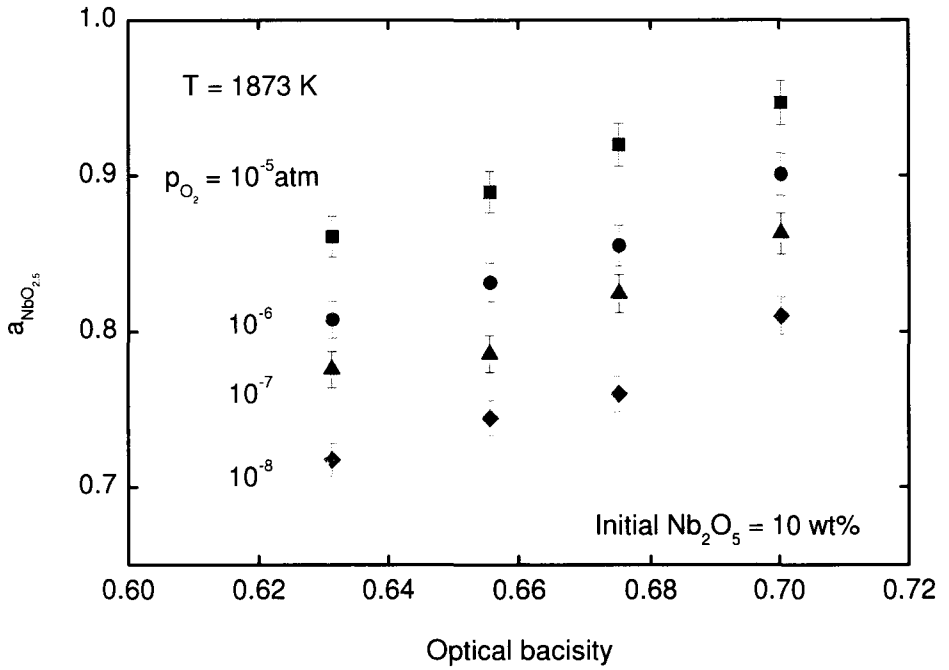

Figure 6.4 Activities of Nb_2O_5 in $CaO\text{-}SiO_2\text{-}NbO_x$ melts at 1600°C as a function of basicities at four oxygen pressures.

It can be seen that $a_{NbO_{2.5}}$ is strongly dependent on slag basicity with the initial 10wt% Nb_2O_5 at 1873K. At a given oxygen potential, $a_{NbO_{2.5}}$ linearly increases with increasing slag basicity in the range of 0.6 to 0.7, calculated from Table 3. This linear relationship is maintained at all oxygen potentials from 10^{-5} to 10^{-8}atm.

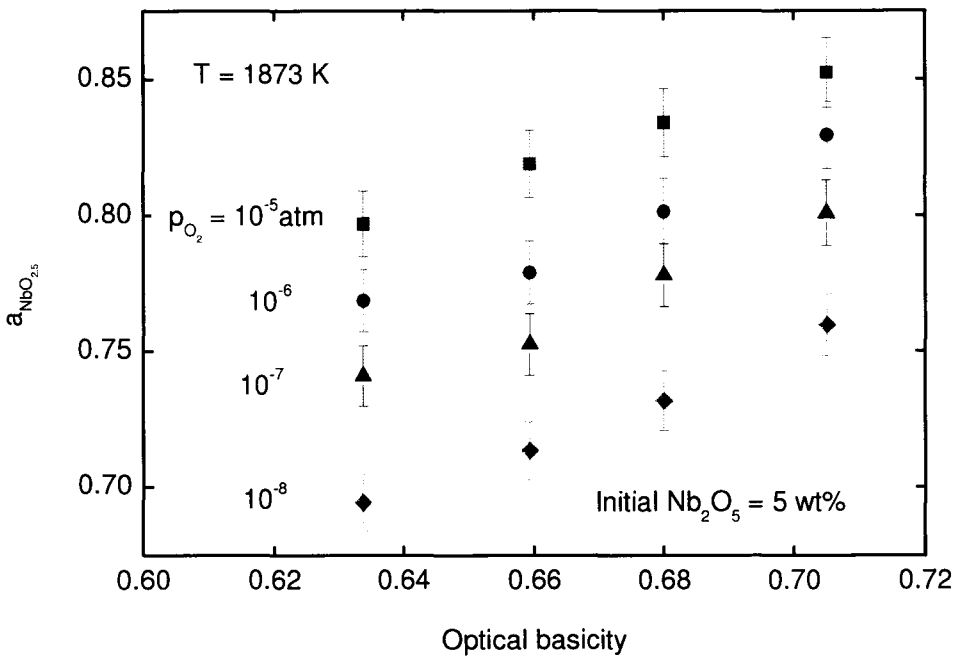

Figure 6.5 Activities of Nb_2O_5 in $CaO-SiO_2-NbO_x$ melts at 1600°C as a function of basicities at four oxygen pressures containing 5 mass pct Nb_2O_5

Additionally, another series of experiments with an initial 5wt% of Nb_2O_5 was conducted varying the CaO/SiO_2 ratios from 0.8 to 1.5 at a constant temperature. The same dependence of $a_{NbO_{2.5}}$ on slag basicity was observed as for 10 wt% Nb_2O_5. However, the lower the initial content of Nb_2O_5, the lower the $a_{NbO_{2.5}}$.

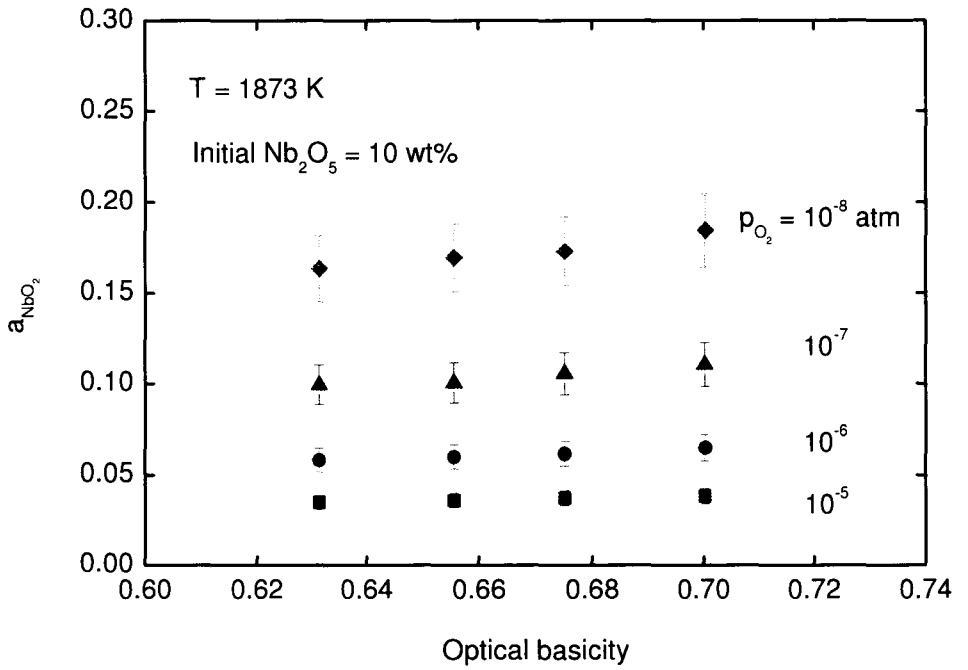

Figure 6.6 Activities of NbO_2 in $CaO\text{-}SiO_2\text{-}NbO_x$ melts at 1600°C as a function of basicities at four oxygen pressures.

Representative plots of the NbO_2 activities in this system, at all p_{O_2} values, are shown in Figure 6.6 and 6.7 (liquid NbO_2 is used as the reference state), where slag basicity is defined by optical basicity. Activity of NbO_2 shows a negligible increase with increasing basicity; however care should be taken in interpreting this result, as a repartitioning of the Nb^{4+}/Nb^{5+} ratio can compensate the effect of basicity. This is seen in the next section where Nb^{4+}/Nb^{5+} changes significantly with basicity. A more informative plot would be that of activity coefficient versus basicity which is shown in Figure 6.10. Comparing Figure 6.4 and 6.6 in the same range of slag basicity, less

dependence of a_{NbO_2} was observed. a_{NbO_2} increases with decreasing oxygen potential, which shows consistency both in 5wt% and 10wt% initial Nb_2O_5 content. However, the dependence of a_{NbO_2} on oxygen partial pressure reverses as shown in Figure 6.4, where $a_{NbO_{2.5}}$ increases with increasing oxygen partial pressure.

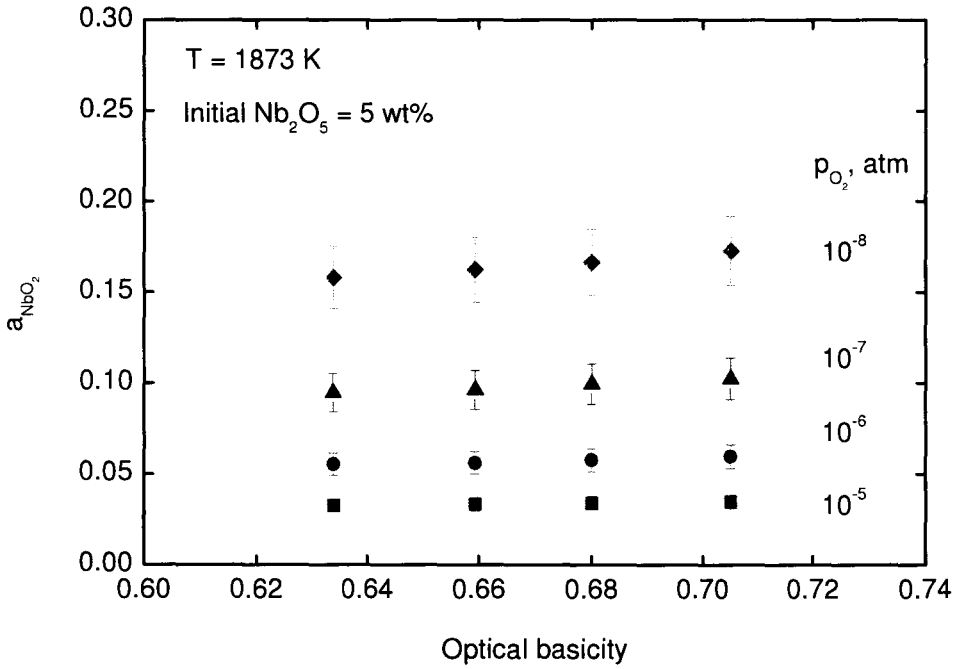

Figure 6.7 Activities of NbO_2 in $CaO\text{-}SiO_2\text{-}NbO_x$ melts at 1600°C as a function of basicities at four oxygen pressures.

6.3.1.3 Nb^{5+}/Nb^{4+} Ratios

It has been shown that both Nb^{4+} and Nb^{5+} are present in the melts corresponding to the conditions of this study and that equilibrium exists between them as discussed

previously. The effect of slag composition on the Nb^{4+} and Nb^{5+} partitioning was examined by varying the CaO/SiO_2 ratio. The measured Nb^{4+}/Nb^{5+} ratios are plotted against the optical basicity at 10 mass pct NbO_x and different oxygen partial pressures in Figure 6.8.

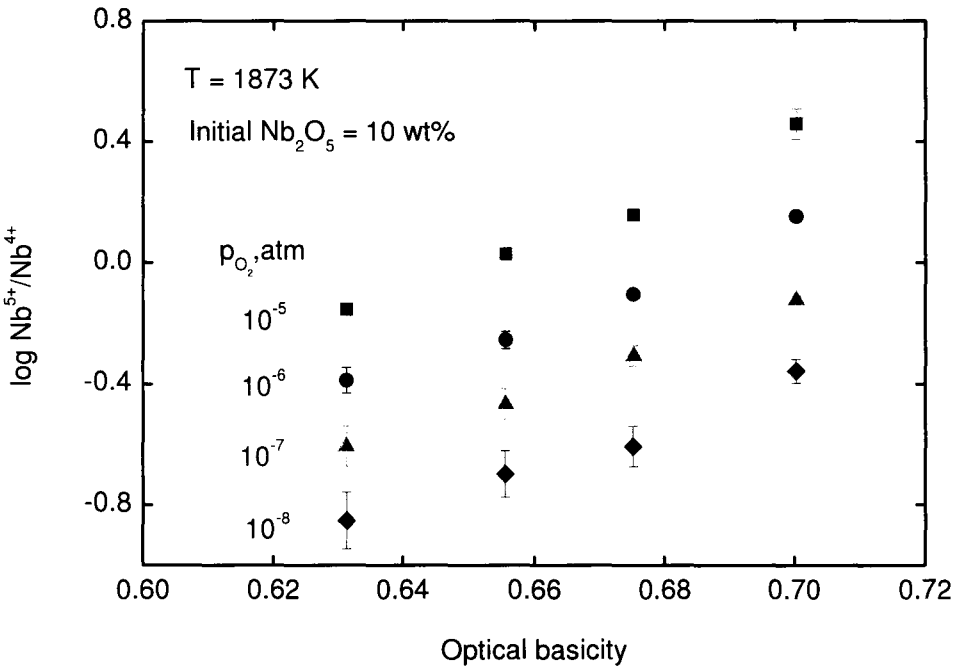

Figure 6.8 Variation of the Nb^{5+}/Nb^{4+} ratio with optical basicity in $CaO-SiO_2-NbO_x$ melts containing 10 mass pct Nb_2O_5 at various oxygen partial pressures

As can be seen in Figure 6.8, the ratios of Nb^{4+}/Nb^{5+} strongly depends on the slag compositions and oxygen partial pressure. The Nb^{5+} content increases with increasing slag basicity while the Nb^{4+} content decreases. In the meantime, the content of Nb^{5+} in the slag system increases with increasing oxygen partial pressure, while that of Nb^{4+}

decreases accordingly at a given temperature. As slag basicity increases, the higher valence state is stabilized.

6.3.1.4. Activity coefficient

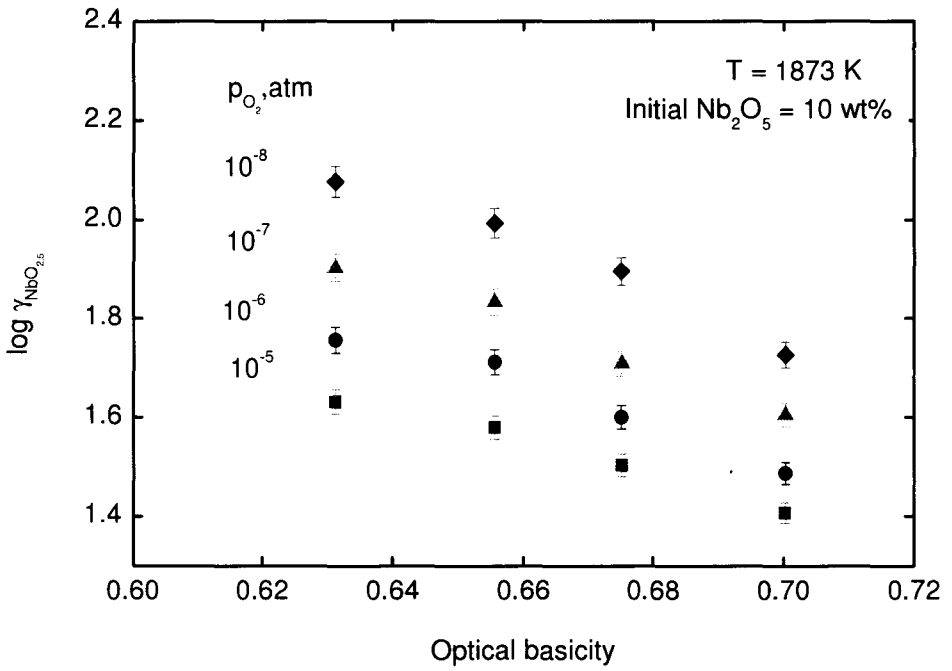

Figure 6.9 Activity coefficient of $NbO_{2.5}$ as a function of melt basicity and p_{O_2} in system $CaO\text{-}SiO_2\text{-}NbO_x$ at 1600°C

The calculated activity coefficients of $NbO_{2.5}$ ($\gamma_{NbO_{2.5}}$) and NbO_2 (γ_{NbO_2}) for melts are plotted as a function of p_{O_2} and melt basicity in Figures 6.9 and 6.10 respectively. It

can be seen that $\gamma_{NbO_{2.5}}$ decreased with increasing basicity, which suggests acidic behaviour for $NbO_{2.5}$ over the entire range of the composition measured in this study, as shown in Figure 6.9. The activity coefficients for $NbO_{2.5}$ are relatively large, indicating a positive deviation from ideality in this slag system.

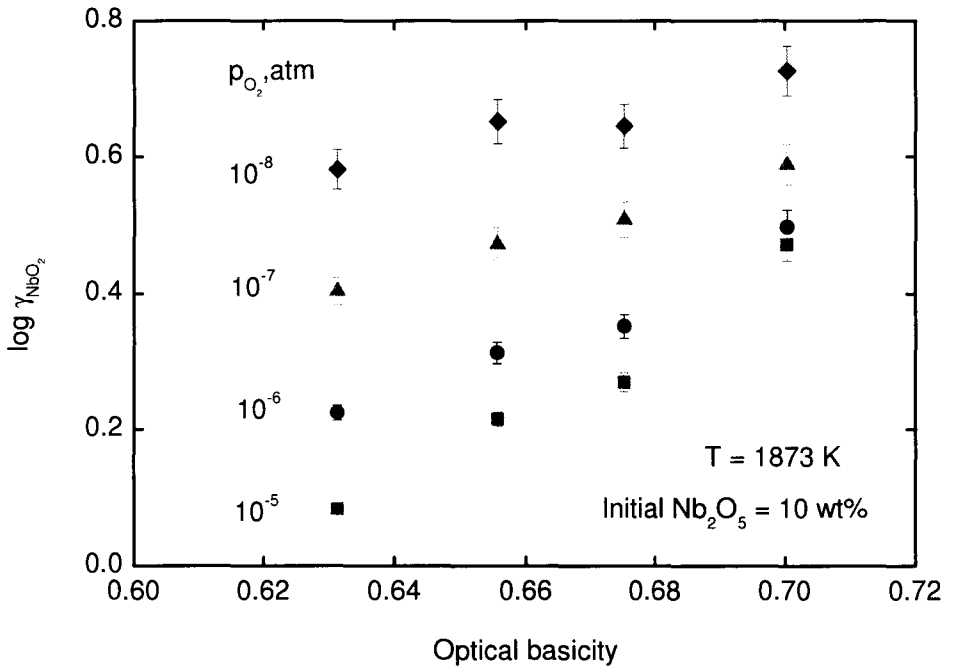

Figure 6.10 Activity coefficient of NbO_2 as a function of melt basicity and p_{O_2} in system $CaO\text{-}SiO_2\text{-}NbO_x$ at 1600°C

The potentiometric technique can quantitively distinguish the valence state and ratios of Nb^{4+}/Nb^{5+}, which enables computation of the activity coefficient of γ_{NbO_2} and $\gamma_{NbO_{2.5}}$ individually. γ_{NbO_2} is shown as a function of slag basicity and oxygen partial

pressure in Figure 6.10, in which log γ_{NbO_2} linearly increases with increasing slag basicity at a given oxygen partial pressure. The dependence of γ_{NbO_2} on slag basicity shows a reverse trend compared with that of $NbO_{2.5}$ in the same slag system, as shown in Figure 6.9. In the mean time, the oxygen partial pressure also presents a different effect on the activity coefficient of NbO_2 and $NbO_{2.5}$, namely, at a given slag basicity, γ_{NbO_2} increases with decreasing oxygen partial pressure while $\gamma_{NbO_{2.5}}$ increases with increasing oxygen partial pressure. This may suggest that NbO_2 appears to behave as a basic oxide in this basicity range of slag melts.

6.3.2 Temperature Dependence

The experimental results of $NbO_{2.5}$ activity, activity coefficient as well as vapour pressure of NbO_2 all present a dependency on temperature as shown in Figures 6.11-6.14. $NbO_{2.5}$ activity increases linearly with increasing temperature in the plot of logarithm of activity against reciprocal temperature as shown in Figure 6.11. The temperature effect on $NbO_{2.5}$ activity is more significant than that of slag compositions.

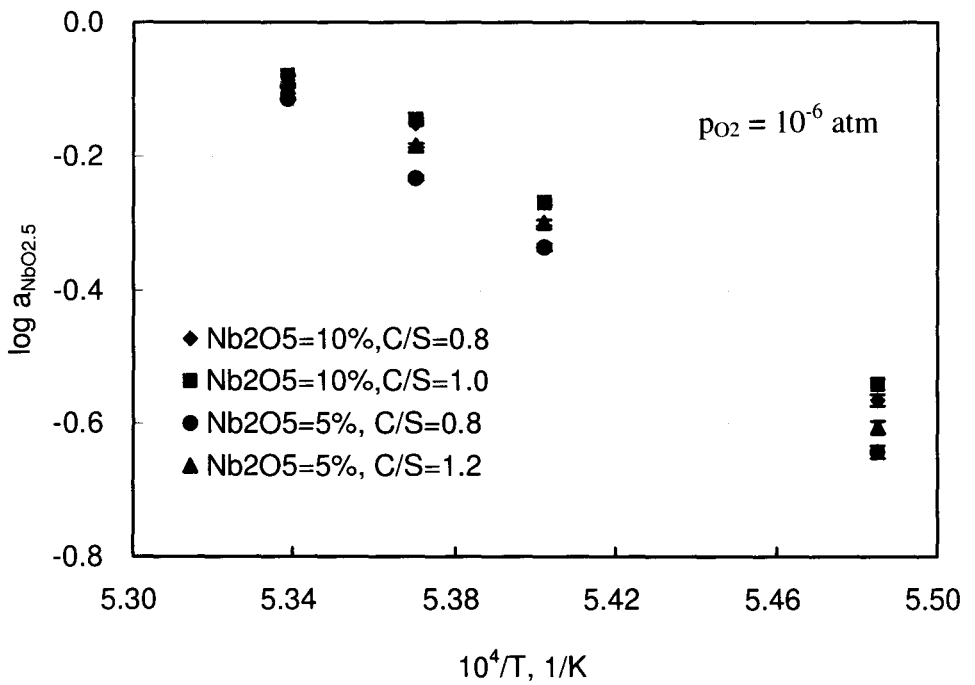

Figure 6.11 Temperature effect on the activity of $NbO_{2.5}$ in $CaO\text{-}SiO_2\text{-}NbO_x$ system at a constant oxygen partial pressure.

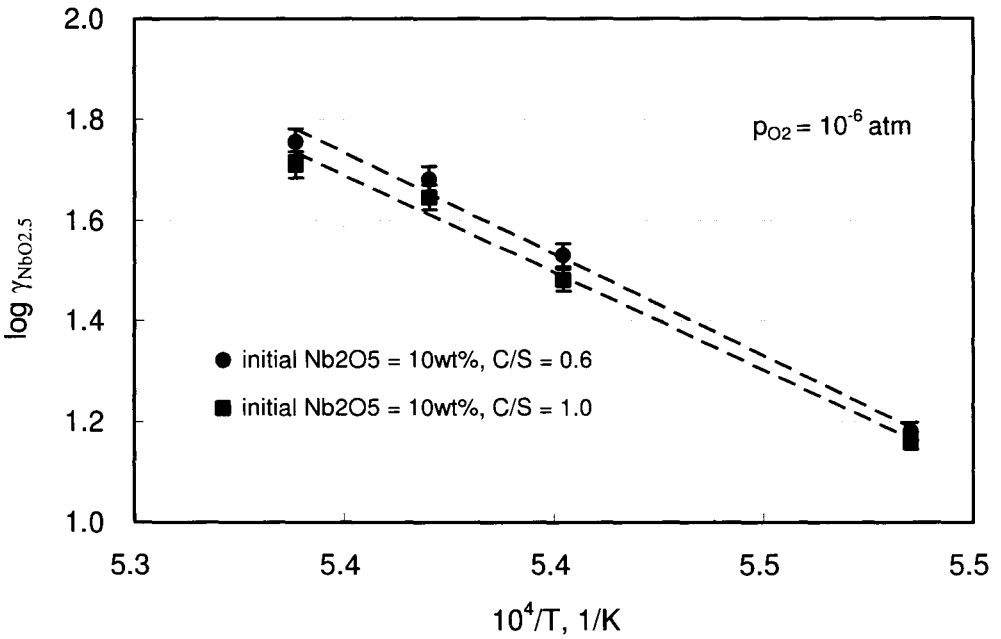

Figure 6.12 Temperature and slag composition effect on the activity coefficient of $NbO_{2.5}$ in $CaO\text{-}SiO_2\text{-}NbO_x$ slag system with constant oxygen pressure.

The activity coefficient of $NbO_{2.5}$, is not only a function of temperature, but also a function of slag basicity as shown in Figure 6.12, however, the effect of C/S ratio is less significant compared to the temperature effect. The vapour pressure of NbO_2 also increases with increasing temperature given that the initial niobium content and partial pressure of oxygen remain the same. With respect to the measured vapour pressure of NbO_2, as seen in Figure 6.13, the effect of slag basicity is insignificant when compared with that of reaction temperature.

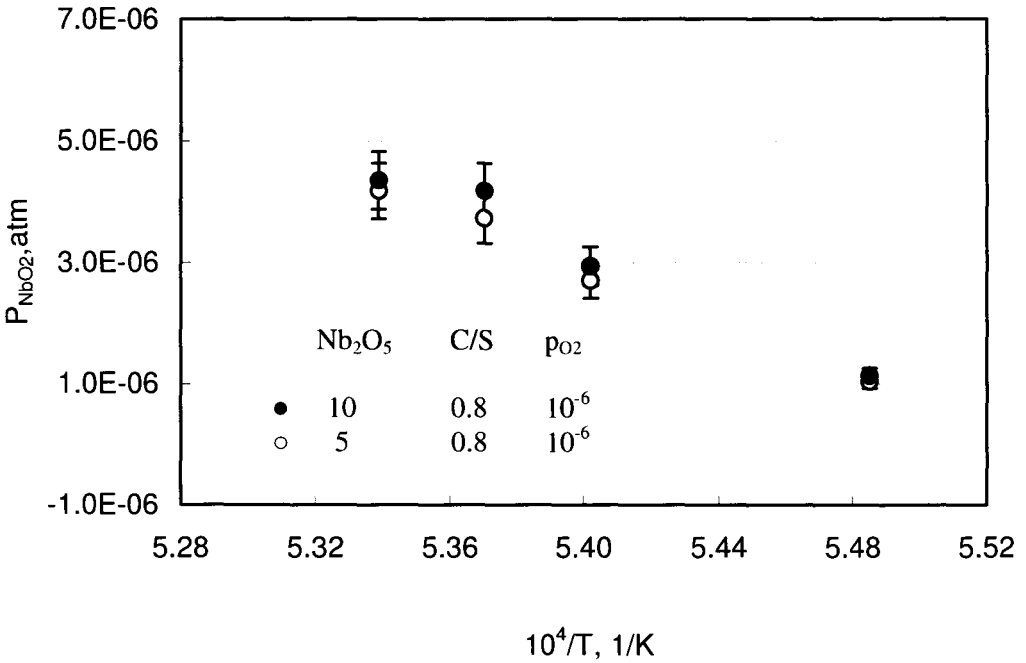

Figure 6.13 Temperature effects on the vapour pressure of NbO_2 in $CaO\text{-}SiO_2\text{-}NbOx$ system at constant vapour pressure of oxygen.

The ratio of $Nb^{5+}/Nb^{4+} \cdot (p_{O_2})^{-1/4}$ shows a decrease with increasing temperature as shown in Figure 6.14. The slag niobium oxide content presents a significant effect on this ratio when compared with the temperature effect.

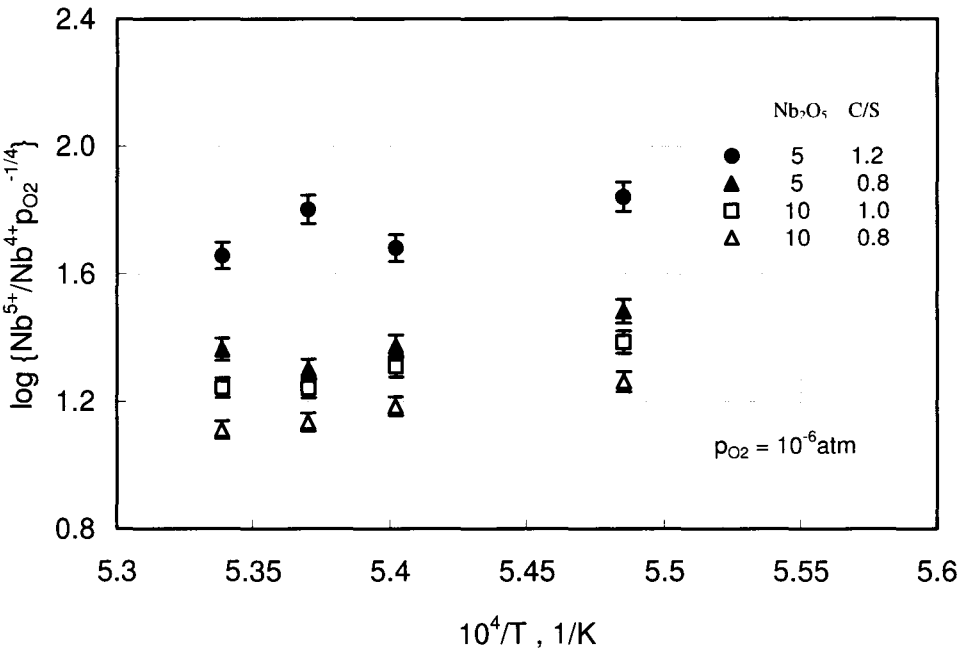

Figure 6.14 Variation of $\log\{Nb^{5+}/Nb^{4+}p_{O_2}^{-1/4}\}$ with reciprocal temperature in various niobium oxide containing slags.

6.3.3 Effect of Partial Pressure of Oxygen

It is well known that many transition cations exist in molten slags and glasses in two valency states, their relative proportions depending on temperature, pressure, composition, and oxygen potential of the system (Turkdogan, 1983).

One of the objectives of the present study was to map the niobium redox behaviour in the $CaO\text{-}SiO_2\text{-}NbO_x$ system under conditions where Nb^{5+} and Nb^{4+} are the predominant oxidation states. The Nb^{5+}/Nb^{4+} ratio was determined as a function of oxygen partial pressure at a constant temperature. The effect of the partial pressure of

oxygen on the vapour pressure of NbO_2 was also well studied by varying the slag compositions at constant temperature.

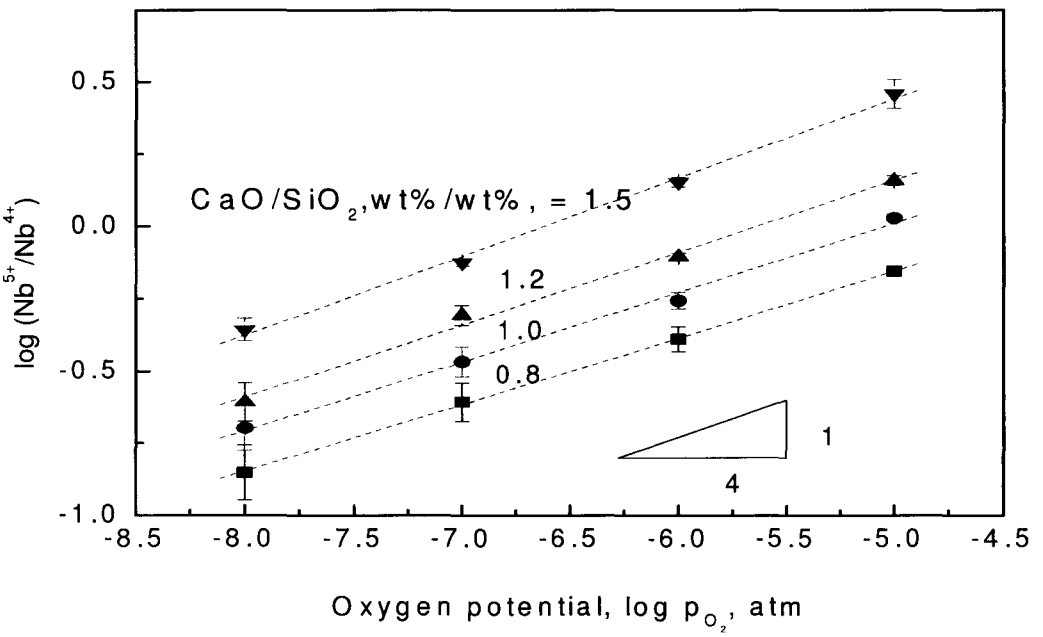

Figure 6.15. Nb^{5+}/Nb^{4+} ratio in $CaO\text{-}SiO_2\text{-}NbO_x$ melts at 1600°C as a function of oxygen pressure and slag composition (total NbO_x content corresponds to 10 wt% Nb_2O_5 in the starting mixture)

As shown in Figure 6.15, the ratio of Nb^{5+}/Nb^{4+} is not only a function of slag composition but also a function of oxygen potential. At a given slag composition, Nb^{5+} increases with increasing oxygen partial pressure, which indicates more Nb^{4+} is oxidized to form Nb^{5+}. This dependence of Nb^{5+}/Nb^{4+} ratio on oxygen partial pressure shows consistency in the slag compositions in this study.

It also can be seen in Figure 6.16 that vapour pressure of NbO_2 is dependent on

the partial pressure of oxygen at a constant temperature. $\log p_{NbO_2}$ linearly increases with $\log p_{O_2}$. However, from Figure 6.16, the effect of oxygen partial pressure on the vapour pressure of NbO_2 is more significant than the effect of various slag compositions. Both initial Nb_2O_5 content and C/S ratio are insignificant.

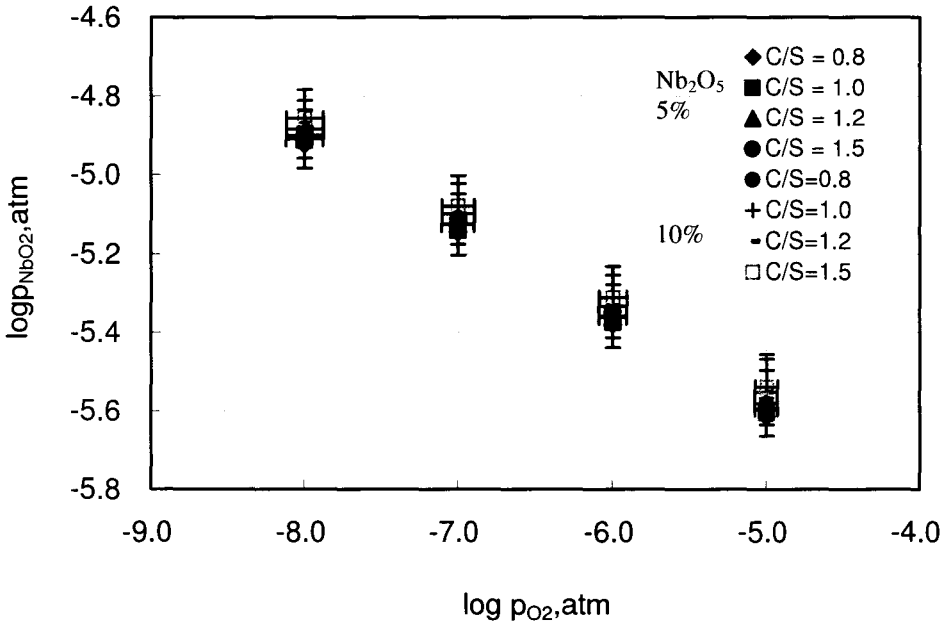

Figure 6.16 Vapour pressure of NbO_2 as a function of oxygen partial pressure measured at 1873K and 5% and 10% initial Nb_2O_5.

6.3.4 Effect of Al_2O_3 Addition

The experiments attempting to investigate the effect of adding Al_2O_3 were conducted with the slag composition similar to those of ladle slags in steelmaking. In this series of experiments, two levels of oxygen partial pressure were chosen in the CaO-SiO_2-Al_2O_3-NbO_x slag system at a constant temperature. The experimental conditions

and slag compositions are tabulated in Table 6.4.

Table 6.4 Overall experimental design

Exp.No.	Temperature (K)	p_{O2} (atm)	CO_2/CO	initial Nb_2O_5 (wt%)	optical basicity	Al_2O_3 content
R1	1873	1.0E-06	2.41	11.86	0.79	0.091
R2	1873	1.0E-06	2.41	12.18	0.76	0.142
R3	1873	1.0E-06	2.41	11.28	0.74	0.171
R4	1873	1.0E-06	2.41	9.94	0.72	0.234
R5	1873	1.0E-06	2.41	11.38	0.70	0.267
S1	1873	1.0E-08	0.24	11.86	0.79	0.096
S2	1873	1.0E-08	0.24	12.18	0.76	0.145
S3	1873	1.0E-08	0.24	9.65	0.74	0.186
S4	1873	1.0E-08	0.24	9.94	0.72	0.236
S5	1873	1.0E-08	0.24	11.15	0.7	0.270

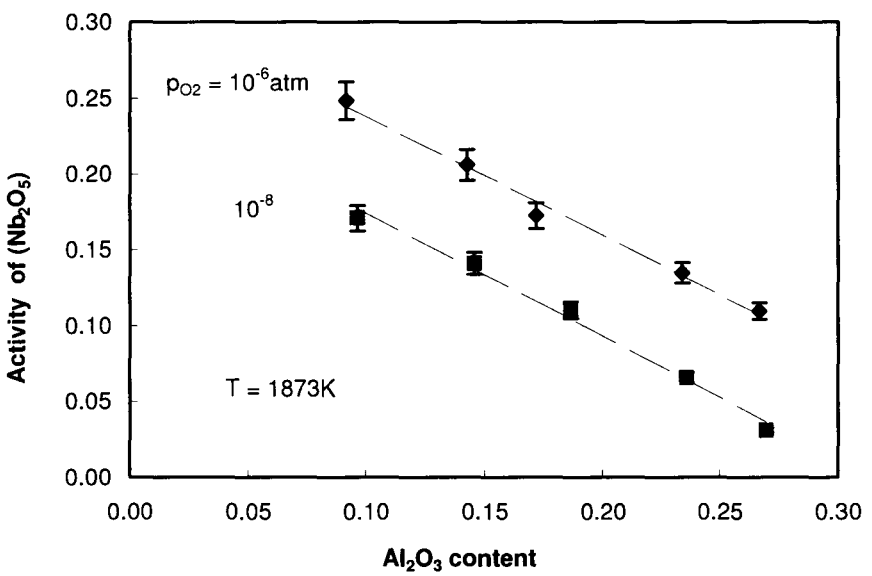

Figure 6.17 Effect of Al_2O_3 addition to the activity of Nb_2O_5 in $CaO\text{-}SiO_2\text{-}Al_2O_3\text{-}NbO_x$ slag system at 1873 K.

The Al_2O_3 content was defined by the molar ratio of $N_{Al_2O_3}/(N_{CaO}+N_{SiO_2}+N_{Al_2O_3}+N_{NbO_{2.5}}+N_{NbO_2})$. The effect of Al_2O_3 content on the activities of niobium oxides, activity coefficient as well as the vapour pressure of NbO_2 are shown in Figure 6.17 through Figure 6.20. The effects of Al_2O_3 addition are detectable in the range of Al_2O_3 content increasing from 0.1 to 0.3. As can be seen, the addition of Al_2O_3 will decrease both the activities of niobium pentoxide and niobium oxide.

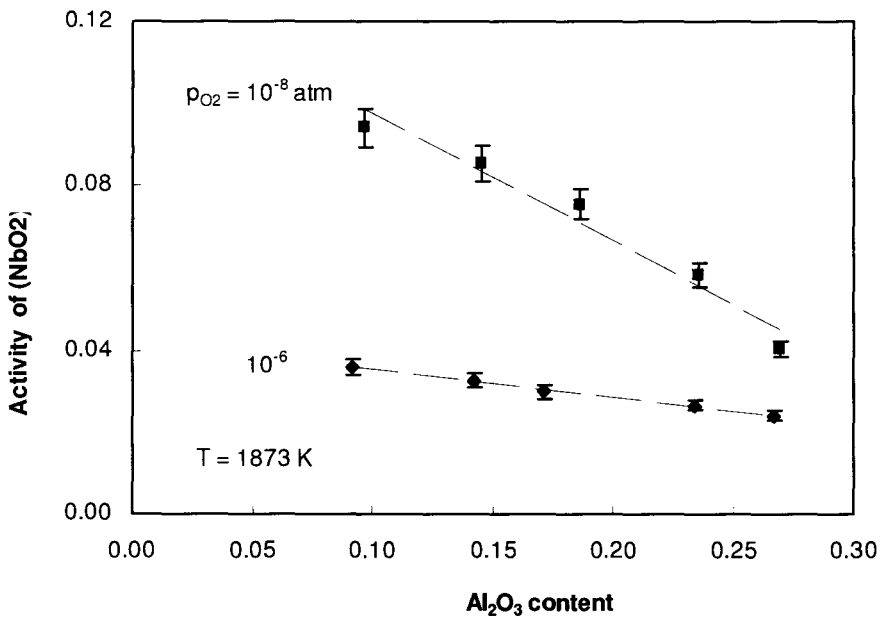

Figure 6.18 Effect of Al_2O_3 addition to the activity of NbO_2 in CaO-SiO_2- Al_2O_3-NbO_x slag system at 1873 K.

The dependence of the activity of niobium pentoxide on Al_2O_3 content shows the same trend in two levels of oxygen partial pressure. However, the activity of NbO_2

slightly decreases by increasing Al_2O_3 content at lower oxygen pressure and rapidly decreases at higher oxygen pressure, as shown in Figure 6.18.

However, Al_2O_3 content increases the activity coefficient of $NbO_{2.5}$ in the range of 0.1 to 0.3 at the two oxygen partial pressure conditions seen in Figure 6.19.

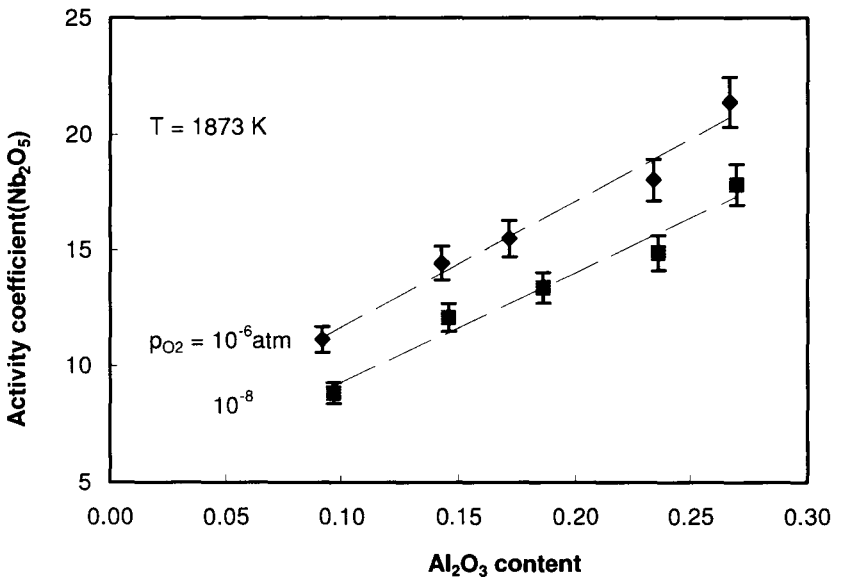

Figure 6.19 Effect of Al_2O_3 addition to the activity coefficient of Nb_2O_5 in CaO-SiO_2- Al_2O_3-NbO_x slag system at 1873 K.

Al_2O_3 addition has indicated an effect on the vapour pressure of NbO_2. As seen in Figure 6.20, the vapour pressure of NbO_2 decreases as Al_2O_3 content increases in the slag composition. On the other hand, vapour pressure of NbO_2 decreases more rapidly at lower oxygen pressure.

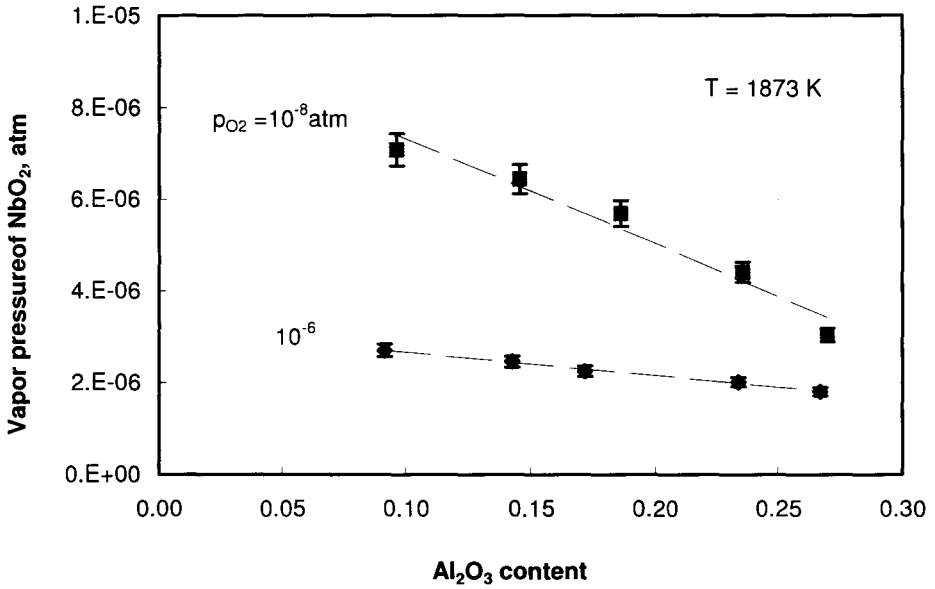

Figure 6.20 Effect of Al_2O_3 addition to the vapour pressure of NbO_2 in CaO-SiO_2- Al_2O_3-NbO_x slag system at 1873 K.

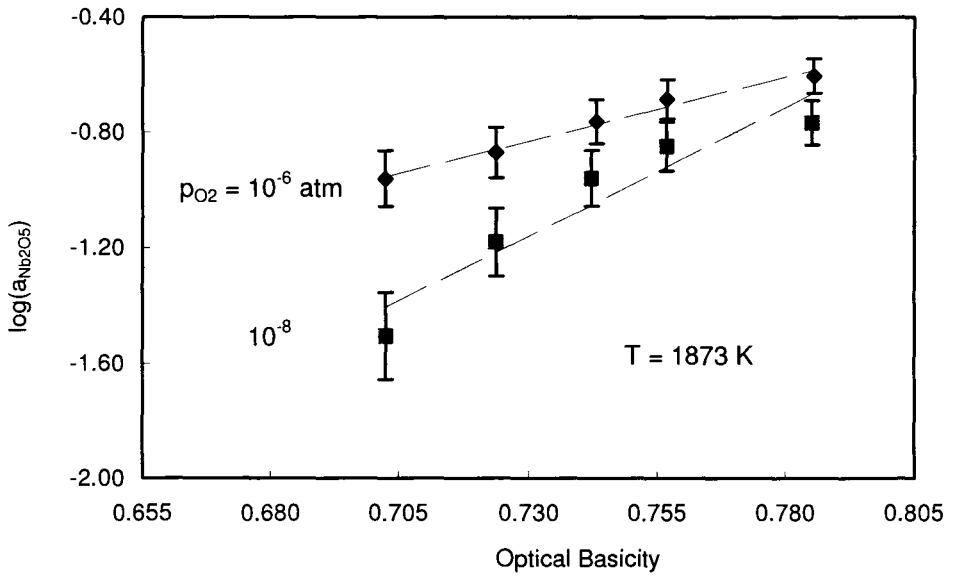

Figure 6.21 Activity of Nb_2O_5 as a function of optical basicity of the slag melts and p_{O_2} in system CaO-SiO_2- Al_2O_3-NbO_x at 1873 K.

For multi-component slags, the activity and activity coefficient of niobium oxides are plotted as a function of melt basicity at levels of $p_{O_2} = 10^{-6}$ and $p_{O_2} = 10^{-8}$ atm, respectively, shown from Figures 6.21 to 6.24.

As shown in Figures 6.21 and 6.22, increasing slag basicity leads to higher activities of niobium oxides in a slag system containing Al_2O_3. This is in agreement with the results from the $CaO\text{-}SiO_2\text{-}NbO_x$ system.

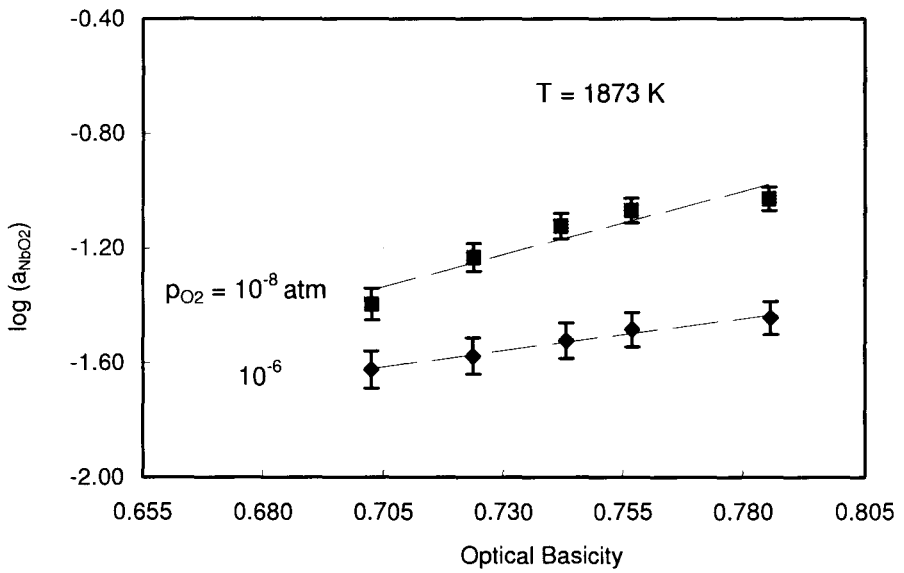

Figure 6.22 Activity of NbO_2 as a function of optical basicity of the slag melts and p_{O_2} in system $CaO\text{-}SiO_2\text{-}Al_2O_3\text{-}NbO_x$ at 1873 K.

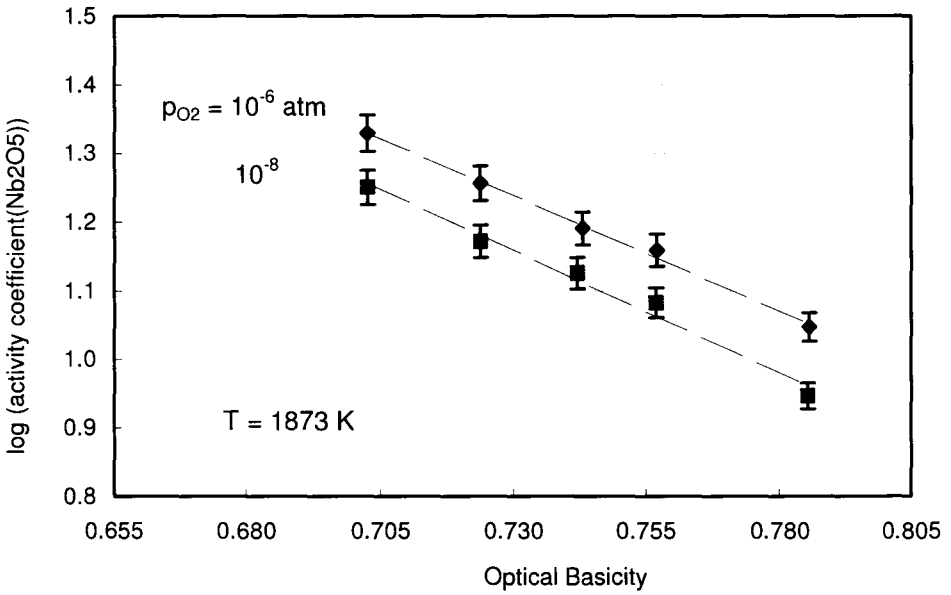

Figure 6.23 Activity coefficient of Nb_2O_5 as a function of optical basicity of the slag melts and p_{O_2} in a CaO-SiO_2-Al_2O_3-NbO_x system at 1873 K.

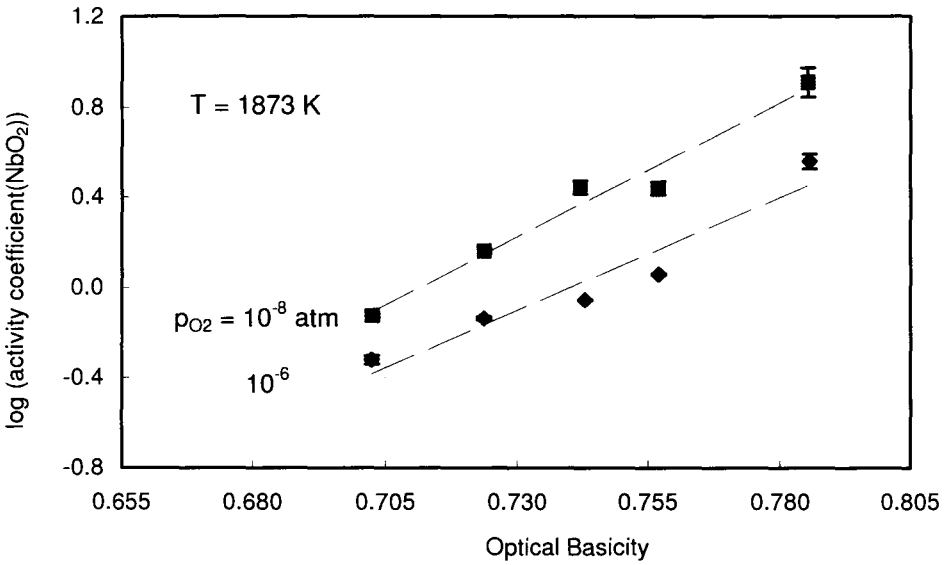

Figure 6.24 Activity coefficient of NbO_2 as a function of optical basicity of the slag melts and p_{O_2} in a CaO-SiO_2-Al_2O_3-NbO_x system at 1873 K.

Figure 6.23 and 6.24 are plots of $\gamma_{Nb_2O_5}$ and γ_{NbO_2}, respectively, as a function of melt basicity. The variation of γ_{NbO_2} and $\gamma_{Nb_2O_5}$ with melt basicity and p_{O_2} is similar to that observed in the $CaO\text{-}NbO_x\text{-}SiO_2$ system; i.e., γ_{NbO_2} increases with increasing melt basicity and decreasing p_{O_2} and $\gamma_{Nb_2O_5}$ decreases with increasing melt basicity and decreasing p_{O_2}.

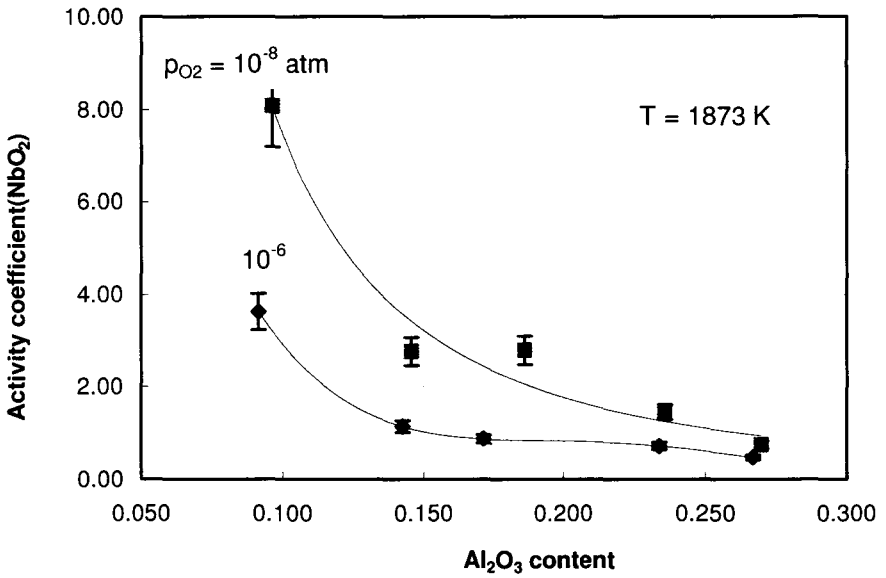

Figure 6.25 Effect of Al_2O_3 addition to the activity coefficient of NbO_2 in a $CaO\text{-}SiO_2\text{-}Al_2O_3\text{-}NbO_x$ slag system at 1873K.

The effect of Al_2O_3 might be explained by the amphoteric nature of Al_2O_3. In basic slags with low Al_2O_3 content, Al_2O_3 behaves as a weak acid as shown in Figure 6.19 since Nb_2O_5 behaves like an acidic oxide. However, when the Al_2O_3 content increases as shown in Figure 6.25, the acidic nature of Al_2O_3 will gradually disappear and

it behaves neutrally. This observation may be consistent with the hypothesis of the amphoteric nature of NbO_2, as discussed shortly.

6.4 Discussion

6.4.1 Effect of Slag Basicity

It is obvious that slag basicity has a remarkable effect on the activity of niobium oxides in a $CaO\text{-}SiO_2\text{-}NbO_x$ slag system under the present study. The higher the slag basicity, the higher the activities of niobium oxides. This may be explained qualitatively by the ionic structure of slags. Although the behaviour of different niobium oxides in slags is not well known, a hypothesis can be determined from two points of view.

First of all, at lower slag basicity, almost all of the niobium cations are associated with the large SiO_2 anionic groups, so that only a few free O^{2-} ions exist. This results in low activities of niobium oxides in these slag melts due to strong complexation with SiO_2. As basic oxides increase, the SiO_2 networks are broken into smaller anion groups and the proportion of free oxygen starts to increase. Therefore, the activities of niobium oxides will increase because the stronger basic metal oxides (CaO) will liberate niobium oxides from the SiO_2 networks in the slag.

Secondly, in a practical operation, the slag composition will be controlled by the amount of CaO addition, so the basicity index, C/S, becomes the only easily controlled

factor. With the substitution of CaO for SiO_2, the activities of the niobium oxides in the slags increase progressively, the slags are easily saturated with NbO_x due to its low solubility at high CaO content (Chase, 1998). The activities of niobium oxides, therefore, are higher in the range of high CaO content. When SiO_2 content increases, the solubility of the niobium oxides increases as well, and may contribute to the decrease in the activities of NbO_2 and $NbO_{2.5}$.

6.4.2 Activity Coefficient

The value of γ_{NbO_2} is strongly dependent on melt composition and increases as the basicity increases. However, γ_{NbO_2} decreases with increasing oxygen partial pressures.

At high p_{O_2}, γ_{NbO_2} shows a large increase with increasing basicity as shown in Figure 6.10. At lower p_{O_2}, γ_{NbO_2} shows a slight increase with increasing basicity. The large increase of γ_{NbO_2} with increasing basicity at high p_{O_2} is expected because Nb^{4+} is destabilized in silicate melts. This relationship is further shown in Figure 6.26, which is a plot of the $\gamma_{NbO_{2.5}} / \gamma_{NbO_2}$ ratios of the melts as a function of melt basicity. As the basicity of the melt decreases, $\gamma_{NbO_{2.5}}$ in the melts increases (Nb^{5+} is destabilized) and γ_{NbO_2} decreases (Nb^{4+} is stabilized), which results in an increase of $\gamma_{NbO_{2.5}} / \gamma_{NbO_2}$.

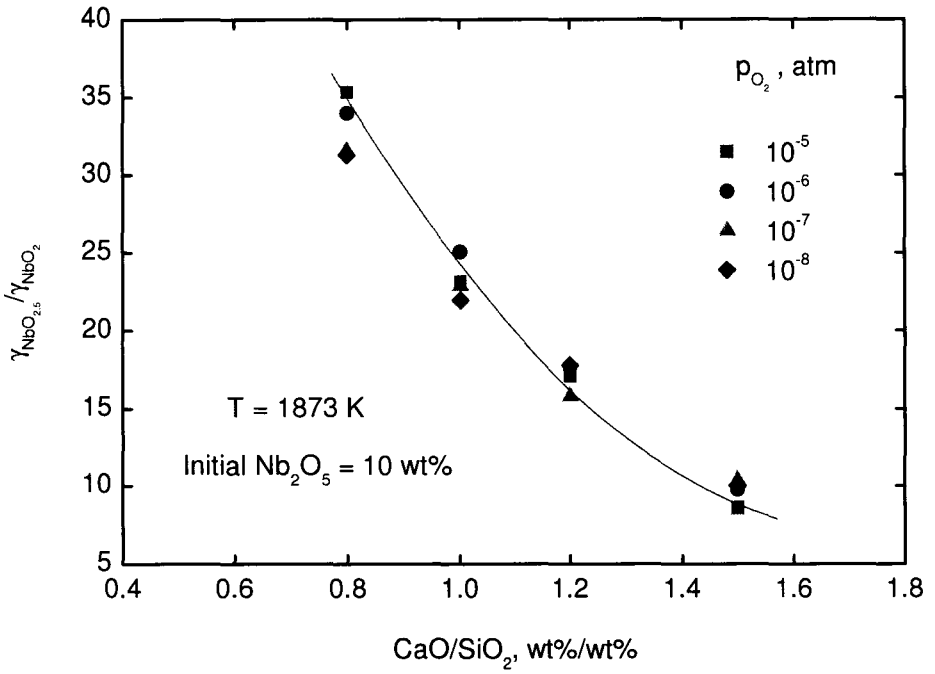

Figure 6.26 $\gamma_{NbO_{2.5}} / \gamma_{NbO_2}$ ratio as a function of the basicity of the melt at various p_{O_2} in the $CaO\text{-}SiO_2\text{-}NbO_x$ system at 1873K

On the other hand, if Nb^{4+} forms silicates in the solid state, there may be some clustering of the NbO^{2+} oxygen complex cations around the silicate anion complexes. This may lead to the lowering of γ_{NbO_2} in the melt. Since γ_{NbO_2} and $a_{O^{2-}}$ change in a similar manner, an increase in γ_{NbO_2} and $a_{O^{2-}}$ with increasing concentrations of network modifier (CaO) brings a decrease in $\gamma_{NbO_{2.5}}$.

In the overall range of optical basicity, the activity coefficient of $NbO_{2.5}$ shows a good agreement with data presented by Tsukihashi, namely, the activity coefficient

decreases with increasing slag basicity, as shown in Figure 6.27.

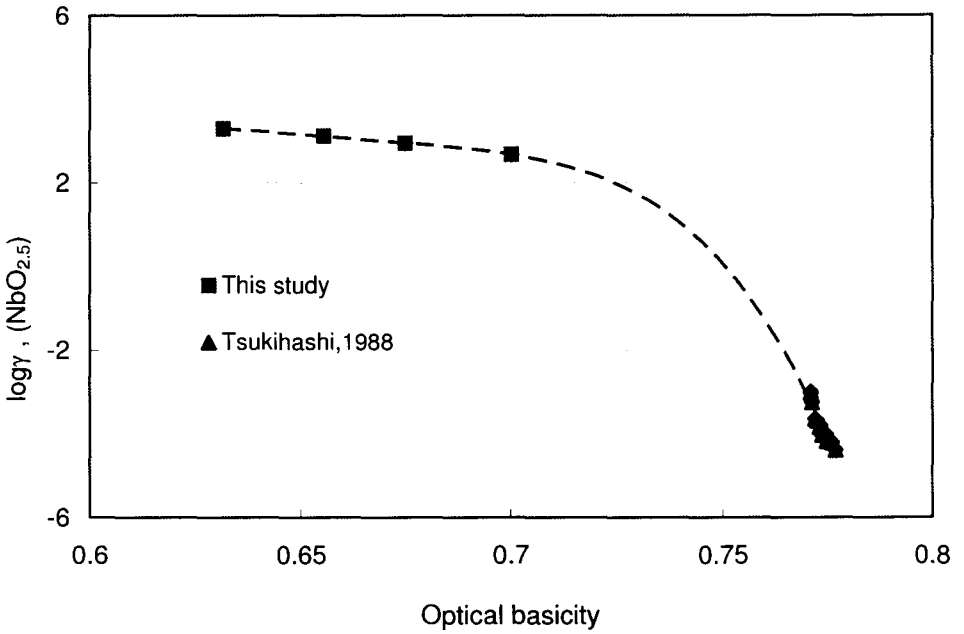

Figure 6.27 Effect of slag basicity on the activity coefficient of $NbO_{2.5}$ for $CaO\text{-}SiO_2\text{-}NbO_x$ system (this study) and $CaO\text{-}Na_2O\text{-}CaF_2\text{-}SiO_2\text{-}NbO_x$ system (Tsukihashi, 1988)

The variation of γ_{NbO_2} with melt composition is plotted in Figure 6.28 as a function of CaO/SiO_2 ratio of melt of $CaO\text{-}SiO_2\text{-}NbO_x$ system. The results of Tsukihashi on the activity of NbO_2 in complex silicate melts are also shown in this figure. γ_{NbO_2} as determined in this study is strongly dependent on composition and increases as the basicity of the melt increases. The results of Tsukihashi, however, show a decrease in γ_{NbO_2} as the basicity of the melts increases. It is difficult to compare qualitatively the results of their work with the results of this study because of the large compositional differences. The melts studies by Tsukihashi were in general more basic than the melts in

the present study. Unfortunately, the melts in this $CaO\text{-}SiO_2\text{-}NbO_x$ system could not be extended to more basic compositions because of the melting point.

In the composition range studied, the γ_{NbO_2} increases as the CaO content of the melt increases. This is expected since CaO is a much stronger base than NbO_2, and would thus preferentially associate with silica.

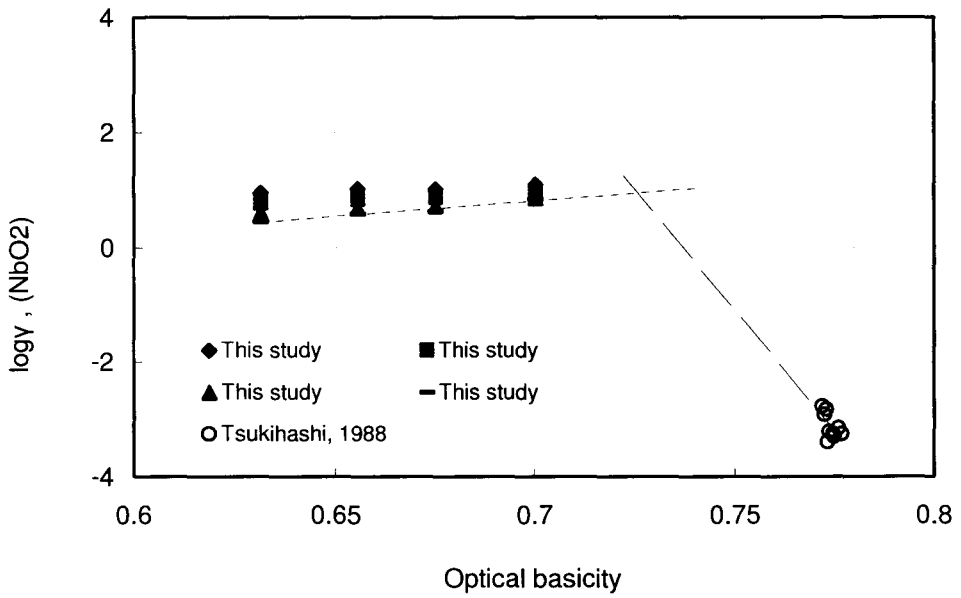

Figure 6.28 The activity coefficient of NbO_2 for the $CaO\text{-}SiO_2\text{-}NbO_x$ system (this study) and $CaO\text{-}Na_2O\text{-}CaF_2\text{-}SiO_2\text{-}NbO_x$ system (Tsukihashi, 1988)

The increase in γ_{NbO_2} with the melt basicity of this study might reach a maximum, as reflected by the change in slope. The results of this study and those of Tsukihashi, would then be complementary and not contradictory. When CaO/SiO_2 is getting larger, γ_{NbO_2} decreases with basicity, indicating an amphoteric property in the overall range of

slag basicity.

Justification for the amphoteric nature of NbO_2 can be found in the behaviour of other transition metal oxides. For example, TiO_2, containing the Ti^{4+} cation, is generally classified an amphoteric oxide, although Ti^{4+} is preferentially regarded as a network forming ion (Furukawa and White, 1979; Greegor et al., 1983) and has demonstrated glass forming properties (Rao, 1964). The network forming properties of TiO_2 are consistent with its repulsion to SiO_2 and moderate attraction to CaO, MnO and FeO (Sommerville and Bell, 1982; Ran and Gaskell, 1981; Banon, et al., 1981). TiO_2, however, appears to weaken the silicate network, judging from its effect on slag viscosity, electrical conductivity, and sulfide capacity (Brown, et al., 1982).

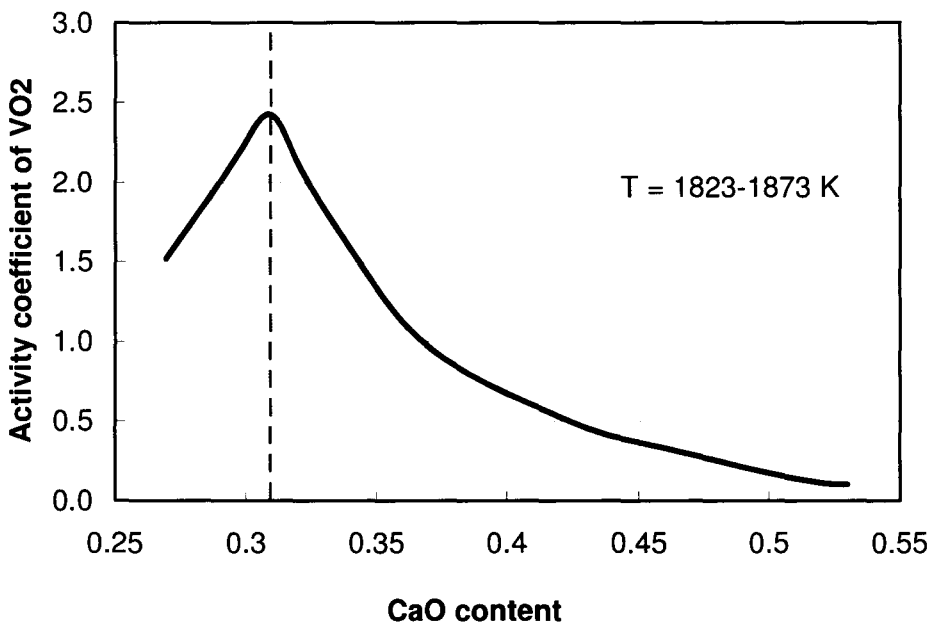

Figure 6.29 Effect of CaO content in the slag on the γ_{VO_2} activity coefficient at 1823-1873 K (Rovnushkin *et al.*, 1989)

VO_2 presents amphoteric character as shown in Figure 6.29. The γ_{VO_2} activity coefficient depends in a complex way on the concentration of CaO. As can be seen from Figure 6.28 there is a maximum in the N_{CaO}=0.3-0.32 region. Apparently, at N_{CaO}<0.3, quadrivalent V is present mainly as the vanadyl ion, VO^{2+}, which forms a sufficiently strong bond with the anion sets. In the N_{CaO}>0.3 region, as N_{CaO} increases the $N_{O^{2-}}$ concentration also increase, quadrivalent V starts forming the VO_4^{4-} type anion sets, and the activity coefficient γ_{VO_2} decreases (Rovnushkin et al., 1989).

Oxide/ion interaction also supports the amphoteric nature of NbO_2 (See section 6.5.1.2).

6.4.3 Nb^{5+}/Nb^{4+} Ratio

It can be seen that the Nb^{5+}/Nb^{4+} ratio increases as slag basicity increases at a given oxygen potential and the proportion of the niobium present in the quadrivalent state decreases with increasing slag basicity. This relationship with melt basicity is in general agreement with observations made previously for Fe^{3+}/Fe^{2+} by Paul and Douglas (Paul and Douglas, 1966) as well as for other transition-metal ions in silicate melts, e.g., Mn^{3+}/Mn^{2+} (Paul and Lahiri, 1966).

From the glass chemistry point of view (Duffy and Ingram, 1976), if we have a metal ion capable of existing in two oxidation states, then the higher state will be

favoured as the optical basicity Λ of the glass is increased, since a high Λ-value means that the oxides are able to donate more negative charge, thereby stabilizing the metal ion. Thus, as the basic oxide content is increased (thus increasing Λ) the upper/lower oxidation state ratio is also increased.

Quinquevalent niobium oxide $NbO_{2.5}$ is an acidic oxide, as shown by Figure 6.9; but there is no published data regarding the interaction between Nb^{4+} and Nb^{5+}. The interaction between quadrivalent and quinquevalent niobium oxides could be large. Coexistence of quadrivalent niobium drastically decreases the activity coefficient of $NbO_{2.5}$. NbO_2 appears to behave as a basic oxide in this basicity range of slag melts. It was also observed in the redox equilibrium experiment that $NbO_{2.5}$ becomes predominant as the slag basicity increases. Therefore, the reaction model between NbO_2 (Nb^{4+}) and $NbO_{2.5}$ (Nb^{5+}) is considered using ionic reactions.

In the range of slag basicity of this study, CaO/SiO_2 ratio is less than 2.0 in the $CaO\text{-}SiO_2\text{-}NbO_x$ slag system. Since $\gamma_{Nb^{4+}}$ increases and $\gamma_{Nb^{5+}}$ decreases with basicity, the possible reactions are presented as shown in Equation 6.10 to 6.12, with the assumption of the formation of NbO^{2+} and NbO_4^{3-} oxygen complex.

$$Nb + O_2 = NbO^{2+} + O^{2-} \tag{6.10}$$

$$Nb + \frac{5}{4}O_2 + \frac{3}{2}O^{2-} = NbO_4^{3-} \tag{6.11}$$

The redox reaction can be described in Equation 6.12

$$NbO^{2+} + \frac{1}{4}O_2 + \frac{5}{2}O^{2-} = NbO_4^{3-} \tag{6.12}$$

6.4.4 Partial Pressure of Oxygen

The distribution of quadrivalent and quinquevalent niobium in the slags equilibrated with oxygen potential is very significant in clarifying the activities of niobium oxides in slags. The distributions of the quadrivalent niobium and quinquevalent niobium can be obtained as follows:

$$NbO_{2.5}(l) = NbO_2(l) + \frac{1}{4}O_2 \tag{6.13}$$

$$\Delta G^0 = -RT \ln \frac{a_{NbO_2} \cdot p_{O_2}^{1/4}}{a_{NbO_{2.5}}} \tag{6.14}$$

The quantitative relation between the oxidation state of niobium and the activity coefficient can be derived from Equation 6.14:

$$\log\left(\frac{Nb^{5+}}{Nb^{4+}}\right) = \frac{\Delta G^0}{2.303RT} - \log\left(\frac{\gamma_{NbO_{2.5}}}{\gamma_{NbO_2}}\right) + 0.25\log(p_{O_2}) \tag{6.15}$$

As shown in Equation 6.15, the ratio $X_{NbO_{2.5}} / X_{NbO_2}$ (expressed as Nb^{5+}/Nb^{4+})

depends on (1) temperature, (2) oxygen partial pressure and (3) slag basicity, since $\gamma_{NbO_{2.5}} / \gamma_{NbO_2}$ is a function of slag composition.

At a constant temperature and constant CaO/SiO_2 ratio, and assuming that $\gamma_{NbO2.5} / \gamma_{NbO_2}$ ratio is not affected by the reduction of Nb^{5+} to Nb^{4+}, Equation 6.15 can be simplified as Equation 6.16

$$\log\left(\frac{Nb^{5+}}{Nb^{4+}}\right) = A + 0.25\log(p_{O_2}) \tag{6.16}$$

Thus, $$\frac{\partial \log\left(\frac{Nb^{5+}}{Nb^{4+}}\right)}{\partial \log(p_{O_2})} = \frac{1}{4} \text{ at constant } CaO/SiO_2 \text{ ratio} \tag{6.17}$$

Where A is a constant, from Equation 6.16, it can be predicted that a plot of experimentally determined values of $\log(p_{O_2})$ vs. $\log(Nb^{5+}/Nb^{4+})$ will yield straight lines of slope 0.25 with intercept A. Such a plot, for various CaO/SiO_2 basicity ratios, is shown in Figure 6.15.

As seen from Figure 6.15, the change in the experimental Nb^{5+}/Nb^{4+} ratio with varying oxygen partial pressure is generally close to the theoretical value of 0.25 predicted by Equation 6.16 in a slag with 10 mass pct NbO_x.

Data from this investigation confirmed the relationship between the Nb^{5+}/Nb^{4+}

ratio and oxygen potential and suggested that the redox ratio (Nb^{5+}/Nb^{4+}) is favoured by increasing slag basicity and oxygen potential, a behaviour common to a number of transition metals.

Oxygen partial pressure has a strong effect on the vapour pressure of NbO_2. The vapour pressure of NbO_2 increases dramatically as the oxygen pressure decreases. The oxygen effect is greater than that of slag composition at a given temperature as shown in Figure 6.16. Since NbO_2 is the only volatile species of niobium oxide under these conditions, a decrease in oxygen pressure will result in more niobium loss through vapourization.

6.4.5 Application of Measurements

Calculated niobium losses to the slag, based on the measured activity coefficients, are presented in Figure 6.30 and 6.31. These figures give the predicted mole fraction of niobium oxide (Nb_2O_5) in the slag and measured vapour pressure of NbO_2 by varying the ratio of CaO/SiO_2 and the Al_2O_3 content respectively.

This calculation was performed by assuming equilibrium to hold between $NbO_{2.5}$ in the slag and Nb(l) in the metal. Data on the activity of niobium of 7.73×10^{-3} in steel was used by Tsukihashi *et al* (Tsukihashi et al., 1988); the partial pressure of oxygen is 10^{-8}atm and the equilibrium niobium content in molten steel is assumed to be 0.01wt%.

$$Nb(l)+\frac{5}{4}O_2 = NbO_{2.5}(l) \qquad \Delta G^0 = -918750+190.6T(J/mole) \quad (6.18)$$

$$x_{NbO_{2.5}} = \exp\left(-\frac{\Delta G^0}{RT}\right)\cdot\left(p_{O_2}\right)^{\frac{5}{4}}\cdot\gamma_{Nb}\cdot x_{Nb}/\gamma_{NbO_{2.5}} \quad (6.19)$$

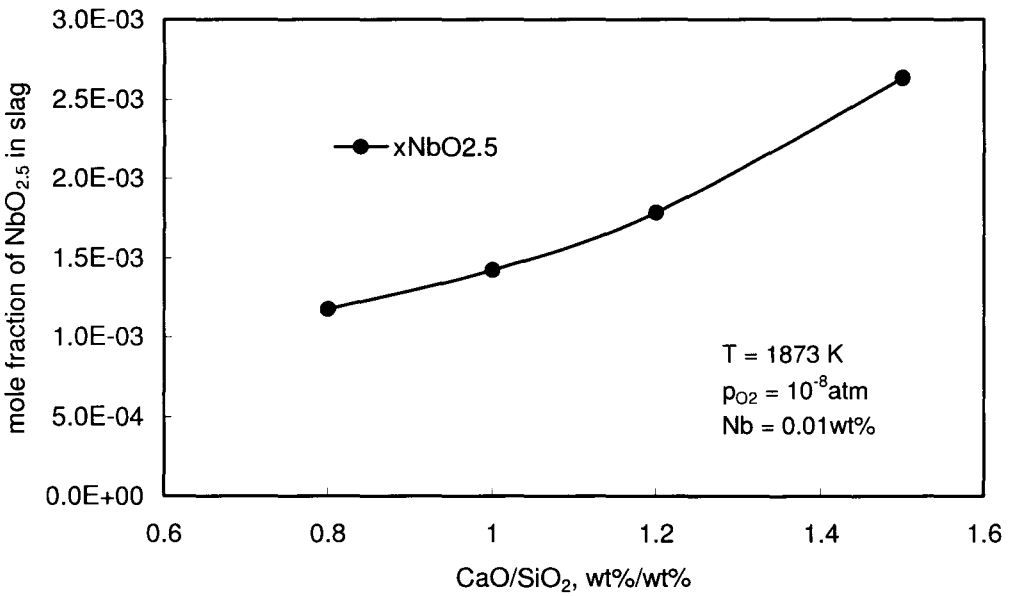

Figure 6.30. Application of experimental data in improving recovery rate of niobium in ladle metallurgy at 1600°C at a given partial pressure of oxygen.

As shown in Figure 6.30, the predicted relationship shows a strong effect of slag basicity on niobium losses. As can be seen, a small increase in the ratio of CaO/SiO_2 yields a large increase in niobium losses as a result of the sharp decrease in the niobium oxide activity coefficient. Therefore, a decrease in slag basicity will benefit the recovery rate of niobium in liquid steel when slag contains CaO, SiO_2 and NbO_x.

In addition, the strong dependence of niobium losses on the slag composition has clear implications for operation of the industrial furnace. As shown in Figure 6.31 small increases in the alumina content in slag from the current level are expected to cause a significant decrease in niobium loss with $CaO\text{-}SiO_2\text{-}Al_2O_3\text{-}NbO_x$ slag system.

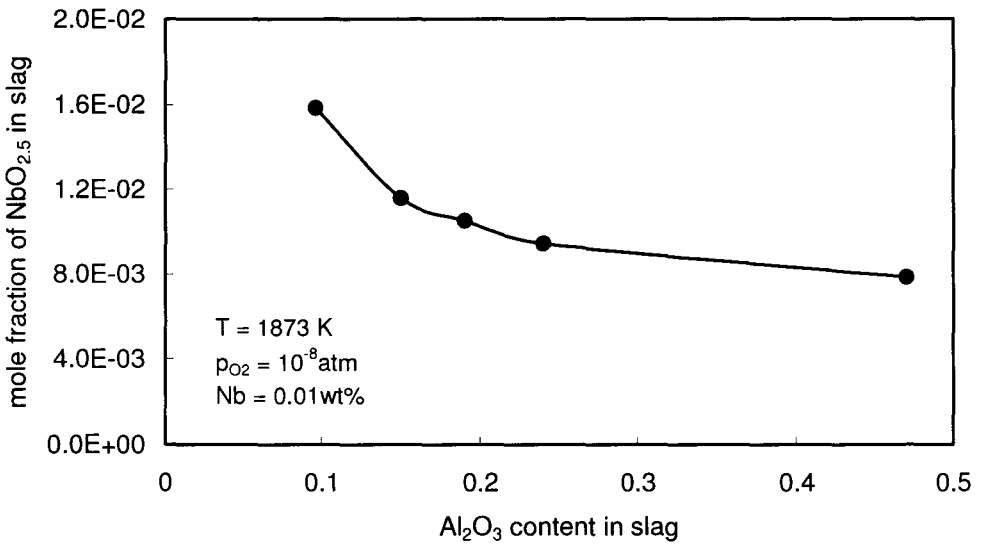

Figure 6.31. Application of experimental data in improving recovery rate of niobium in ladle metallurgy at 1600°C at a given partial pressure of oxygen for $CaO\text{-}SiO_2\text{-}Al_2O_3\text{-}NbO_x$ slag system.

On the other hand, in the vacuum degasser, niobium may be lost by forming vapours of niobium oxide. Higher $\gamma_{NbO2.5}$ which, gave high p_{NbO2} in these experiments, would give lower losses to slag.

6.5 Mathematical Approach of Niobium Oxide Activity

6.5.1 Assessment of the Model Parameters

6.5.1.1 Introduction

The applicability of the regular solution model in various slag systems has been investigated for over 30 years by different researchers. The investigated slag systems with respect to the regular solution model contain the following components: Al_2O_3, CaO, CoO, Cu_2O, FeO, Fe_2O_3, MgO, MnO, NiO, P_2O_5, PbO, SiO_2, TiO_2 and ZnO (Jahanshahi and Wright, 1992). However, for the slags containing niobium oxides, there were not yet any publication found to describe their thermodynamic properties with the regular solution model.

Significant work fitting experimental data to obtain interaction energies and conversion parameters for the regular solution model has been achieved by Lumsden and Ban-Ya. The data fitting method was explained in detail in the reference (Lumsden, 1961). However, the parameters required for a $CaO\text{-}SiO_2\text{-}NbO_x$ melt were not available in the literature. In addition, the application of these data fitting methods failed because of insufficient experimental data in the literature.

In previous assessment work, multiple linear-regression analysis has been used as a quick and convenient method for determining the model parameters (Jahanshahi and

Wright, 1992). The assessment was processed from binary $CaO\text{-}SiO_2$ to multicomponent systems. The experimental data in the $CaO\text{-}SiO_2$ system were taken from the literature (Sharma and Richardson, 1962; Rein and Chipman, 1965). The obtained interaction energy parameters were optimized mathematically. The conversion energies for changing the standard state of activity coefficient from the hypothetical regular solution to the traditional pure solid or pure liquid were also optimized simultaneously. Still, this method is not applicable to the present study due to the shortage of thermodynamic data of niobium oxides in slag melt.

Ban-Ya (Ban-Ya, 1993) associated the interaction energy with other physico-chemical properties. The interaction energy between cations can be written as follows in the regular solution

$$\alpha_{ij} = (ZN_0/2)(2U_{ij} - U_{ii} - U_{jj}) \tag{6.20}$$

where U_{ij} is the bond energy of the (i cation)-O-(j cation) ion pair, and Z and N_0 are coordination number of cation and Avogadro's number respectively.

However, the lack of bond energy data of ion pairs is still a barrier in these applications. Therefore, seeking a new method of obtaining the parameters becomes necessary for the application of the regular solution model to $CaO\text{-}SiO_2\text{-}NbO_x$ melt.

6.5.1.2 Definition of Basicity and Acidity by Ion-oxygen Attraction

Ward (Ward, 1962) defined that an acidic oxide will absorb oxygen ions when dissolved in a basic melt, while a basic oxide provides oxygen ions when dissolved in a melt.

An examination of the properties of oxides shows that they form a continuous series from those with strongly basic to those with strongly acidic behaviour. The attractive force between a metal ion and an O^{2-} ion has often been used as a parameter by which to describe the degree of basicity or acidity of an oxide (Ward, 1962).

The electrostatic attraction between two point charges (a^-, b^+) separated by a distance d is given by the usual inverse square law relation as :

$$F = \frac{a \cdot b}{d^2} \tag{6.21}$$

In the case of an oxygen ion ($a = 2e$) and a cation ($b = ze$), the force is given by

$$F = \frac{2ze^2}{d^2} \tag{6.22}$$

where z is the valence of the cation and as e^2 is common to all such calculations it is commonly omitted, and the resulting expression is defied as the 'ion-oxygen attraction (Bockris et al, ,1952)

$$I = \frac{2z}{d^2} \tag{6.23}$$

Values of the ion-oxygen attraction are given in Table 6.5 for niobium cations, calculated from the ionic radii of Pauling.

Table 6.5 Dependence of Ion-Oxygen Attraction on Cationic Radius

oxide	cationic radius,pm	oxygen ion radius,pm	valence of cation	ion-oxygen attraction
NbO_2	0.069	0.140	4	1.83
Nb_2O_5	0.070	0.140	5	2.27

As defined by Ward, cations with ion-oxygen attractions less than 1.0 have predominantly basic behaviours, and their oxides dissociate in solution giving O^{2-} ions which can then break down the silicate networks (the 'network modifiers' of glass technology). Conversely, acidic oxides ($I > 2.0$) certainly absorb O^{2-} ions in solution to form complex ions ('network formers'). However, intermediate cations ($I = 1.0 - 2.0$) may show either basic or acidic characteristics according to their environment, and their behaviour cannot successfully be predicted. This supports the hypothesis Nb_2O_5 behaves as an acidic oxide while NbO_2 is amphoteric.

6.5.1.3 Correlation between Ion-oxygen Attraction and Interaction Energy

The ion-oxygen attraction data reveal a correlation between ionic radius and

interaction energies in the regular solution model showing that the ion-oxygen attraction is a fairly good parameter for correlating these data, listed in Table 6.6. Interaction energy plotted as a function of Ion-oxygen attraction is shown in Figure 6.32. A good correlation is found among the ionic radius, valence and interaction parameter.

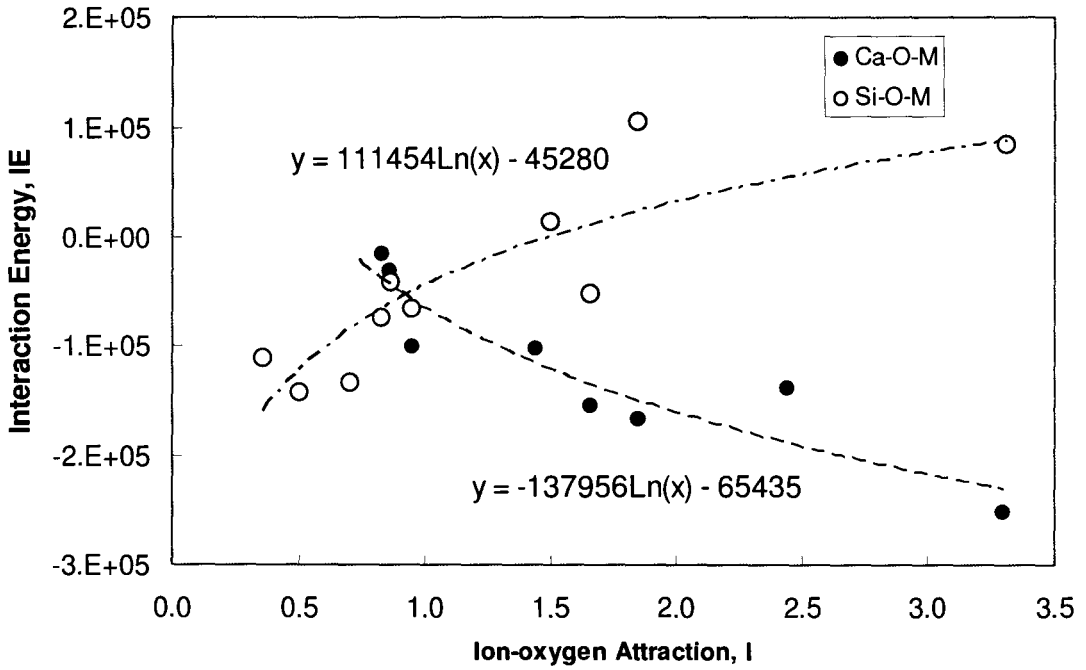

Figure 6.32 Correlations between ion-oxygen attractions and interaction energy in the regular solution model.

6.5.2 Comparison between Calculated and Measured Activities of Niobium Oxides in Slags

The interaction energies can be obtained by the correlation between ion-oxygen

attraction and interaction energies presented in this study. Based on the ionic radii, the calculated ion-oxygen attraction is summarized in Table 6.6. The fitted curve and its model was used to obtain the interaction energies for Ca-Nb^{5+}, Ca-Nb^{4+}, Si-Nb^{5+} and Si-Nb^{4+}, as presented in Table 6.6.

For the CaO-SiO_2-NbO_x system, assigning NbO_2(1), $NbO_{2.5}$(2), SiO_2(3), CaO(5), the calculation is shown below.

$$RT\ln\gamma_{NbO_2} = \alpha_{12}x_{NbO_{2.5}}^2 + \alpha_{13}x_{SiO_2}^2 + \alpha_{15}x_{CaO}^2 + (\alpha_{12}+\alpha_{13}-\alpha_{23})x_{NbO_{2.5}}x_{SiO_2} + (\alpha_{12}+\alpha_{15}-\alpha_{25})x_{NbO_{2.5}}x_{CaO} + (\alpha_{13}+\alpha_{15}-\alpha_{35})x_{SiO_2}x_{CaO} \quad (6.24)$$

$$RT\ln\gamma_{NbO_{2.5}} = \alpha_{12}x_{NbO_2}^2 + \alpha_{23}x_{SiO_2}^2 + \alpha_{25}x_{CaO}^2 + (\alpha_{12}+\alpha_{23}-\alpha_{13})x_{NbO_2}x_{SiO_2} + (\alpha_{12}+\alpha_{25}-\alpha_{15})x_{NbO_2}x_{CaO} + (\alpha_{23}+\alpha_{25}-\alpha_{35})x_{SiO_2}x_{CaO} \quad (6.25)$$

The comparison between the calculated activities and those experimentally measured in the niobium-containing slag systems is shown in Figure 6.33 and 6.34. According to these comparison results, considering the existence of a certain degree of scatter in the experimental data, the results give an acceptable agreement.

Table 6.6 Selected Cations of Interaction Energy and Ion-Oxygen Attraction

cations	interaciton energy IE	reference	cations	ion-oxygen attraction I	Pauling Radii	reference
Ca^{2+} - Fe^{2+}	-31380	Ban-Ya,1993	Fe^{2+}	0.86	0.76	Ward, 1962
Ca^{2+} - Fe^{3+}	-102510	*ibid*	Fe^{3+}	1.44	0.60	*ibid*
Ca^{2+} - Mn^{2+}	-16740	*ibid*	Mn^{2+}	0.83	0.80	*ibid*
Ca^{2+} - Mg^{2+}	-100420	*ibid*	Mg^{2+}	0.95	0.65	*ibid*
Ca^{2+} - Al^{3+}	-154810	*ibid*	Al^{3+}	1.66	0.50	*ibid*
Ca^{2+} - Ti^{4+}	-167360	*ibid*	Ti^{4+}	1.85	0.68	*ibid*
Ca^{2+} - Si^{4+}	-138490	*ibid*	Si^{4+}	2.44	0.41	*ibid*
Ca^{2+} - P^{5+}	-251040	*ibid*	P^{5+}	3.31	0.34	*ibid*
Si^{4+} - Fe^{2+}	-41840	*ibid*	Nb^{5+}	2.27	0.70	*ibid*
Si^{4+} - Fe^{3+}	13390	*ibid*	Nb^{4+}	1.83	0.69	*ibid*
Si^{4+} - Mn^{2+}	-75310	*ibid*	Fe^{2+}	0.87	0.76	*ibid*
Si^{4+} - Mg^{2+}	-66940	*ibid*	Fe^{3+}	1.50	0.64	*ibid*
Si^{4+} - Al^{3+}	-52300	*ibid*	Ca^{2+}	0.70	0.99	*ibid*
Si^{4+} - Ti^{4+}	104600	*ibid*	Li^{+}	0.50	0.60	*ibid*
Si^{4+} - Ca^{2+}	-138490	*ibid*	Na^{+}	0.36	0.95	*ibid*
Si^{4+} - P^{5+}	83680	*ibid*				
Si^{4+} - Li^{+}	-142130	*ibid*				
Si^{4+} - Na^{+}	-111290	*ibid*				
			data fitting models			
Ca^{2+} - Nb^{5+}	-178529	this study	IE = -137956 ln(I) - 65435			this study
Ca^{2+} - Nb^{4+}	-148804	this study				
Si^{4+} - Nb^{5+}	46088	this study	IE = 111454 ln(I) - 45280			this study
Si^{4+} - Nb^{4+}	22073	this study				

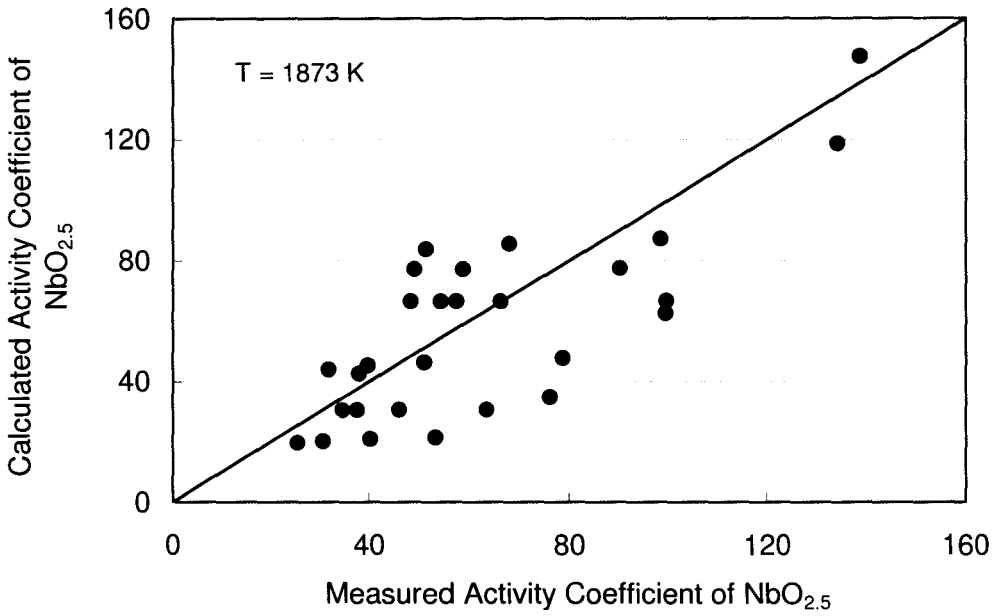

Figure 6.33 Comparison of calculated results with those measured activity coefficients of $NbO_{2.5}$

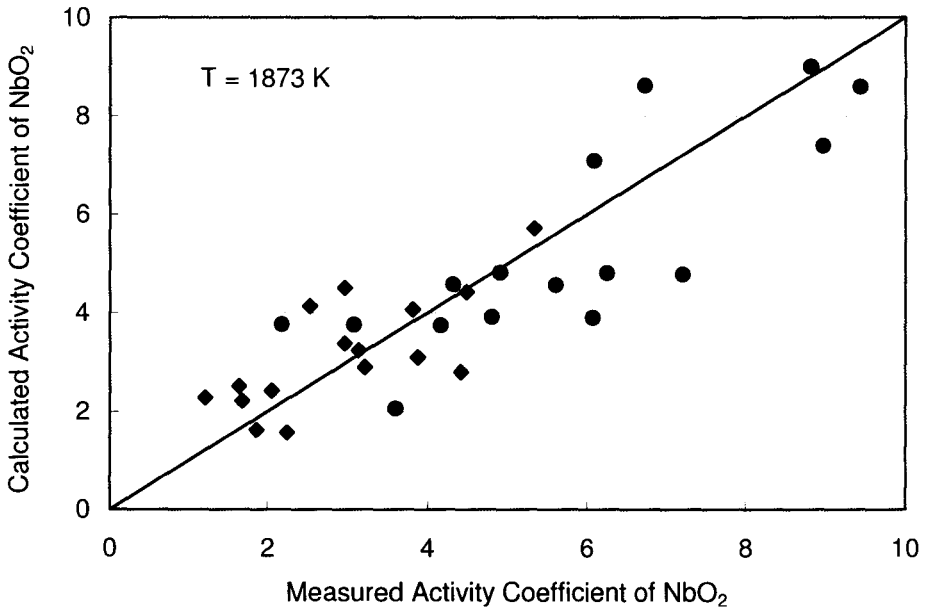

Figure 6.34 Comparison of calculated results with those measured activity coefficients of NbO_2

6.6 Summary

60 conditions and 120 experiments have been conducted to determine the volatility of niobium oxide and thermodynamic properties of niobium oxides in the slag systems $CaO\text{-}SiO_2\text{-}NbO_x$ and $CaO\text{-}SiO_2\text{-}Al_2O_3\text{-}NbO_x$. It was found that the optical basicity has a profound effect on vapour pressure, activity and activity coefficient of niobium oxide. The Nb^{5+}/Nb^{4+} ratio is also significantly affected by temperature, partial pressure of oxygen and optical basicity. By observing the dependence of the activity coefficient on slag basicity in the composition range studied, Nb_2O_5 shows the characteristics of an acidic oxide and the NbO_2 behave like an amphoteric oxide if a wider basicity range is applied.

In the application of the regular solution model to slag melts, it was found that the interaction energy is associated with ion-oxygen attraction. When these assessments of interaction energy were applied to the regular solution model, it resulted in a fairly good agreement between the measured and calculated values.

Chapter 7 Conclusions

7.1 Conclusions

An experimental study has been made, using the transpiration method, of the volatility and thermodynamic properties of niobium oxides in $CaO\text{-}SiO_2\text{-}NbO_x$ slag melts. To ensure the accuracy and precision of the measurements, Chapter 3 and 4 addressed the approach for the well-controlled atmosphere, calibration work and self-consistency experiments which can be summarized below:

- A more efficient method to dissolve the slag sample has been developed. Slags containing niobium oxide were brought into solution by acid attack without introducing new elements, leading to stable and repeatable ICP readings. An effective dissolution method, along with the following potentiometric titration has been developed resulting in improved accuracy.

- The temperature at the specimen-setting position was measured before and after the run by using a Pt-6 pct Rh/Pt-30 pct Rh thermocouple. The measuring thermocouple was compared periodically with other standardized thermocouples. The hot zone of the furnace was about 40 mm and the accuracy of the temperature measurements was estimated to be within ±1°C.

- Individual flow controller for CO_2 and CO gases was calibrated frequently. The

difference between short and long term calibration was not significant and it ensured the precision of flow rate control during longer experimental time periods. The total flow rate was controlled within an error of ± 0.1 mL/min. The gas composition monitor utilized was propagated to the error of the oxygen partial pressure of ± 2%.

- The transpiration technique for the determination of the thermodynamic activity of a component in a binary liquid alloy was presented and applied to liquid gold-silver alloys as a test. The reliability and the sensitivity of the technique were demonstrated with gold-silver alloys in the concentration range of 20-80 mol% of silver at 1350K. It has been found that this technique yields reliable results for the transpiration method, compared with other techniques applied in the literature, yielding the same thermodynamic properties, thus demonstrating the accuracy and validity of this transpiration method.

In Chapter 5, the vapour pressure of NbO_2 above liquid Nb_2O_5 were measured under controlled oxygen partial pressure and the follow conclusions can be drawn,

- Better control of oxygen partial pressure is the crucial condition in the vapourization study of niobium oxides. Vapour pressure of NbO_2 was measured as a function of partial pressure of oxygen at a fixed temperature, indicating a good agreement with the dissociation reaction of Nb_2O_5. The vapour pressure of NbO_2 above liquid Nb_2O_5 via a least-square treatment, is given as follows:

$$\log p_{NbO_2} = -0.252 \log p_{O_2} - 6.777 \qquad \text{at } 1873\text{K}$$

- NbO_2 is confirmed to be the vapour species through the dependence of vapour pressure of niobium oxides on the oxygen pressure; Nb_2O_5 vapourizes according to the equilibrium: $Nb_2O_5(l) = 2NbO_2(g) + 1/2O_2(g)$

- Logarithm of vapour pressure of NbO_2 linearly increases with reciprocal temperature at a fixed partial pressure of oxygen. The vapour pressure of NbO_2 in the range of $1798 \le T \le 1873\ K$ can be expressed by the equation

$$\log p_{NbO2,} atm = \frac{(-1.2 \pm 0.2) \times 10^4}{T} + (1.5 \pm 0.2)$$

- The enthalpy of vapourization in that temperature range is 229.7 ± 38.2 kJ/mol although the slope in the plot of logarithm of vapour pressure vs. reciprocal temperature is observed to be in fairly good agreement with that of the literature.

The thermodynamic properties of niobium oxide in a slag system were systematically studied for the first time. The essence of the overall research is presented in Chapter 6, where the thermodynamic properties of niobium oxide in the slag systems $CaO\text{-}SiO_2\text{-}NbO_x$ and $CaO\text{-}SiO_2\text{-}Al_2O_3\text{-}NbO_x$ were measured by varying the experimental conditions of slag basicities, slag compositions, temperature and oxygen partial pressures. The following conclusions can be drawn:

- Optical basicity has a strong effect on the activity of Nb_2O_5 in $CaO\text{-}SiO_2\text{-}NbO_x$ melts. The activity of Nb_2O_5 increases with increasing optical basicity at a

constant partial pressure of oxygen at 1873K. The activity of NbO_2 shows a negligible change with basicity, however, this is a reflection of the repartitioning of the valence states which masks a much more significant change in activity coefficient. The dependence of activity of niobium oxide on optical basicity is consistent between the two initial niobium oxide contents.

- vapour pressure of NbO_2 slightly increases with increased slag basicities at a fixed oxygen partial pressure; the higher the initial content of niobium oxide in the slag melt, the higher the vapour pressure of NbO_2 if all other conditions remain the same

- Slag composition and oxygen partial pressure show a strong effect on the ratios of Nb^{4+}/Nb^{5+}. As slag basicity increases, Nb^{5+} is stabilized and the Nb^{5+} content increases with increasing slag basicity, whereas Nb^{4+} content decreases. The content of Nb^{5+} in the slag system also increases with increasing oxygen partial pressure, while that of Nb^{4+} decreases accordingly at a given temperature; Nb^{5+}/Nb^{4+} ratio increases with increasing oxygen pressure and the dependence is in an agreement with the expression $\partial \log\left(\frac{Nb^{5+}}{Nb^{4+}}\right) / \partial \log\left(p_{O_2}\right) = \frac{1}{4}$

- activity coefficient of Nb_2O_5 decreases with increasing basicity at a given partial pressure of oxygen while that of NbO_2 in a silicate system slightly increased with increasing basicity in this study; $\gamma_{NbO_{2.5}}$ decreases with increasing basicity, suggesting acidic behavior of $NbO_{2.5}$ over the entire range of the composition in

this study; NbO_2 appears to behave as a basic oxide. For a wider range of optical basicity, NbO_2 may demonstrate amphoteric behaviour in the $CaO\text{-}SiO_2\text{-}NbO_x$ system.

- Al_2O_3 additions to the $CaO\text{-}SiO_2\text{-}NbO_x$ system decrease both activities of niobium pentoxide and niobium oxide; $\gamma_{NbO_{2.5}}$ increases with the Al_2O_3 content of the melts; the effect of Al_2O_3 on γ_{NbO_2} is not significant at higher Al_2O_3 contents.

- The application of these experimental results suggest that the recovery rate of niobium in ladle metallurgy can be improved by decreasing CaO/SiO_2 to minimize the vapourization of $NbO_2(g)$, an optimization suitable for the steelmaking practice has been proposed. The strong dependence of niobium losses on the slag composition has clear implications for the operation of an industrial furnace. Small decreases in alumina content from the current level are expected to cause a large decrease in niobium oxide loss in $CaO\text{-}SiO_2\text{-}Al_2O_3\text{-}NbO_x$ slag system.

- A new correlation between the ion-oxygen attraction and interaction energy has been found and the assessment of interaction energy applied to the regular solution model results in a fairly good agreement between the measured values and calculated ones. The validity of the regular slag model in niobium-oxide-containing slags has been investigated by applying the present experimental results.

7.2 Future work

In this study, the activity coefficient of NbO_2 increases with increasing optical basicity, indicating basic oxide behaviour. The hypothesis of amphoteric behavior was present within literature with both niobium dioxide and vanadium oxide exhibiting similar amphoteric behavior. Due to the limitation of experimental conditions, the author could not verify this hypothesis in a wider range of slag compositions. Thus, the suggested future work is as follows

- Measuring the activity coefficient of NbO_2 over a wider range, mostly, the higher range of optical basicity to prove the amphoteric character of NbO_2
- Slag chemistry, reducing the SiO_2 content close to the refining multiple slag components like FeO for the regular solution model.
- In the regular solution model, the interaction coefficient was associated with ionic distance, optimization work to be done to refine this coefficient on a larger quantity of data analysis.

Bibliographies

Albers M., Sai Baba M., Kath D., Miller M. and Hilpert K., Physical Chemistry, 1992, vol.96, p.1663

Alcock C.B and .Hooper G.W, in Physical Chemistry of Process Metallurgy, Part I, edited by St. Pierre G.R., Metallurgical Society. AIME, 1959, p.325

Alcock C.B. and .Hooper G.W, Proceedings of the Royal Society A, 1960, vol.254, p.551

Alyamovskii S.N., Shveikin G.P. and Gel'd P.V., Zhur.Neorg.Khim., 1958, p.2437

Anthonisamy S., Ananthasivan K., Kaliappan I., Chandramouli V., Vasudeva P.R., Rao, Mathew C.K., and Jacob K.T. Metallurgical and Materials Transactions. A, 1996, vol.27A ,p.1919

Banon S., Chatillon C. and Allibert M., Canadian Metallurgical Quarterly, 1981,vol.20, p.79

Ban-ya S., ISIJ International, 1993, vol 33, no.1, p. 2

Belton G.R. and Worrell W.L., Heterogeneous Kinetics at Elevated Temperatures, Plenum press, New York-London, 1970

Bencze L. and Hilpert K., Metallurgical and Materials Transactions, A., 1996, 27A, p. 2673

Bockris J.O'M., Kitchener J.A., Ignatowicz S. and Tomlinson J.W., Transactions of the Farady Society, 1952, 48, p.75

Bodsworth C. and Bell H.B., Physical Chemistry of Iron and Steel Manufacture, Longman, 1972, p.96

Bonnet K.D. and Coley K.S., Steelmaking Conference Proceedings, 2001, p.965

Borgianni C. and Granati P., Metall. Trans., 1979, 10B, p.21

Brodowsky H. and Schaller H.-J (eds), Thermochemistry of Alloys, Academic Publishers, Dordrecht, 1989

Brown S.D., Roxburgh R.J., Ghita I., and Bell H.B., Ironmaking and Steelmaking, 1982, vol.9, p.163

Chang L.L. and Phillips B., Journal of the American Ceramic Society, 1969, vol.52, p.527

Chase, M. W. NIST-JANAF Thermochemical Tables, 4th edition, American Chemical Society ,1998

Chen W.Q, Zhou R.Z. and Lin Z.C. Journal of University of Science and Technology Beijing, 1989, vol. 11. no. 6, p. 526

Deeley P. D., Kundig K.J.A., Spendelow H. R., Ferroalloys & Alloying Additives Handbook, Metallurgy Alloy Corp., 1981, p.37

Duffy J.A., Ingram M.D. and Sommerville I.D., Journal of the Chemical Society. Faraday Transactions I, 1978, vol. 74, p.1410

Duffy J.A. and Ingram M.D., Journal of Non-crystalline Solids, 1976, vol. 21, p.373

Eckert M., Bencze L., Kath D., Nickel H. and Hilpert K., Physical Chemistry, 1996, vol. 100, p.418

Fincham C.J.B. and Richardson F.D., Proc. Roy. Soc., 1954, vol. 223, p.40

Flood H. and Knapp W.J., J. Am. Ceram. Soc., 1963, vol. 46, p.61

Fujita M. and Maruhashi S., Tetsu-to-Hagané, 1970, vol 56, no.7, p.830

Furukawa T. and White W.B., Physics and Chemistry of Glasses, 1979,vol.20.,p. 69

Gaskell D.R. Application of Thermodynamics to Metallurgical Processes, 104th AIME annual meeting, New York, Feb. 16-20,1975

Gaskell D.R., Met. Trans B, 1977, vol. 8B, p. 131

Geiger F., Busse C.A. and Loehrke R.I., International Journal of Thermophysics, 1987, vol. 8, no.4, p.425

Gilles P.W. Journal of the American Ceramic Society,1975, vol 58, no.7-8, p.279

Golubtsov I.V., Lapitskii A.V.and Shiryaev V.K. Izv.Vysshekh Uchebn.Zavedenii, Khim.i Khim.Tekknol., 1960, vol.3, p.571

Greegor R.B., Lytle F.W., Sandstrom D.R., Wong J., and Schultz P., Journal of Non-Crystalline Solids, 1983,vol.55, pp.27-43

Grieveson P. Hooper G.W. and Alcock B.C. in Physical Chemistry of Process Metallurgy, Part I, edited by St.Pierre G.R., Metallurgical Society. AIME, 1959, p.341

Hallstedt B., Hillert M., Selleby M. and Sundman B., Calphad. 1994, vol. 18, no.1, p.31

Haskell R.W. and Byrne J.G. "Treatise on Materials Science and Technology", H. Herman(Ed.),1, Academic Press, New York, 1972

Hastie, J.W. High Temperature Vapors, New York/ San Francisco/London, 1975

Hilpert K. "Advances in Mass Spectrometry" 7A, (N.R.Daly,Ed.) Heyden, London 1978

Hirth J.P. and Pound G.M., Progr. Materials Sci., 1963, vol 11

Hultgren R., Desai P.D.,Hawkins D.T., Gleiser M., Kelley K.K., and Wagman D.D., Selected values of the Thermodynamic Properties of the Elements. American Society for Metals, 1971

Inoue R. and Suito H., Tetsu-to-Hagané 69, 1983 , vol. 69, p.1129

Lepore J.V.and Van Wazer J.R.,U.U.Atomic Engergy Commission, MDDC- , 1948, p.1188

Jahanshahi S. and Wright S., 4th International Conference on Molten Slags and Fluxes, 1992, Sendai, ISIJ , p.61

Jahanshahi S. and Wright S., ISIJ international, 1993, vol.33, p.195

Jiang G.-C, Xu K-D. and Wei S.-K., ISIJ international, 1993, vol.33, p.20

Kamegashira N., Matsui T., Harada M. and Naito K., Journal of Nuclear Materials, 1981, vol.101, p.207

Kapala J., Kath D. and Hilpert K., Metallurgical and Materials Transactions A, 1996, 27A, p.2673

Kapoor M.L., Mehrotra G.M. and Frohberg M.G , Archiv. Eisenhuttenw, 1974, vol. 45, p. 213

Kolthoff I.M. and Elving P.J (Ed), Treatise on Analytical Chemistry, part II, Interscience Publishers, New York, 1964, vol. 6, p.226

Komarek K.L. and Ipser H., Pure and Applied Chemistry, 1984, vol 56, p.1511

Komarek K.L., Ber. Bunsenges, Physical Chemistry, 1977, vol.81, p.936

Komarek K.L. Metallurgical Chemistry, ed. by O.Kubaschewski, Proceedings of A Symposium held at Brunel University and The National Physical Laboratory on the 14, 15 and 16 July , 1971, p.75

Kubaschewski O. and Alcock C.B. Metallurgical Thermochemistry, 5th,Pergamon Press, Oxford, 1979

Kubaschewski O., Physica, 1981, 103B, p.101

Kubaschewski O., Alcock, C.B. and Spencer P.J. Materials Thermochemisry,6th edition, Pergamon Press, Oxford, 1993

Kubaschewski O., Evans E.LL., Alcock C.B. Metallurgical thermochemistry,4th edition, 1967

Kubaschewski O. and Evans E.L., Metallurgical Thermochemistry, 3rd Edition (rev.), Pergamon Press, New York , 1958

Kvande H. and Wahlbeck P.G., Acta Chemica Scandinavia, 1976, A30, p.297

Lin P.L. and Pelton A.D., Metall. Trans., 1979, 10B, p.21

Lumsden J., in Physical Chemistry of Process Metallurgy ,St. Pierre G.R., ed., AIME, Interscience, New York, 1961, Part 1, p.165

Lumsden J., Thermodynamics of Alloys, 1952, p.129

Margrave J.L., in Physicochemical Measurements at High Temperatures, Bockris J.O'M. (editor), Academic Press, New York, 1959, p.225

Masson C.R., Glass 1977, Proc. 11th International Congress on Glass, Gotz J.(editor), Prague, 1977, vol. 1, p.3

Masson C.R., Smith I.B. and Whiteway S.G., Can. J. Chem., 1970, vol. 48, p. 1456

Matsui T. and Naito K., International Journal of Mass Spectrometry and Ion Physics, 1983, vol.47, p.253

Matsui T. and Naito K., Journal of Solid State Chemistry, 1985, v 59, no. 2, p. 228

Matsui T. and Naito K., Journal of .Nuclear Materials, 1981, vol.102, p.227

Matsui T. and Naito K., Journal of Nuclear Materials, 1982, vol.107, p.83

McCabe C.L and Birchenall C.E., Journal of Metals , 1953, May, p.707

McCabe C.L., Schadel H.M. and Birchenall C.E. , Journal of Metals, 1953, vol.5, p.709

McLean A., Yang Y.D., Sommerville I.D., Uchida Y. and Iwase M., High Temperature Materials and Processes, 2001, vol.20, p.185.

Merten U., Journal of Physical Chemistry, 1959, vol.63, p.443

Merten U. and Bell W.E., The Characterization of High-Temperature Vapors, Margrave J.L.(editor), 1967

Miller M. and Gingerich K.A., Metallurgical and Materials Transactions A, 1994, vol. 25A, p.857

Mills K.C., ISIJ International, 1993, vol.33, p.148

Mysen B.O., Earth-Science Rev., 1990, vol.27, p.281

Mysen B.O., Structure and Properties of Silicate Melts, Elseviewr Sci. Publishers B.V, 1988

Nagabayashi R., Hino M. and Ban-ya S. , Transactions of the Iron and Steel Institute of Japan International, 1989, vol.29, p.140

Naito K., Kamegashira N. and Sasaki N., Journal of Solid State Chemistry, 1980, vol. 35, p.305

Niwa K. and Yokokawa T., Trans. Jpn. Inst. Met., 1969, vol. 10, p.3

Neckle A., Thermochemistry of Alloys, Recent Developments of Experimental Methods, (Brodowsky H. and Schaller H.-J.,Ed.) Kluwer Academic Publishers, 1989

Nesmeyanov A.N. Vapor Pressures of the Elements, Elsevier Publishing Company, Amsterdam, 1963

Nukui A., Tagai H., Morikawa H. and Iwai S.I., Journal of the American Ceramic Society, 1978, vol.61, p.174

Onderka B, Wypartowicz J. and Hämäläinen M., CALPHAD 1993, vol.17, p.1

Oriani R.A., Acta Met., 1956, vol.4, p.15

Park J.H., Min D.J. and Song H.S., Metallurgical and Materials Transactions B. vol. 35B, p.269

Paul A. and Douglas R.W., Physics and Chemistry of Glasses, 1966, vol.7, p.1

Paul A. and Lahiri D., Journal of the American Ceramic Society, 1966, vol. 49, p.565

Paule R.C. and Margrave J.L., The Characterization of High Temperature Vapours, edited by Margrave J.L , John Wiley and Sons, New York, 1967, p.130

Peltner H.E. and Herzig C., Acta Metallurgica , 1981, vol. 29, p. 1107

Pichelin G. and Rouanet A., Chemical Engineering Science, 1991, vol. 46, no.7, p. 1635

Pichelin G. and Rouanet A., High temperatures-High Pressures, 1992, vol.24 , p.97

Ran B.K.D.P. and .Gaskell D.R, Metallurgical Transactions B, 1981,vol.12B, p.469

Rao B.V.J., Journal of the American Ceramic Society, 1964,vol.47, p.455

Rao Y.K., Stoichiometry and Thermodynamics of Metallurgical Processes, Cambridge University Press, Cambridge, 1985, p.892

Rapp R.A., Physicochemical measurements in metals research, New York , Interscience Publishers, 1968

Regnault H.V. Ann.Chim., 1845, vol.15, p.129

Rein R.H.and Chipman J., Transactions of the Metallurgical Society of AIME, 1965, vol 233 ,p.415

Reyes R.A. and Gaskell D.R. Metallurgical Transactions B, 1983, vol. 14B, p.725

Richardon F.D. and Alcock C.B., Physicochemical Measurements at High Temperatures, J.O'M. Bockris (Editor), Academic Press, New York, 1959, p.135

Richards A.W. and Thorne D.F.J., Physical Chemistry of Process Metallurgy, Part 1(ed. St. Pierre G.R.), AIME, Interscience, New York, 1961, p.277

Richardson F.D. Physical Chemistry of Melts in Metallurgy , v1, Academic Press, London, New York, 1974

Rovnushkin V.A., Nikiforov S.V. and Toporishchev G.A., Russian Metallurgy, 1989, no.5

Sano N., Lu W-K., Riboud P.V., Advanced Physical Chemistry for Process Metallurgy, Academic Press, 1997

Sano N. and Tsukihashi F., High Temperature Materials and Processes, 2001, vol.20, p.263

Sato A., Aragane G., Kasahara A., Kori M. and Yoshimatsu S., Tetsu-to-Hagané , 1987, vol.73, p.275

Schadel H.M.Jr and Birchenall C.E. Journal of Metals, September 1950, Transactions AIME, vol. 188, p. 1134

Schaefer H., Chemical Transport Reactions, Academic Press, New York, 1964

Schulze K.K., Jehn H.A. and Hörz G., Journal of Metals, 1988, October, p.25

Schwerdtfeger K. and Turkdogan E.T. "Techniques of Metals Research" (Rapp R.A., Ed.), vol.IV, Wiley, New York, 1970

Schwerdtfeger K. Mirzayousef-Jadid A.-M., 2000 Belton Symposium Proceedings, 2000, p.108

Semenov G.A. and Lopatin S.I., Russian Journal of Applied Chemistry, 2001, vol. 74, no.6, p.901

Sharma R.A. and Richardson F.D., The Journal of the Iron and Steel Institute, 1962, vol.200, p. 373

Shchukarev S.A., Semenov G.A. and Frantseva K.E., Dokl.Acad.Nauk SSSR, 1962,vol. 145, p.119.

Shchukarev S.A., Semenov G.A. and Frantseva K.E., Izv.Vysshekh Uchebn.Zavedenii, Khim.i Khim.Tekhnol. 1962, vol.5, p.691.

Shchukarev S.A., Semenov G.A. and Frantseva K.E., Russian Journal of Inorganic Chemisrty, 1966, vol.11, p.129.

Shchukarev S.A., Semenov G.A. and Frantseva K.E., Russian Journal of Inorganic Chemistry, 1959, vol. 4, p.1217

Sismanis P.G. and Argyropoulos S.A., Transactions of the ISS, 1989, July, p.39

Slag Atlas,edited by Verein Deutscher Eisenhüttenleute (VDEh),Verlag Stahleisent GmbH, 1995

Sommerville I.D. and .Bell H.B., Canadian Metallurgical Quarterly, 1982, vol.21, p 145

Son A.H. and Tsukihashi F. ISIJ International, 2003, vol.43, no.10 , p.1356

Thomson G.W., Technique of Organic Chemistry,1, Weissberger A.(Editor), Physical Methods of Organic Chemistry, Part I, 3rd Edition, Interscience, New York, 1959, p.401

Toop G.W. and Samis C.S., Trans. Metall. Soc. AIME, 1962, vol. 224, p.873

Tsukihashi F., Tagaya A. and Sano N., Transactions of the Iron and Steel Institute of Japan, 1988, vol.28, p.164

Turkdogan E.T. and Bills P.M., Ceramic Bulletin., 1960, vol.39, p. 682

Turkdogan E.T. Physical Chemistry of High Temperature Technology, Academic Press, 1980

Turkdogan E.T., Transactions of the Iron and Steel Institute of Japan , 1984, vol.24, p.591

Vidal R. and Poos A., in "The Steel Industry and the Environment" (J. Szekely, Ed.), Dekker, New York, 1973

Wachter A. Journal of the American Chemical Society, 1932, vol.54, p.4609

Wahlbeck P.G. High Temperature Science, 1986, vol.21, p.189

Ward R.G., An introduction to the physical Chemistry of ion & steel making, Edward Arnold LTD, 1962

Warren B.E., Journal of the American Ceramic Society, 1934, vol.17, p.249

Wilfred W.Scott,Sc.D. Standard Methods of Chemical Analysis, Fifth edition D.van nostrand company, inc, New York, 1939, p.331

Zachariasen W.H, Journal of the American Chemical Society, 1932, vol.54, p.3841

Appendix A Uncertainty Analysis

A.1 Introduction

By transpiration method, the results of vapor pressure are performed on a few measurements using a number of constants. The constants are free of error. However, the problem is to estimate the error of vapor pressure resulting from the uncertainties. The idea in this section is to develop a general formula for the propagation of errors.

Generally, the formulation of the problems is as follows:

Given a function

$$y = f(x_1, x_2, \cdots, x_i) \tag{A.1}$$

Where $x_1, x_2, \cdots, x_i$ are independent variables and the standard deviations are given by $\sigma_{x_1}, \sigma_{x_2}, \cdots, \sigma_{x_i}$ .If the errors of these measurements of $x_1, x_2, \cdots, x_i$ are independent of each other, the standard deviation of y is provided by the following formula:

$$\sigma_y^2 = \left(\frac{\partial f}{\partial x_1}\right)^2 \sigma_{x_1}^2 + \left(\frac{\partial f}{\partial x_2}\right)^2 \sigma_{x_2}^2 + \cdots + \left(\frac{\partial f}{\partial x_i}\right)^2 \sigma_{x_i}^2 \tag{A.2}$$

From this general formula, the following special cases are easily derived:

(a) *Case of subtraction and addition*

For,

$$y = K + a_1 x_1 + a_2 x_2 + \cdots + a_i x_i \tag{A.3}$$

where K is a constant, and $a_1, a_2, \cdots, a_i$ are any real numbers ,substituting (A.3) into (A.2) and reorganizing ,we obtain

$$\sigma_y = \sqrt{a_1^2 \sigma_{x_1}^2 + a_2^2 \sigma_{x_2}^2 + \cdots + a_i^2 \sigma_{x_i}^2} \tag{A.4}$$

(b) *Case of multiplication*

For expression, $$y = K \cdot x_1^{a_1} \cdot x_2^{a_2} \cdot \cdots \cdot x_i^{a_i} \tag{A.5}$$

Substitution of (6.25) to (6.222), we have

$$\sigma_y^2 = \frac{a_1^2 \cdot y^2 \cdot \sigma_{x_1}^2}{x_1^2} + \frac{a_2^2 \cdot y^2 \cdot \sigma_{x_2}^2}{x_2^2} \sigma_{x_2}^2 + \cdots + \frac{a_i^2 \cdot y^2 \cdot \sigma_{x_i}^2}{x_i^2} \sigma_{x_i}^2 \tag{A.6}$$

Therefore,

$$\frac{\sigma_y}{y} = \sqrt{a_1^2 \left(\frac{\sigma_{x_1}}{x_1}\right)^2 + a_2^2 \left(\frac{\sigma_{x_2}}{x_2}\right)^2 + \cdots + a_i^2 \left(\frac{\sigma_{x_i}}{x_i}\right)^2} \tag{A.7}$$

From Equation A.4 note that the errors of additive terms are not additive; only their squares are additive. Similarly, it follows from Equation A.7 that for multiplicative expressions, the squares of the relative errors are additive, not the relative errors themselves.

A.2 Propagation of Errors

The uncertainties for the vapor pressure measurements are mainly considered to be a combination of the uncertainties in temperature, weight-loss determination, flow rate and gas composition. The uncertainty sources and estimation are listed in Table 6.4. It has been noticed that the major contribution to the maximum uncertainty are mass determination and the concentration determination by ICP, which leads to a maximum uncertainty in derived apparent vapor pressures of about ±11.4%.

Table A.1 Uncertainty sources and estimation

Source	uncer.contribution	estimation	relative uncertainty %	symbol
ICP	concentration	std solution	±6%	e_1
scale	Mass	0.0001g/0.001g	±10%	e_2
flow controller	flow rate	calibration	±0.7%	e_3
time	flow volume	3min/1050min	±0.3%	e_4
temperature		1k/1873k	±0.05%	e_5
propagation of uncertainty			±11.40%	

Appendix B Experimental Results

Table B.1 Dissoication Vapor Pressure of Nb_2O_5 at 1873K

Temperature K	CO_2/CO	Total Flow Rate mL/min	p_{O2} atm	p_{NbO2} atm
1873	7.552	40.4	9.75E-06	2.75E-06
1873	2.384	40.4	9.72E-07	6.99E-06
1873	0.752	40.0	9.67E-08	8.95E-06
1873	0.236	40.3	9.52E-09	1.44E-05
1873	0.076	40.2	9.88E-10	3.49E-05

Appendix B Experimental Results

Table B.2 Experimental results on $CaO\text{-}SiO_2\text{-}NbO_x$ slag system

label	T	CaO/SiO_2	opt B	Nb_2O_5 in premelt	$p_{NbO2} \times 10^5$	log p_{O2}	$a_{NbO2.5}$	$\gamma_{NbO2.5}$	a_{NbO2}	γ_{NbO2}	Nb^{5+}/Nb^{4+}
	K	wt%/wt%		wt%	atm	atm					
B1	1873	0.7984	0.63147	10.4855	1.2311	-8	0.7176	119.2755	0.1633	3.8147	0.1405
E1	1873	0.7984	0.63138	10.4855	0.7481	-7	0.7755	80.0531	0.0992	2.5338	0.2473
F1	1873	0.7984	0.63126	10.4855	0.4382	-6	0.8078	56.9549	0.0581	1.6753	0.4087
G1	1873	0.7984	0.6311	10.4855	0.2627	-5	0.8611	42.7906	0.0349	1.2100	0.6986
			0.6313								
B2	1873	1.001	0.65585	9.8034	1.2769	-8	0.7443	98.4896	0.1694	4.4879	0.2002
E2	1873	1.001	0.65571	9.8034	0.7576	-7	0.7853	68.0433	0.1005	2.9748	0.3416
F2	1873	1.001	0.65554	9.8034	0.4512	-6	0.8318	51.3953	0.0599	2.0519	0.5547
G2	1873	1.001	0.65528	9.8034	0.2714	-5	0.8895	37.9272	0.0360	1.6401	1.0684
B3	1873	1.2003	0.67556	10.5542	1.3033	-8	0.7597	78.5764	0.1729	4.4174	0.2470
E3	1873	1.2003	0.67528	10.5542	0.7955	-7	0.8246	51.0583	0.1055	3.2268	0.4938
F3	1873	1.2003	0.67504	10.5542	0.4640	-6	0.8552	39.7664	0.0616	2.2477	0.7853
G3	1873	1.2003	0.67472	10.5542	0.2806	-5	0.9199	31.8265	0.0372	1.8580	1.4424
B4	1873	1.4993	0.70082	10.8011	1.3901	-8	0.8103	53.2144	0.1844	5.3267	0.4398
E4	1873	1.4993	0.70048	10.8011	0.8325	-7	0.8630	40.2861	0.1105	3.8792	0.7523
F4	1873	1.4993	0.70005	10.8011	0.4886	-6	0.9007	30.6880	0.0648	3.1469	1.4247
G4	1873	1.4993	0.69964	10.8011	0.2888	-5	0.9467	25.5199	0.0383	2.9688	2.8743

Table B.2 (Continued)

label	T	CaO/SiO_2	opt B	Nb_2O_5 in premelt	$p_{NbO2} \times 10^5$	log p_{O2}	$a_{NbO2.5}$	$\gamma_{NbO2.5}$	a_{NbO2}	γ_{NbO2}	Nb^{5+}/Nb^{4+}
	K	wt%/wt%		wt%	atm	atm					
A1	1873	0.8019	0.6339	6.7815	1.1910	-8	0.6943	138.6779	0.1580	6.0855	0.1928
H1	1873	0.8019	0.6338	6.7815	0.7148	-7	0.7409	90.1508	0.0948	4.1650	0.3610
J1	1873	0.8019	0.6337	6.7815	0.4170	-6	0.7686	58.6782	0.0553	3.0892	0.7314
K1	1873	0.8019	0.6336	6.7815	0.2431	-5	0.7969	49.0546	0.0323	2.1828	1.0994
A2	1873	1.0037	0.6595	5.1955	1.2238	-8	0.7134	134.1983	0.1624	8.9612	0.2934
H2	1873	1.0037	0.6594	5.1955	0.7259	-7	0.7525	99.5279	0.0963	6.0648	0.4761
J2	1873	1.0037	0.6593	5.1955	0.4226	-6	0.7789	66.2049	0.0561	4.7961	1.0065
K2	1873	1.0037	0.6592	5.1955	0.2498	-5	0.8188	57.3809	0.0331	3.6042	1.5519
A3	1873	1.2026	0.6802	5.5565	1.2554	-8	0.7318	99.3421	0.1666	9.4315	0.4171
H3	1873	1.2026	0.6801	5.5565	0.7506	-7	0.7780	76.0354	0.0996	6.7262	0.6911
J3	1873	1.2026	0.6799	5.5565	0.4348	-6	0.8014	54.2944	0.0577	5.6046	1.4342
K3	1873	1.2026	0.6798	5.5565	0.2544	-5	0.8340	48.3543	0.0338	4.3200	2.2073
A4	1873	1.5029	0.7054	6.9912	1.3032	-8	0.7596	63.3839	0.1729	8.8098	0.6107
H4	1873	1.5029	0.7051	6.9912	0.7725	-7	0.8008	46.0194	0.1025	7.2013	1.2226
J4	1873	1.5029	0.7049	6.9912	0.4499	-6	0.8294	37.5377	0.0597	6.2436	2.3109
K4	1873	1.5029	0.7047	6.9912	0.2600	-5	0.8524	34.6107	0.0345	4.9031	3.5000

Table B.3 Experimental results on $CaO-SiO_2-Al_2O_3-NbO_x$ slag system at 1873 K

label	p_{NbO2} atm	log p_{O2} atm	opt B	$X(Al_2O_3)$	a_{Nb2O5}	γ_{Nb2O5}	a_{NbO2}	γ_{NbO2}	Nb^{5+}/Nb^{4+}
R1	2.70E-06	-6	0.7856	0.0914	0.2486	11.1562	0.0359	3.6217	4.4964
R2	2.46E-06	-6	0.7569	0.1424	0.2060	14.4185	0.0327	1.1413	0.9980
R3	2.25E-06	-6	0.7430	0.1714	0.1723	15.4702	0.0299	0.8759	0.6529
R4	1.99E-06	-6	0.7237	0.2338	0.1348	18.0481	0.0264	0.7228	0.4085
R5	1.80E-06	-6	0.7024	0.2668	0.1097	21.3668	0.0239	0.4741	0.2041
S1	7.09E-06	-8	0.7853	0.0963	0.1709	8.8383	0.0941	8.0851	3.3215
S2	6.45E-06	-8	0.7568	0.1454	0.1415	12.1048	0.0857	2.7536	0.7516
S3	5.69E-06	-8	0.7421	0.1860	0.1099	13.3375	0.0755	2.7791	0.6069
S4	4.41E-06	-8	0.7237	0.2358	0.0660	14.8437	0.0585	1.4462	0.2199
S5	3.03E-06	-8	0.7025	0.2697	0.0312	17.8217	0.0403	0.7468	0.0651

Table B.4 Experimental results on temperature effect in $CaO-SiO_2-NbO_x$ slag system

label	Temperature	CaO/SiO_2	p_{O2}	p_{NbO2}	opt B	$a_{NbO2.5}$	γ_{Nb2O5}	a_{NbO2}	γ_{NbO2}	Nb^{5+}/Nb^{4+}
	K	wt%/wt%	atm	atm						
O1	1823	0.7984	1.00E-06	1.24E-06	0.6312	0.2721	15.1517	0.0380	1.2262	0.58
O2	1823	1.0010	1.00E-06	1.31E-06	0.6315	0.2879	14.5168	0.0402	1.5596	0.77
O3	1823	0.8019	1.00E-06	1.04E-06	0.6332	0.2279	14.9971	0.0318	2.0088	0.96
O4	1823	1.2026	1.00E-06	1.13E-06	0.6338	0.2481	14.2832	0.0346	4.3844	2.20
P1	1851	0.7984	9.60E-07	3.15E-06	0.6312	0.5384	33.9492	0.0770	2.3317	0.48
P2	1851	1.0010	9.60E-07	3.15E-06	0.6315	0.5383	30.2717	0.0770	2.7722	0.64
P3	1851	0.8019	9.60E-07	2.70E-06	0.6333	0.4613	34.9750	0.0660	3.7034	0.74
P4	1851	1.2026	9.60E-07	2.93E-06	0.6338	0.5018	33.1013	0.0718	7.1127	1.50
Q1	1862	0.7984	9.81E-07	4.50E-06	0.6312	0.7067	48.0695	0.1021	2.9871	0.43
Q2	1862	1.0010	9.81E-07	4.56E-06	0.6316	0.7164	44.3139	0.1035	3.5222	0.55
Q3	1862	0.8019	9.81E-07	3.73E-06	0.6333	0.5848	48.8015	0.0845	4.4430	0.63
Q4	1862	1.2026	9.81E-07	4.17E-06	0.6338	0.6549	38.8920	0.0946	11.2326	2.00